8-7-2018

Mechanistic Studies on D-arginine Dehydrogenase and Functional Annotation of a Novel NADH:quinone Oxidoreductase (PA1024)

Jacob A. Ball
Georgia State University

MECHANISTIC STUDIES ON D-ARGININE DEHYDROGENASE AND FUNCTIONAL ANNOTATION OF A NOVEL NADH:QUINONE OXIDOREDUCTASE (PA1024)

by

JACOB BALL

Under the Direction of Giovanni Gadda, PhD

ABSTRACT

Pseudomonas aeruginosa D-arginine dehydrogenase (*Pa*DADH) is an FAD-dependent enzyme that catalyzes the oxidative deamination of D-arginine to generate the corresponding α-keto acid and ammonia. The enzyme is similar to D-amino acid oxidase, except that *Pa*DADH is a strict dehydrogenase with no oxygen reactivity. The enzyme exhibits broad substrate specificity and can oxidize 17 of the 20 common amino acids. The best substrates for the enzyme are D-arginine and D-lysine based on the second order rate constant k_{cat}/K_m values.

The 3D structure of the DADH-iminoarginine complex suggests that E87 engages in an electrostatic interaction with the positively charged guanidinium group of D-arginine. The 3D structure also displays a hydrogen bonding network of water molecules that connects H48 to the substrate α-amine, suggesting it may serve as catalytic base. E87 and H48 were mutated to

produce E87L and H48F variants, and pH effect kinetic approaches with zwitterionic and cationic substrates were employed. The data, in combination with previous results on Y53 and Y249 variants, suggests that there is no catalytic base, since the catalytic pK_a is present in all variants. The results are also consistent with E87 required to be deprotonated to bind cationic substrates.

In the second part of this dissertation, a presumed nitronate monooxygenase from *P. aeruginosa*, PA1024, is characterized. PA1024 is determined to not possess NMO activity and instead catalyze the two-electron reduction of quinones via the oxidation of NADH. The enzyme has a strict preference for NADH over NADPH. The functional annotation and bioinformatics identifies a novel class of FMN-dependent NADH:quinone oxidoreductases (NQO) with a TIM-barrel fold. The pH effects reveal that PA1024 has two regimes of activity at low and high pH dictated by the deprotonation of an enzymatic residue with pK_a ~7. In addition, the 3D X-ray structure of PA1024 in complex with the reaction product NAD^+ is solved. The structure reveals the structural basis for the strict NADH specificity, which relies on a steric constraint imposed by a nearby P78 and Q80. The structure also reveals a conformational gating mechanism of Q80 and an unusual interrupted helix structural pattern to bind the pyrophosphate of NAD^+.

INDEX WORDS: flavin, oxidoreductase, NADH, quinones, D-arginine dehydrogenase, pH effects, enzyme kinetics

MECHANISTIC STUDIES ON D-ARGININE DEHYDROGENASE AND FUNCTIONAL ANNOTATION OF A NOVEL NADH:QUINONE OXIDOREDUCTASE (PA1024)

by

JACOB BALL

A Dissertation Submitted in Partial Fulfillment of the Requirements for the Degree of

Doctor of Philosophy

in the College of Arts and Sciences

Georgia State University

2018

MECHANISTIC STUDIES ON D-ARGININE DEHYDROGENASE AND FUNCTIONAL ANNOTATION OF A NOVEL NADH:QUINONE OXIDOREDUCTASE (PA1024)

by

JACOB BALL

Committee Chair: Giovanni Gadda

Committee: Dabney Dixon

Donald Hamelberg

Electronic Version Approved:

Office of Graduate Studies

College of Arts and Sciences

Georgia State University

August 2018

DEDICATION

This dissertation is dedicated to my parents Hollis and Cookie Ball.

ACKNOWLEDGEMENTS

I would like to thank my family for supporting me through this journey. My parents, Hollis and Cookie, and siblings – brothers Butler, Adam, Jeremy, and sister, Carrie – all have been a crucial support this entire time. I would like to thank my advisor, Dr. Giovanni Gadda, for pushing me in the right direction to become the driven individual I am today. I am forever indebted to him for lending his expertise and knowledge. I never envisioned myself obtaining a PhD, but he helped me realize I did have the strength and ability to do so. I am grateful for my committee members. Dr. Dabney Dixon – thank you for asking tough questions and helping me improve my CV to a high standard. Dr. Donald Hamelberg – thank you for being an outstanding professor in physical chemistry and offering advice. I would like to thank lab members past and present – Swathi, Francesca, Crystal, Yvette, Rizuan, Elvira, Dan, Daniel, Quan, Archana, Renata, Hossein, Elias, Chris, and Maria – and many more. Swathi, you were an excellent mentor when I first joined the lab as an undergraduate. Finally, I would like to thank my girlfriend, Beibei, who improved many aspects of my life and gave me constant support and encouragement. Completion of this degree would not have been possible without you all. The work presented in this dissertation was supported by an MBD graduate fellowship.

TABLE OF CONTENTS

LIST OF TABLES

LIST OF FIGURES

LIST OF SCHEMES

LIST OF ABBREVIATIONS

FMN, flavin mononucleotide; FAD; flavin adenine dinucleotide; *Pa*DADH, D-arginine dehydrogenase from *Pseudomonas aeruginosa*; DAAO, D-amino acid oxidase; pDAAO, D-amino acid oxidase from pig kidney; *Rg*DAAO, D-amino acid oxidase from *Rhodoturula gracilis*; *h*DAAO, D-amino acid oxidase from human; DASPO, D-aspartate oxidase; NMDA, N-methyl-D-aspartate; CephC, Cephalosporin C; D-DOPA, D-3,4-dihydroxyphenylalanine; PMS, Phenazine methosulfate; NMO, nitronate monooxygenase; P3N, propionate 3-nitronate; 3-NPA, 3-nitropropionic acid; IPTG, isopropyl-1-thio-β-D-galactopyranoside; Cyt *c*, Cytochrome *c*; superoxide dismutase, SOD; NADH, reduced nicotinamide adenine dinucletide; NAD^+, oxidized nicotinamide adenine dinucleotide; NADPH, reduced nicotinamide adenine dinucleotide phosphate; $NADP^+$, oxidized nicotinamide adenine dinucleotide phosphate; NADH:quinone oxidoreductase 1, NQO1; ribosyldihydronicotinamide:quinone reductase, NQO2.

1 INTRODUCTION

1.1 Substrate specificity of flavoenzymes that oxidize D-amino acids

1.1.1 Abstract

The oxidation of D-amino acids is relevant to neurodegenerative diseases, detoxification, and nutrition in microorganisms and mammals. It is also important for the resolution of racemic amino acid mixtures and the preparation of chiral building blocks for the pharmaceutical and food industry. Considerable biochemical and structural knowledge has been accrued in recent years on the enzymes that carry out the oxidation of the C_α-N bond of D-amino acids. These enzymes contain FAD as a required cofactor, share similar overall three-dimensional folds and highly conserved active sites, but differ in their specificity for substrates with neutral, anionic, or cationic side-chains. Here, we summarize the current biochemical and structural knowledge regarding substrate specificity on D-amino acid oxidase, D-aspartate oxidase, and D-arginine dehydrogenase, for which a wealth of biochemical and structural studies is available.

1.1.2 Introduction

The oxidation of D-amino acids is important from both fundamental and applied standpoints.[1] The reaction is relevant to neurodegenerative diseases, detoxification, nutrition, and other biological processes in microorganisms and mammals. It is also important for the resolution of racemic amino acid mixtures, the preparation of chiral building blocks for the pharmaceutical industry, and the food industry. In this review article, we present a brief overview of the importance of D-amino acids regarding biochemical processes and industrial applications, and summarize the current biochemical as well as structural knowledge on the flavoenzymes that oxidize α-D-amino acids with emphasis on substrate specificity. The enzymes covered within the scope of this review include D-amino acid oxidase (DAAO), D-arginine

dehydrogenase (DADH), and D-aspartate oxidase (DASPO), for which a wealth of biochemical and structural studies is available. These enzymes are divided into three categories, depending on their preference for D-amino acid substrates with neutral, cationic, or anionic side-chains. Mutant variants of the enzymes that had an impact on substrate specificity are also discussed. We conclude with some general principles about structure and specificity for the oxidation of α-D-amino acids by flavoenzymes. The mechanistic aspects of the enzymes that oxidize the C_α-N bond of D-amino acids have been recently reviewed by Fitzpatrick and are not covered here.[2]

1.1.3 Importance of D-amino acids

Due to a lack of detection methods for D-amino acids for most of the 20th century, with only isolated cases of detection mostly in invertebrates[3-5], studies investigating L-amino acids have eclipsed those of D-amino acids. Analysis of D-amino acids changed with the advent of improved analytical techniques in the 1990s, such as gas chromatography, high performance liquid chromatography, and the use of chiral columns, which allow separation of D/L-racemic mixtures and the detection of trace amounts of D-amino acids.[4, 6] In bacteria, D-Ala and D-Glu have been detected as important components of the bacterial peptidoglycan and contribute to the overall strength of the cell wall.[5] In humans, D-Ser has been detected at high concentrations in the brain and serves as the endogenous agonist of N-methyl-D-Asp (NMDA) receptors.[7] D-Asp has been detected in the β-amyloid peptides of patients with Alzheimer's disease [8], the crystallin peptides of patients with cataracts [9], and the αA-crystallin peptides of the elastic fibers in sun-damaged skin.[10] Thus, the emergence of knowledge on D-amino acids is fairly recent and remains underappreciated in many fields of biochemistry.

D-amino acid derivatives are increasingly attractive chiral building blocks for drug discovery.[11] Many natural and synthetic antibiotics contain D-amino acid groups, such as

penicillins and cephalosporins.[12] The inherent resistance to protease cleavage demonstrated by antibiotic peptides containing D-amino acids greatly reduces the rate of their inactivation. Several drugs containing D-amino acids have surfaced in recent years including Nafarelin, which is used in the treatment of estrogen-dependent conditions such as endometriosis.[13] D-cycloserine has been reported to have antibacterial properties through its inhibition of bacterial DAAOs.[13] Furthermore, recent findings suggest that human DAAO may play a significant role in the pathogenesis of schizophrenia due to its metabolic action on the neuromodulator D-Ser.[14]

Because many routine commercial methods to synthesize amino acids result in a racemic mixture, L-amino acids must often be purified from D-amino acids. Several enzymatic systems that use D-amino acid oxidizing enzymes have been designed to resolve racemic amino acid mixtures.[12] D-amino acid detection is of paramount importance in the food industry, where spontaneous racemization due to heat and processing conditions can generate D-amino acids that contaminate food preparations.[15, 16] Enzymes that oxidize D-amino acids have been shown to accomplish rapid D-amino acid detection in mixtures, with a low cost and accuracy comparable to classical analytical techniques, such as high-performance liquid chromatography that are more expensive and time-consuming.[17]

1.1.4 Flavoenzymes and C_α-N bond oxidation

Enzymes that are known to oxidize the C_α-N bond of D-amino acids with high stereospecificity for the D-isomer are flavoenzymes. Flavoenzymes are versatile catalysts that utilize a covalently, or more often, non-covalently bound FMN or FAD as a cofactor (**Figure 1.1**).[18] The reactive portion of FMN or FAD is the 7,8-dimethylisoalloxazine ring (**Figure 1.1**), which is a fusion of xylene, pyrazine and pyrimidine rings, allowing for multifunctional capabilities.[19] The general reaction of D-amino acid oxidation by flavoenzymes entails the

oxidation of the bond between the C_α atom and the amine N atom to generate the corresponding imino acid (**Scheme 1.1**). Non-enzymatic hydrolysis of the imino acid product yields the α-keto acid and ammonia. The reduced flavin cofactor donates electrons to an acceptor to regenerate the oxidized flavin. As illustrated in **Scheme 1.1**, oxidases utilize oxygen as electron acceptor, whereas dehydrogenases utilize electron acceptors other than oxygen. Although the hydrolysis reaction occurs non-enzymatically in solution, recent studies have reported an imine deiminase enzyme from the Rid protein family that can accelerate the breakdown of the imino acid to the corresponding α-keto acid.[20, 21]

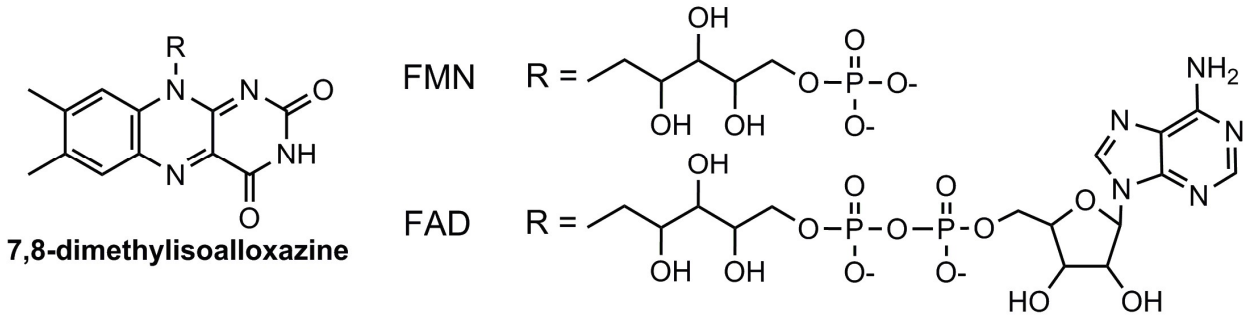

Figure 1.1 Structure of FMN, FAD, and 7,8-dimethylisoalloxazine.

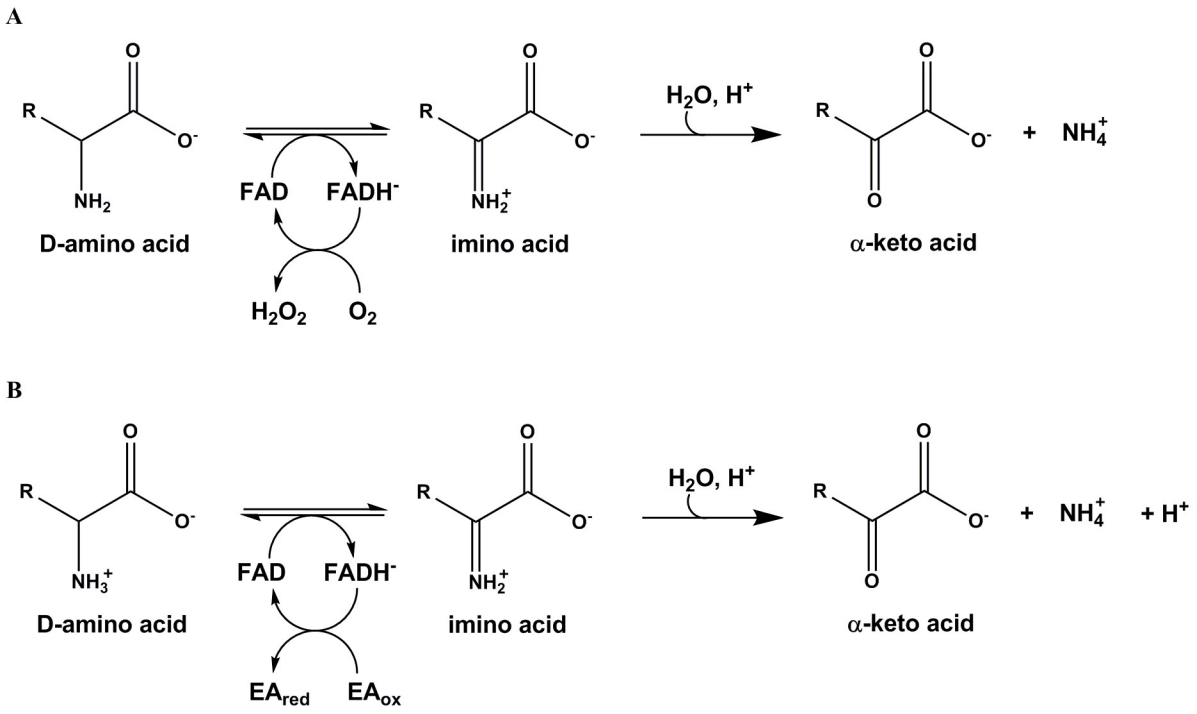

Scheme 1.1 General scheme of the reaction catalyzed by A) D-amino acid oxidases and B) D-arginine dehydrogenase.
EA_{ox}: oxidized electron acceptor; EA_{red}: reduced electron acceptor. The D-amino acid substrate in the DAAO reaction loses the amino group proton prior to forming the ES complex.[2]

The oxidation of D-amino acids is found in key life processes, such as regulatory processes, neurotransmission,[22-24] cell-signaling,[25] and metabolism.[26] As a result, imbalance in the regulation or function of these enzymes is proposed to cause neurodegenerative diseases and even cell death.[22, 25] The oxidation of the C_α-N bond of D-amino acids by flavoenzymes can be harnessed for the preparation of α-keto acids and chirally-active pharmaceutical precursors.[27] Among the several flavoenzymes reported that oxidize the C_α-N bond of D-amino acids, a wealth of biochemical information is available for D-amino acid oxidase from pig kidney (*p*DAAO), *Rhodoturula gracilis* (*Rg*DAAO), and human (*h*DAAO), as well as *Pseudomonas aeruginosa* D-arginine dehydrogenase (*Pa*DADH), and DASPO (**Table 1.1**). X-Ray crystallographic data are available for all the enzymes except DASPO, for which we have built here a 3D model of the

enzyme from beef kidney (*b*DASPO) using SWISS-MODEL and the coordinates of *p*DAAO (PDB code: 1KIF), which share 43% identity in the amino acid sequence. These enzymes show similar overall three-dimensional structures (**Figure 1.2**), highly conserved active sites (**Figure 1.3**), contain a non-covalently bound FAD, adopt a Rossmann fold to bind the cofactor,[28] but show different substrate specificity (**Table 1.2**).

Table 1.1 Select flavoenzymes that oxidize the Cα-N group of D-amino acids.

Enzyme	Source	Cofactor	Electron acceptor	EC number	PDB
D-amino acid oxidase	Pig kidney	FAD	Oxygen	1.4.3.3	1KIF
D-amino acid oxidase	*Rhodoturula gracilis*	FAD	Oxygen	1.4.3.3	1C0I
D-amino acid oxidase	Human	FAD	Oxygen	1.4.3.3	2DU8
D-arginine dehydrogenase	*Pseudomonas aeruginosa*	FAD	Unknown (PMS *in vitro*)	1.4.99.6	3NYC
D-aspartate oxidase	Various	FAD	Oxygen	1.4.3.1	Unavailable

Table 1.2 Preferred and select biologically relevant D-amino acid substrates for *p*DAAO, *Rg*DAAO, *h*DAAO *Pa*DADH, and *b*DASPO.

Substrate	k_{cat}/K_m, M^{-1} s^{-1}	k_{cat}, s^{-1}	K_m, mM
	***p*DAAO**[a]		
D-Pro	9,200	87.2	9.5
D-Ala	5,500	12.7	2.3
D-Met	4,800	143	30
D-Phe	4,500	55.9	12.3
	***Rg*DAAO**[b]		
D-Trp	530,000	160	0.3
D-Phe	358,000	105	0.3
D-Met	265,000	106	0.4
D-Ala	129,000	103	0.8
CephC	18,000	91	5.0
	***h*DAAO**[c]		
D-Cys	14,600	8.6	0.6
D-Tyr	13,500	14.8	1.1
D-DOPA	6,750	40.5	6.0
D-Ala	4,000	5.2	1.3
D-Ser	400	3	7.5
	***Pa*DADH**[d]		
D-Arg	3,400,000	204	0.06
D-Lys	530,000	141	0.26
D-Tyr	27600	23	0.8
D-Met	14800	154	10
D-Phe	6900	75	11
	***b*DASPO**[e]		
NMDA	20600	30.9	1.5
D-Asp	6090	22.5	3.7
D-Glu	213	1.2	5.6

Enzyme activity was measured varying concentrations of the desired amino acid and 21% O_2 (oxidase) or 1 mM PMS (dehydrogenase) at 25 °C and [a]pH 8.5, [b]pH 8.5, [c]pH 8.5 (except D-Tyr - pH 8.3), [d]pH 8.7 and [e]pH 7.2

[a]standard errors were not reported.[29]

[b]standard errors reported to be ≤33%.[17]

[c]standard errors reported to be ≤22%.[30-32]

[d]standard errors reported to be ≤15%.[33]

[e]standard errors were not reported.[34]

CephC – Cephalosporin C; D-DOPA – D-3,4-dihydroxyphenylalanine

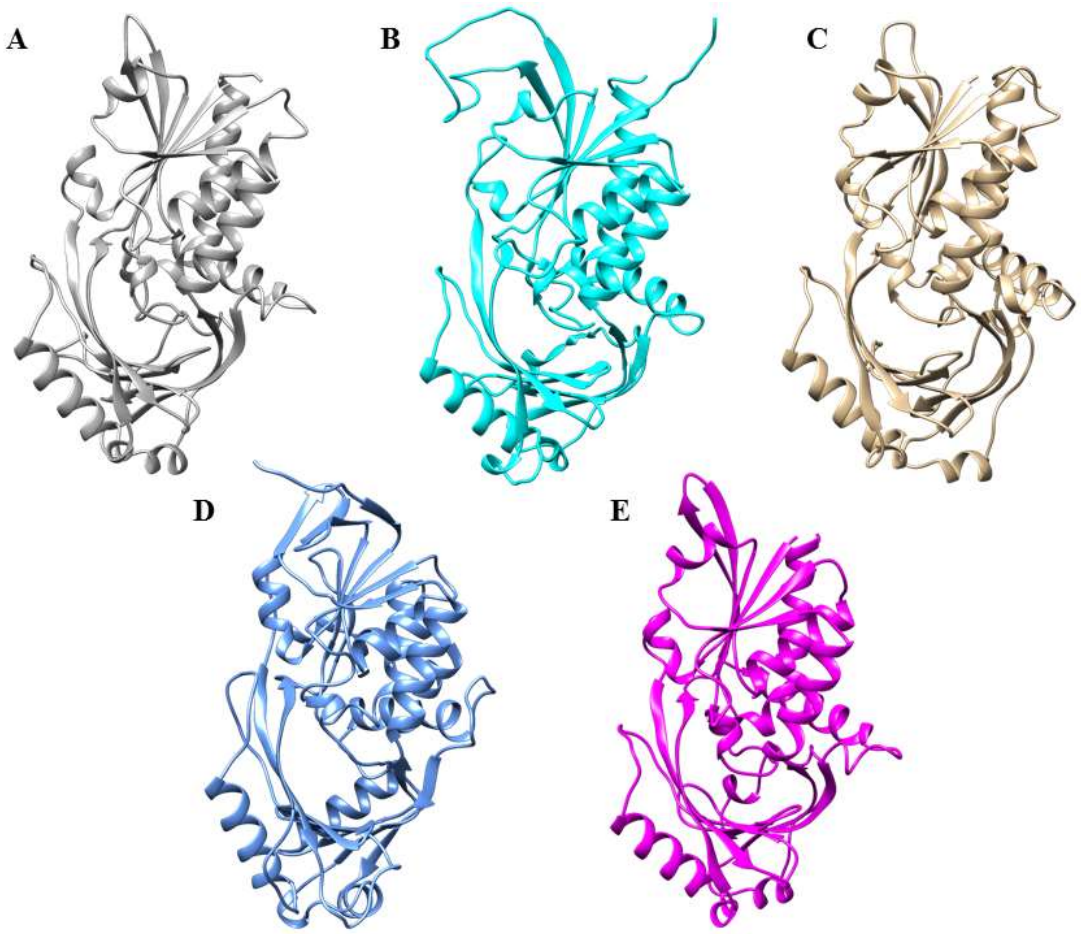

Figure 1.2 Three-dimensional structure of: (A) *p*DAAO (PDB 1KIF); (B) *Rg*DAAO (PDB 1C0I); (C) *h*DAAO (PDB 2DU8); (D) *Pa*DADH (PDB 3NYC); and (E) three-dimensional model of *b*DASPO (model template: 1KIF).
Each panel is shown with the same orientation of the subunit for ease of comparison.

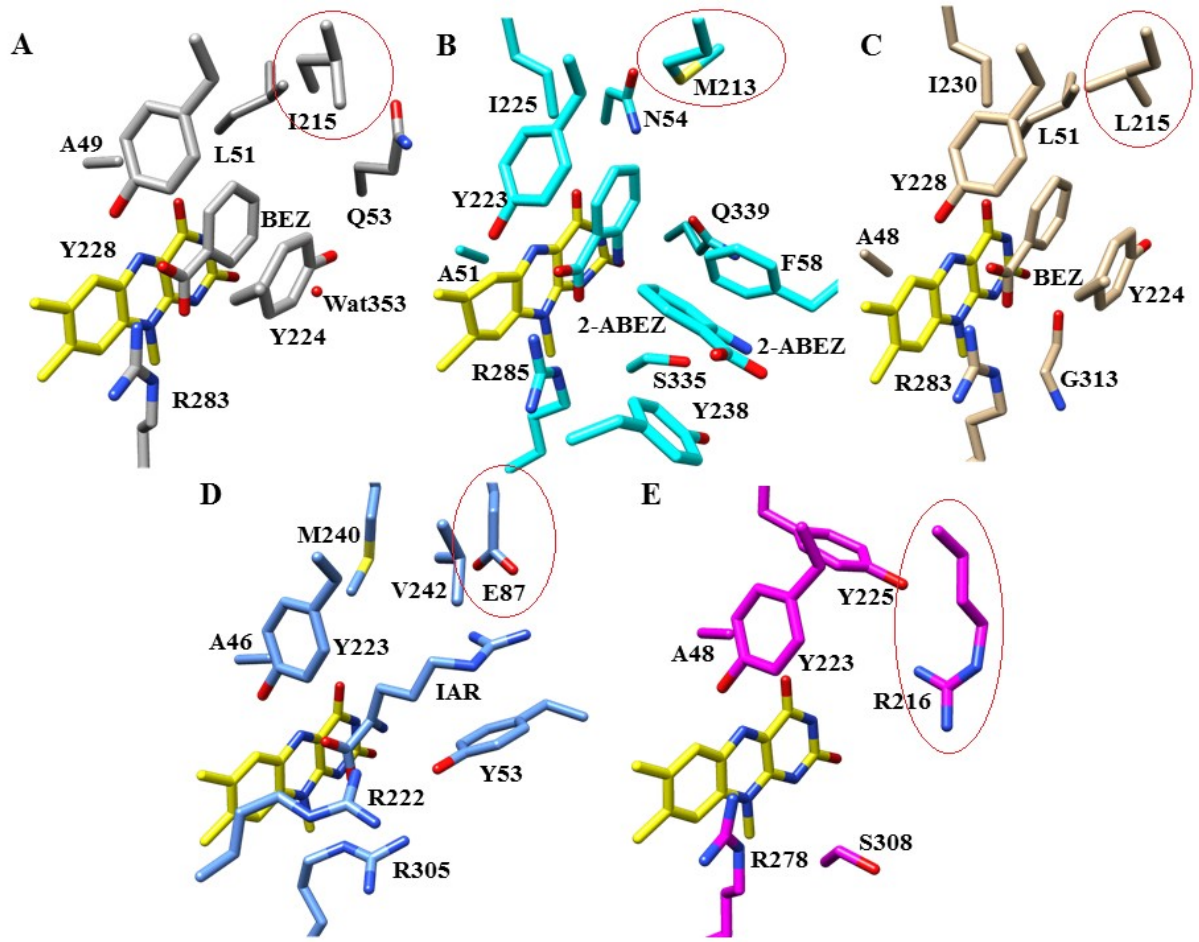

Figure 1.3 Active site of: (A) *p*DAAO in complex with benzoate (BEZ); (B) *Rg*DAAO in complex with 2-amino benzoate (2-ABEZ); (C) *h*DAAO in complex with benzoate (BEZ); (D) *Pa*DADH in complex with iminoarginine (IAR); and (E) model of the active site of *b*DASPO. The FAD carbons are shown in yellow. Some residues and/or water molecules have been omitted for clarity. FAD is shown with the same orientation in each panel for ease of comparison. The residues circled in red indicate the residue that chiefly defines the substrate specificity.

1.1.5 D-amino acid oxidase: an enzyme with preference for neutral substrates

Pioneering studies by the groups of Massey and Yagi established DAAO as the archetype of the flavin-dependent oxidase/dehydrogenase enzymes.[35-48] DAAO is found in various animals and microorganisms. The enzyme catalyzes the oxidative deamination of D-amino acids to imino acids with concomitant flavin reduction. Subsequent reoxidation of the flavin by molecular oxygen produces hydrogen peroxide (**Scheme 1.1A**). Two protons are released during the

reaction; the first proton is released from the amino acid amino group prior to binding to the ES complex and the second proton is released from the amino acid α-hydrogen.[49] Apart from being one of the initial discoveries in the flavin field by Krebs,[50] DAAO has spurred a myriad of studies on several topics, including the versatility of the flavin cofactor, substrate specificity, biotechnological applications, and physiological role of the enzyme. Interest in this enzyme has never dwindled in part because of the controversy surrounding the accepted catalytic mechanism of amino acid oxidation, i.e., hydride transfer versus carbanion, along with the discovery of the enzyme in humans.[2, 4, 51-53] DAAO serves a regulatory role in humans via the degradation of the neurotransmitter D-Ser, a co-agonist of the NMDA receptor, as hypofunction of the NMDA receptor is hypothesized to contribute to schizophrenia.[54] In bacteria and fungi DAAO functions in a catabolic role to convert D-amino acids into carbon and nitrogen sources.[54]

Pig kidney D-amino acid oxidase

The *p*DAAO contains one FAD cofactor for each 40 kDa-subunit (**Figure 1.2A**).[51, 55] The enzyme has been detected in multiple oligomeric states in solution depending on the protein concentration.[4] The different oligomeric states can alter certain aspects of the kinetics, such as product release and inhibitor binding.[36] *p*DAAO is most active with hydrophobic substrates, such as D-Pro, D-Ala, D-Met, and D-Phe (**Table 1.2**). [56] The bulky D-Tyr and D-Trp are slowly oxidized as well.[56] The enzyme does not react with the anionic amino acids D-Asp and D-Glu and displays marginal activity against the cationic amino acids D-Arg and D-Lys.[56] (**Figure 1.3A**).[51] Thiazolidine-2-carboxylic acid is also a substrate for the enzyme with catalytic turnover numbers similar to D-Pro.[57] A hydrophobic cage comprised of L51, I215, Y224, and Y228 that surrounds the substrate side-chain explains why charged substrates display poor reactivity with

*p*DAAO (**Figure 1.3A**).[51] The volume of the active site cavity is 160 Å^3, permitting substrates with side-chains of 4-6 C atoms to bind optimally.[51, 56] However, the structure of the iminotryptophan complex revealed some degree of plasticity of the active site in *p*DAAO, enabling it to expand the volume for bulky amino acids.[52] Stabilization of the substrate α-carboxylate is provided by interactions with Y228 and R283, whereas the α-amino group is within hydrogen bond distance to the hydroxyl group of Y224 and a buried water molecule (Wat352) (**Figure 1.3A**).

Mutagenesis of Y224 to phenylalanine indicated that the hydroxyl group does not play a role in the substrate specificity of *p*DAAO since the k_{cat}/K_m values with D-Ala, D-Pro, D-Met, and D-Phe were largely unchanged as compared to the wild-type enzyme.[29] In contrast, the k_{cat}/K_m value for the Y228F variant was roughly 20-fold lower for D-Ala and D-Phe, 10-fold lower for D-Pro, and 6-fold lower for D-Met than in the wild-type enzyme, suggesting the hydroxyl of Y228 affects the substrate specificity of *p*DAAO.[29] A recent study that investigated Y224A and Y228A variants reported a significant reduction in specific activity against all substrates, demonstrating the importance of the phenyl ring of Y224 and Y228 in *p*DAAO for substrate specificity and catalytic function.[58] Replacement of H307 with leucine provided evidence that this residue is involved in proper orientation of FAD for binding to the enzyme as the dissociation constant for FAD was 28-fold greater in the H307L variant as compared to the wild-type enzyme.[59] Conversion of *p*DAAO into an R-stereoselective amine oxidase was recently accomplished by a double variant of I230A/R283G.[60]

Rhodotorula gracilis D-amino acid oxidase

The *Rg*DAAO is a homodimer of 80 kDa with one molecule of FAD bound per subunit (**Figure 1.2B**). The enzyme is most active with D-Trp, but can also process small neutral amino acids, such as D-Ala, as shown in **Table 1.2**.[61, 62] *Rg*DAAO exhibits 14,800- and 370-fold lower k_{cat}/K_m values with D-Asp and D-Arg as compared to D-Trp, respectively.[63] The amino acid sequence identity between *p*DAAO and *Rg*DAAO is 30% and their overall topology is highly similar (**Figure 1.2A-B**), yet *Rg*DAAO possesses a more open active site architecture than *p*DAAO (**Figure 1.3A-B**). An active site volume of ~230 $Å^3$ is estimated with Caver Analyst 1.0 (J. Ball and G. Gadda; unpublished results), providing a rationale for *Rg*DAAO exhibiting a preference for bulky substrates like D-Phe and D-Trp. (**Figure 1.3B**). The α-carboxylate of the amino acid substrate forms an electrostatic interaction with R285 and a hydrogen bond with the side-chains of Y223 and Y238 (**Figure 1.3B**). The α-amino group of the ligand establishes a hydrogen bond with the side chain of S335 and a water molecule (Wat72), which is fixated in space through hydrogen bond interactions with N54 and Q339.[64] *Rg*DAAO is highly sought after for biotechnological applications due to its overall higher catalytic efficiency than *p*DAAO, high thermal and operational stability[65], and its ability to oxidize Cephalosporin C as part of a two-step process to produce the antibiotic precursor 7-aminocephalosporic acid.[66]

Considerable efforts have been undertaken to produce *Rg*DAAO variants with altered substrate specificities due to its biotechnological potential. M213 is especially important because it resides ~3 Å from the β-carbon of D-F_3-Ala bound to the enzyme and presumably interacts with the side-chain of the substrate.[67] M213 of *Rg*DAAO was mutated to arginine and the resulting M213R variant acquired activity with D-Asp as substrate,[68] with a k_{cat}/K_m value for D-Asp similar to the value reported with *b*DASPO (**Table 1.2**); however, the k_{cat}/K_m of M213R for

D-Ala was 220-fold lower in comparison to the wild-type enzyme.[68] The M213G variant was shown to oxidize unnatural aromatic amino acids such as D-2-naphthylglycine, which is a component of Nafarelin.[17]. Mutations at R285 severely depleted the enzymatic activity of the enzyme, consistent with this residue being essential to the general reactivity with amino acids as it binds the α-amino group of the substrate.[63, 69] Y238 was later mutated to generate the Y238F and Y238S variants, which demonstrated enhanced catalytic efficiency with D-Phe and D-Tyr without compromising D-Ala activity.[17] A directed evolution study that employed an error-prone PCR approach identified three *Rg*DAAO variants, i.e., L118H, T60A/Q144R/K152E, and Q144R/G199D/Y223C/H329R, which were active on all D-amino acids with significantly improved catalytic efficiency with D-Ala, D-Arg, and D-Asp than past mutagenic efforts. Intriguingly, most of the mutations identified by error-prone PCR that increased the catalytic activity of *Rg*DAAO were not in the active site but they were clustered on the surface of the enzyme, but not far away from the substrate entrance.[70] It was concluded that these surface residues synergistically enhance the catalytic turnover and substrate affinity by modulating the protein dynamics and/or stability.[70]

Human D-amino acid oxidase

The *h*DAAO is a homodimer of 80 kDa that binds one FAD per subunit (**Figure 1.2C**).[32, 71] *h*DAAO shares 85% amino acid sequence identity with *p*DAAO. The activation of *h*DAAO by pLG72, which elevates the biodegradation of the D-Ser, a potent activator of the NMDA receptor, has been associated with the pathophysiology of schizophrenia.[72] A distinctive feature of *h*DAAO is that it demonstrates the weakest binding affinity of the FAD cofactor, with a K_d value of 8 μM, among known DAAOs.[32] A hydrophobic stretch ($V^{47}AAGL^{51}$) in *h*DAAO, which

is fully conserved in *p*DAAO, was shown to be in a different conformation than the pig enzyme, and this difference was proposed to be responsible for the weaker binding of FAD in the human enzyme.[31] D-Cys is the best substrate for the enzyme as indicated by a k_{cat}/K_m value of 14,600 $M^{-1}s^{-1}$ (**Table 1.2**), [30] and it was proposed that D-Cys might be the physiological substrate of the enzyme in some tissues.[30] Due to the high levels of D-Ser in the brain it was also proposed that D-Ser might be the physiological substrate for *h*DAAO in the brain, although the enzyme has a low k_{cat}/K_m value of 400 $M^{-1}s^{-1}$, which would suggest otherwise.[73] D-Glu and NMDA are not substrates for *h*DAAO, whereas D-Asp exhibits a low k_{cat}/K_m value of 4 $M^{-1}s^{-1}$.[30] As shown in **Figure 1.3C**, the side-chain of the D-amino acid extends into a fairly hydrophobic pocket, which explains the specificity for neutral substrates.[74, 75] The active site volume is ~220 $Å^3$, making it larger than *p*DAAO and explaining the higher kinetic efficiency with D-Tyr than *p*DAAO.[75] The α-carboxylate group of the ligand interacts with the guanidino group of R283 and the hydroxyl group of Y228, while the α-amino group participates in hydrogen bond interactions to the flavin O4 atom and the main-chain amide oxygen atom of G313 (**Figure 1.3C**).[74-76]

Most of the mutations of *h*DAAO have focused on variants related to disease states. The R199W variant has been associated with familial amyotrophic lateral sclerosis, and biochemical investigations have shown that this mutation promotes protein instability and decreases kinetic efficiency with D-Ser.[77] A W209R variant of the enzyme, which is also deposited in the single nucleotide polymorphisms database, exhibited greater D-Ser activity and higher affinity for FAD.[77] It was proposed that the increased production of hydrogen peroxide by the W209R variant as a result of increased D-Ser oxidation might be the feature affecting cell viability.[77] Two variants associated with an increased risk of schizophrenia, D31H and R279A, showed an increased kinetic efficiency for D-Ser and tighter binding of the FAD cofactor.[78] A recent study

reported that a Y55A variant, which is located on a loop on the border between the active site and the hydrophobic substrate binding pocket, increased the specific activity of *h*DAAO and *p*DAAO towards D-His, D-Met, D-Phe, D-Tyr, and D-Trp by facilitating solvent and substrate access.[58]

1.1.6 D-arginine dehydrogenase: an enzyme with preference for cationic substrates

*Pa*DADH is a 42 kDa monomer that binds one FAD molecule (**Figure 1.2D**).[33] *Pa*DADH catalyzes the same chemical reaction as DAAO, except it employs an electron acceptor other than molecular oxygen to reoxidize the flavin (**Scheme 1.1B**). Phenazine methosulfate is used *in vitro* as the physiological electron acceptor remains unknown.[79] The enzyme functions as the first step in a novel two-enzyme coupled system in *P. aeruginosa* that racemizes D-Arg to L-Arg.[26] The second enzyme is an NAD(P)H-dependent L-arginine dehydrogenase that combines ammonia and the α-keto acid to produce L-Arg. The three-dimensional structures of *Pa*DADH in both a ligand-free and product-bound conformation, and that of the enzyme with an N5-iminoleucine adduct, are available.[33, 80]

*Pa*DADH has a broad substrate specificity with the ability to oxidize all of the 19 common D-amino acids except D-Asp and D-Glu.[33] The cationic amino acids, D-Arg and D-Lys, are the best substrates for the enzyme as judged by the high k_{cat}/K_m values shown in **Table 1.2** (10^5-10^6 $M^{-1}s^{-1}$).[33] The position of iminoarginine bound to *Pa*DADH suggests that the side-chain of the D-Arg substrate forms an electrostatic interaction with E87. The presence of E87 rationalizes the lack of reactivity with D-Asp and D-Glu. Similar to *p*DAAO, a hydrophobic cage formed by the side-chains of Y53, M240, V242 and Y249 (**Figure 1.3D**) engages in favorable van der Waals and π-π interactions with aliphatic and aromatic side-chains of the substrate, consequently D-Met

and D-Tyr are oxidized in the 10^4 $M^{-1}s^{-1}$ range. The active site volume of *Pa*DADH, which is calculated to be ~320 Å with Caver Analyst 1.0 (unpublished results; J. Ball and G. Gadda), is large enough to provide the necessary space to accommodate bulky substrates, such as D-Arg, D-Tyr and D-Trp. Contrary to the single arginine used to bind the α-carboxylate of the substrate in DAAOs, *Pa*DADH employs two arginine residues, R222 and R305, to bind the substrate α-carboxylate (**Figure 1.3D**).

Mutagenic work on *Pa*DADH established the importance of E87 to be unprotonated for optimal binding of cationic substrates.[81] Although the E87L variant did not lose the ability to oxidize D-Arg, the k_{cat}/K_m value was down 20-fold compared to the wild-type enzyme.[81] An H48F variant decreased the k_{cat}/K_m value with D-Arg only by 2-fold, indicating this residue does not significantly affect substrate specificity.[81] Overall, the mutagenic work suggests there is no catalytic base operative in the mechanism, and the catalytic p*K*a seen, irrespective of the substrate or variant, belongs to the substrate α-amino group.[81, 82] A base not being required for the chemical step of catalysis was also proposed for DAAO.[63, 67] A recent and extensive review on *Pa*DADH can be found here.[83]

1.1.7 D-aspartate oxidase: an enzyme with preference for anionic substrates

DASPO is a specialized enzyme of 39 kDa that oxidizes the anionic amino acids D-Asp and D-Glu.[84, 85] The enzyme catalyzes the oxidative deamination of D-Asp to generate 2-ketoglutarate, ammonia, and hydrogen peroxide. In the brain, D-Asp functions as a neurotransmitter.[86] DASPO has been biochemically and kinetically characterized from various mammalian sources, including human brain, beef kidney, pig kidney, mouse, and octopus.[85, 87-90] DASPO has also been characterized from the yeast *Cryptococcus humicola*.[91] Purified *b*DASPO

forms a homotetramer while purified pig kidney DASPO is monomeric.[85, 88] The enzyme from all sources has a higher catalytic efficiency with D-Asp as compared to D-Glu. The major difference between human brain, beef kidney, pig kidney, and mouse DASPO to octopus DASPO is that the latter exhibits a lower activity against NMDA than the former enzymes.[88, 90] Increasing evidence has linked DASPO to schizophrenia in mammals, where enhanced activity of DASPO in the *post-mortem* dorsolateral prefrontal cortex of patients with schizophrenia contributes to dysfunctional NMDA transmission.[92-94] DASPO is proposed to play a role in the assimilation and detoxification of D-Asp in yeast.[95]

The three-dimensional structure of DASPO has yet to be solved, but a structural model of *b*DASPO using SWISS-MODEL with the *p*DAAO (PDB: 1KIF; 43% sequence identity) as template is shown in **Figure 1.2E and Figure 1.3E**. The position of R216 in the model suggests it might form an electrostatic interaction with the side-chain of D-Asp (**Figure 1.3E**). It appears the α-amino group may interact with S308 or Y223 (**Figure 1.3E**). Biochemical studies on R237 from mouse DASPO, which corresponds to R278 of *b*DASPO, suggests it serves to bind the α-carboxylate group of D-Asp, and does not significantly affect the strict specificity for anionic amino acids.[96] Lower levels of turnover and higher K_m values were detected with D-Glu, indicating an active site framework that is finely tuned for the one-carbon shorter D-Asp.[34]

Mutations on DASPO have focused on R216 and S308, which are conserved between *b*DASPO and mouse DASPO. An R216L variant of mouse DASPO acquired the ability to oxidize D-Phe and D-His, but at the cost of appreciably lower activity against D-Asp and NMDA than the wild-type enzyme.[96] Replacement of S308 with glycine doubled the specific activity (U/mg) of mouse DASPO against D-Asp and nearly tripled the specific activity against NMDA.[97] H56 of yeast DASPO has been shown to be important for the substrate specificity of

the enzyme as the H56A and H56N variants of the enzyme lost the ability to oxidize D-Asp, but gained the ability to oxidize neutral substrates, such as D-Met, D-Phe, and D-Gln.[98]

1.1.8 Active site lid

*p*DAAO (^{I}215-225^{N}), *h*DAAO (^{T}216-228^{Y}), and *Pa*DADH (^{R}33-56^{P}) contain a flexible loop region which acts as an "active site lid" (**Figure 1.4**).[33, 51, 55, 99] The iminotryptophan complex of *p*DAAO demonstrated the flexibly of active site loop in *p*DAAO (**Figure 1.4A**). It has been proposed by Mattevi and coworkers that when in the closed conformation this loop primes *p*DAAO for the hydride transfer by desolvation of the active site.[52] The active site lid is also thought to regulate substrate entry and exit.[51] Specific inhibitors of *h*DAAO have been shown to stabilize the open conformation of the lid (**Figure 1.4B**).[99] A similar active site lid is absent in *Rg*DAAO, which may contribute to differences in substrate specificity and the reason FAD reduction is rate-limiting for *Rg*DAAO instead of product release, contrary to *p*DAAO and *h*DAAO.[64] Nonetheless, *Rg*DAAO does have a residue Y238 that corresponds to Y224 of *p*DAAO and is proposed to exert a similar role in capping the active site.[100] Structural models of a newly characterized DAAO from *Rubrobacter xylanophilus* (*Rx*DAAO), which shows a strict specificity for D-Val, indicate there is a L215 in the corresponding spatial position of Y224 in *p*DAAO, and it was proposed this residue might contribute to the unique substrate specificity of *Rx*DAAO.[101] The flexible loop region comprised in *Pa*DADH has been observed in both an open and closed conformations, representing the ligand-free enzyme and product-bound conformations, respectively.[33] Y53 of *Pa*DADH, which corresponds to Y224 of *p*DAAO, in the ligand-free enzyme points away from the active site, but in the product-bound conformation it swings inward to shield the active site from bulk solvent (**Figure 1.4C**).[33]

Deletion of the active site lid loop in both *p*DAAO and *h*DAAO results in variants deficient in activity or inactive towards most substrates.[58] Mutagenesis of the I215-N225 loop region of *p*DAAO to the corresponding region of human brain DASPO (R216-G220) granted *p*DAAO the ability to oxidize D-Asp.[102] Molecular dynamics studies on *Pa*DADH indicated the loop is highly flexible and the loop variants S45A and A46G, which are two residues that reside on the "hinge" region of the loop (**Figure 1.4C**), suggested these mutations modulate the dynamics of the gate to a more open conformation and this negatively affects the ability of *Pa*DADH to capture and oxidize D-amino acid substrates.[103] The functional character of this loop and its flexibility are major determinants for the substrate specificity of flavoenzymes oxidizing the C_{α}-N bond of D-amino acids.

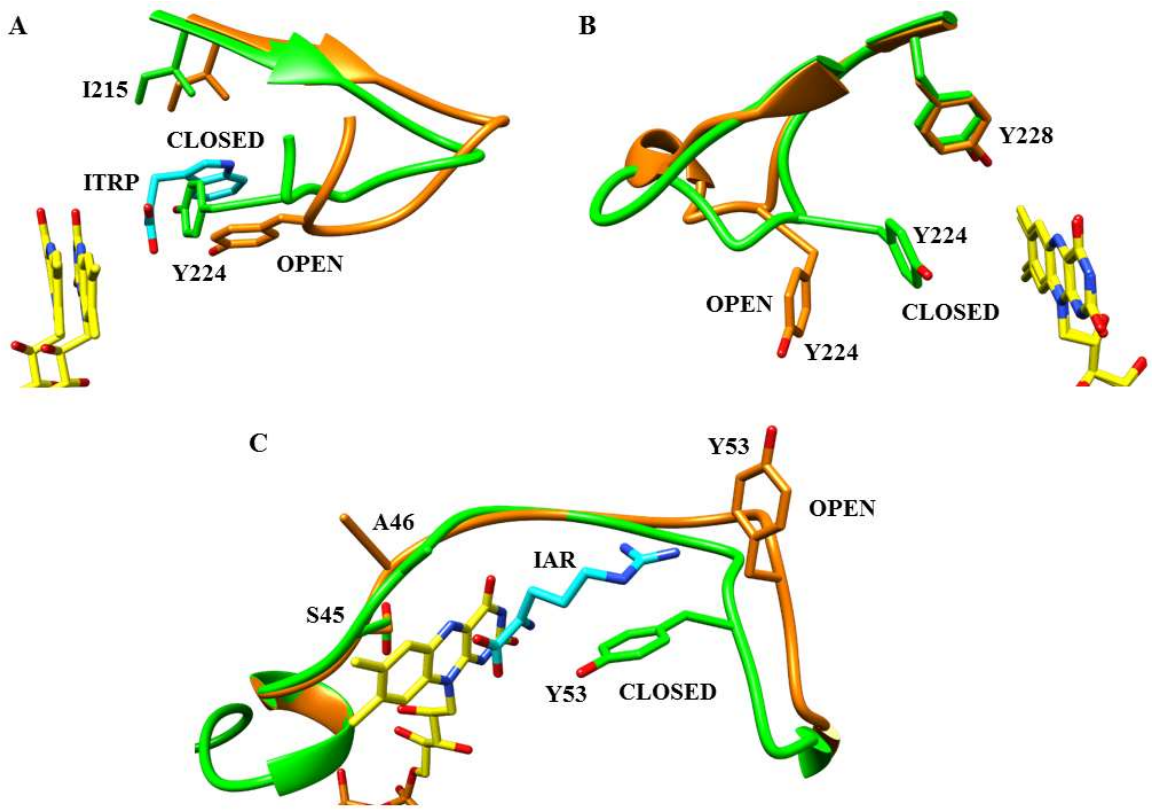

Figure 1.4 Active site loops of: (A) *p*DAAO (PDBs 1KIF and 1DDO) (B) *h*DAAO (PDBs 2DU8 and 4QFD) and (C) *Pa*DADH (PDB 3NYE).
ITRP – iminotryptophan; IAR – iminoarginine. Each open conformation is shown in orange. Each closed conformation is shown in green. FAD carbons shown in yellow. ITRP and IAR carbons are shown in cyan. Benzoate was removed from panel A and 3-(7-hydroxy-2-oxo-4-phenyl-2H-chromen-6-yl)propanoic acid and benzoate were removed from panel B for clarity.

1.1.9 General principles about structure and specificity

The active site in the flavoenzymes that oxidize D-amino acids is generally located at the interface of the flavin- and substrate-binding domains with conservation of key active site residues that enable the amino acid main-chain to bind and the hydride transfer possible (**Figure 1.3**). The topology of the flavin-binding domain is similar while subtle modifications in the substrate side-chain pocket render differential specificity for D-amino acid substrates. The α-

carbon of the amino acid substrate must be within striking distance (<5 Å) of the N5 of the flavin in order to transfer a hydride equivalent. The ideal hydride transfer distance is achieved by tethering both the N and C terminus of the amino acid to the protein through a combination of electrostatic interactions and hydrogen bonds. Salt-bridge stabilization of the carboxylate group is made possible by an arginine residue(s). A tyrosine, serine, or water molecule is typically positioned to form hydrogen bond interactions with the α-amino group of the substrate. The cationic substrates are captured by E87 in *Pa*DADH; the anionic substrates are captured by R216 in *b*DASPO; *p*DAAO, *h*DAAO, and *Rg*DAAO capture neutral substrates with I215, L215, and M213, respectively. M213 of *Rg*DAAO could possibly be engaging in favorable sulfur-π interactions with the aromatic rings of D-Trp and D-Phe. An alanine is behind the N5 atom of the FAD in all the enzymes and may modulate the flavin redox potential. Another major factor is the active site cavity volume, which physically limits the size of substrates that can fit into the active site. A flexible loop that functions as an active site lid is present in most of the enzymes and plays a role to allow these enzymes to adjust the active site for a diverse range of amino acids. Lastly, the absence of a strong base in the proximity of the substrate α-C prevents reactions with α-hydroxy acids, which typically have much higher pK_a values than the α-amino group on amino acids.[2]

1.1.10 Closing thoughts and future directions

A single enzyme is not sufficient to oxidize at equal rates all the various D-amino acids, which differ in charge, size, and shape. Nature has designed different architectures for substrate-binding sites. The opposite charge of anionic and cationic D-amino acids requires distinctive binding pockets for the side-chain. The varying size and shape of D-amino acids necessitates

characteristic active site volumes. Movements of flexible loops contribute to the active site plasticity, which broadens the substrate scope of the enzymes. Many of the factors governing the substrate specificity of enzymes that oxidize D-amino acids have been elucidated, yet most of the focus has been on active site residues and utilized a rational design approach. Mutagenesis of distal surface residues offers intriguing possibilities in altering the substrate specificity and would open new paradigms in the relationship between enzyme structure and substrate specificity. Future directions could focus on how the dynamic behavior and molecular motions of enzymes that oxidize D-amino acid influence the kinetics in order to develop a more complete understanding of their structure-function relationships. This information will help elaborate how a relatively rigid protein structure is fine-tuned by its internal motions to optimize catalysis for neutral, charged, as well as hydrophobic D-amino acid substrates. Another important aspect centers on engineering oxidases from dehydrogenases, i.e., DADH, to aid the industrial utilization of the enzymes that oxidize D-amino acids. A question that deserves attention is the physiological fate of the other product of reaction formed in the oxidation of D-amino acids, i.e., hydrogen peroxide or other reduced electron acceptors. Do these molecules play an active role in regulatory processes and neurotransmission, cell-signaling, and metabolism? The recent decades have witnessed incredible advances in our understanding of the structure-function of the enzymes that oxidize D-amino acids. The future offers intriguing questions whose answers will take synthetic biology a step closer to the *de novo* design of targeted catalytic activities for the oxidation of specific D-amino acids for industrial and biotechnological use.

1.1.11 References

[1] Genchi, G. (2017) An overview on D-amino acids, Amino Acids 49, 1521-1533.

[2] Fitzpatrick, P. F. (2010) Oxidation of amines by flavoproteins, Arch Biochem Biophys 493, 13-25.

[3] Corrigan, J. J. (1969) D-amino acids in animals, Science (New York, N.Y.) 164, 142-149.

[4] Pilone, M. S. (2000) D-Amino acid oxidase: new findings, Cell Mol Life Sci 57, 1732-1747.

[5] Cava, F., Lam, H., de Pedro, M. A., and Waldor, M. K. (2011) Emerging knowledge of regulatory roles of D-amino acids in bacteria, Cell Mol Life Sci 68, 817-831.

[6] Ohide, H., Miyoshi, Y., Maruyama, R., Hamase, K., and Konno, R. (2011) D-Amino acid metabolism in mammals: biosynthesis, degradation and analytical aspects of the metabolic study, J Chromatogr B Analyt Technol Biomed Life Sci 879, 3162-3168.

[7] Martineau, M., Baux, G., and Mothet, J. P. (2006) D-serine signalling in the brain: friend and foe, Trends Neurosci 29, 481-491.

[8] Roher, A. E., Lowenson, J. D., Clarke, S., Wolkow, C., Wang, R., Cotter, R. J., Reardon, I. M., Zurcher-Neely, H. A., Heinrikson, R. L., Ball, M. J., and et al. (1993) Structural alterations in the peptide backbone of beta-amyloid core protein may account for its deposition and stability in Alzheimer's disease, J Biol Chem 268, 3072-3083.

[9] Fujii, N., Takata, T., Fujii, N., and Aki, K. (2016) Isomerization of aspartyl residues in crystallins and its influence upon cataract, Biochim Biophys Acta 1860, 183-191.

[10] Fujii, N., Tajima, S., Tanaka, N., Fujimoto, N., Takata, T., and Shimo-Oka, T. (2002) The presence of D-beta-aspartic acid-containing peptides in elastic fibers of sun-damaged

skin: a potent marker for ultraviolet-induced skin aging, Biochem Biophys Res Commun 294, 1047-1051.

[11] Feng, Z., and Xu, B. (2016) Inspiration from the mirror: D-amino acid containing peptides in biomedical approaches, Biomol Concepts 7, 179-187.

[12] Gao, X., Ma, Q., and Zhu, H. (2015) Distribution, industrial applications, and enzymatic synthesis of D-amino acids, Appl Microbiol Biotechnol 99, 3341-3349.

[13] Martinez-Rodriguez, S., Martinez-Gomez, A. I., Rodriguez-Vico, F., Clemente-Jimenez, J. M., and Las Heras-Vazquez, F. J. (2010) Natural occurrence and industrial applications of D-amino acids: an overview, Chem Biodivers 7, 1531-1548.

[14] Sacchi, S., Rosini, E., Pollegioni, L., and Molla, G. (2013) D-amino acid oxidase inhibitors as a novel class of drugs for schizophrenia therapy, Curr Pharm Des 19, 2499-2511.

[15] Friedman, M. (2010) Origin, microbiology, nutrition, and pharmacology of D-amino acids, Chem Biodivers 7, 1491-1530.

[16] Friedman, M. (1999) Chemistry, nutrition, and microbiology of D-amino acids, J Agric Food Chem 47, 3457-3479.

[17] Frattini, L., Rosini, E., Pollegioni, L., and Pilone, M. S. (2011) Analyzing the D-amino acid content in biological samples by engineered enzymes, J Chromatogr B Analyt Technol Biomed Life Sci 879, 3235-3239.

[18] Ghisla, S., and Edmondson, D. E. (2001) Flavin Coenzymes, In eLS, John Wiley & Sons, Ltd.

[19] Massey, V. (2000) The chemical and biological versatility of riboflavin, Biochem Soc Trans 28, 283-296.

[20] Hodge-Hanson, K. M., and Downs, D. M. (2017) Members of the Rid protein family have broad imine deaminase activity and can accelerate the Pseudomonas aeruginosa D-arginine dehydrogenase (DauA) reaction in vitro, PLoS One 12, e0185544.

[21] Degani, G., Barbiroli, A., Regazzoni, L., Popolo, L., and Vanoni, M. A. (2018) Imine Deaminase Activity and Conformational Stability of UK114, the Mammalian Member of the Rid Protein Family Active in Amino Acid Metabolism, Int J Mol Sci 19.

[22] Wolosker, H., D'Aniello, A., and Snyder, S. H. (2000) D-aspartate disposition in neuronal and endocrine tissues: ontogeny, biosynthesis and release, Neuroscience 100, 183-189.

[23] Zaar, K., Kost, H. P., Schad, A., Volkl, A., Baumgart, E., and Fahimi, H. D. (2002) Cellular and subcellular distribution of D-aspartate oxidase in human and rat brain, J Comp Neurol 450, 272-282.

[24] Billard, J. M. (2012) D-Amino acids in brain neurotransmission and synaptic plasticity, Amino Acids 43, 1851-1860.

[25] Sasabe, J., Miyoshi, Y., Suzuki, M., Mita, M., Konno, R., Matsuoka, M., Hamase, K., and Aiso, S. (2012) d-Amino acid oxidase controls motoneuron degeneration through d-serine, Proc Natl Acad Sci U S A 109, 627-632.

[26] Li, C., and Lu, C.-D. (2009) Arginine racemization by coupled catabolic and anabolic dehydrogenases, Proc Natl Acad Sci U S A 106, 906-911.

[27] Brodelius, P., Nilsson, K., and Mosbach, K. (1981) Production of alpha-keto acids Part I. Immobilized cells ofTrigonopsis variabilis containing D-amino acid oxidase, Appl Biochem Biotechnol 6, 293-307.

[28] Rossmann, M. G., Moras, D., and Olsen, K. W. (1974) Chemical and biological evolution of nucleotide-binding protein, Nature 250, 194-199.

[29] Pollegioni, L., Fukui, K., and Massey, V. (1994) Studies on the Kinetic Mechanism of Pig-Kidney D-Amino-Acid Oxidase by Site-Directed Mutagenesis of Tyrosine-224 and Tyrosine-228, J Biol Chem 269, 31666-31673.

[30] Murtas, G., Sacchi, S., Valentino, M., and Pollegioni, L. (2017) Biochemical Properties of Human D-Amino Acid Oxidase, Front Mol Biosci 4, 88.

[31] Kawazoe, T., Tsuge, H., Imagawa, T., Aki, K., Kuramitsu, S., and Fukui, K. (2007) Structural basis of D-DOPA oxidation by D-amino acid oxidase: Alternative pathway for dopamine biosynthesis, Biochem Biophys Res Commun 355, 385-391.

[32] Molla, G., Sacchi, S., Bernasconi, M., Pilone, M. S., Fukui, K., and Polegioni, L. (2006) Characterization of human D-amino acid oxidase, FEBS lett 580, 2358-2364.

[33] Fu, G., Yuan, H., Li, C., Lu, C. D., Gadda, G., and Weber, I. T. (2010) Conformational changes and substrate recognition in Pseudomonas aeruginosa D-arginine dehydrogenase, Biochemistry 49, 8535-8545.

[34] Negri, A., Tedeschi, G., Ceciliani, F., and Ronchi, S. (1999) Purification of beef kidney D-aspartate oxidase overexpressed in Escherichia coli and characterization of its redox potentials and oxidative activity towards agonists and antagonists of excitatory amino acid receptors, Biochim Biophys Acta 1431, 212-222.

[35] Fitzpatrick, P. F., Ghisla, S., and Massey, V. (1985) 8-Azidoflavins as photoaffinity labels for flavoproteins, J Biol Chem 260, 8483-8491.

[36] Fitzpatrick, P. F., and Massey, V. (1982) The kinetic mechanism of D-amino acid oxidase with D-alpha-aminobutyrate as substrate. Effect of enzyme concentration on the kinetics, J Biol Chem 257, 12916-12923.

[37] Ghisla, S., Entsch, B., Massey, V., and Husein, M. (1977) On the structure of flavin-oxygen intermediates involved in enzymatic reactions, Eur J Biochem 76, 139-148.

[38] Ghisla, S., and Massey, V. (1989) Mechanisms of flavoprotein-catalyzed reactions, Eur J Biochem 181, 1-17.

[39] Ghisla, S., and Massey, V. (1986) New flavins for old: artificial flavins as active site probes of flavoproteins, Biochem J 239, 1-12.

[40] Massey, V., Palmer, G., and Bennett, R. (1961) The purification and some properties of D-amino acid oxidase, Biochim Biophys Acta 48, 1-9.

[41] Ronchi, S., Minchiotti, L., Galliano, M., Curti, B., Swenson, R. P., Williams, C. H., Jr., and Massey, V. (1982) The primary structure of D-amino acid oxidase from pig kidney. II. Isolation and sequence of overlap peptides and the complete sequence, J Biol Chem 257, 8824-8834.

[42] Swenson, R. P., Williams, C. H., Jr., Massey, V., Ronchi, S., Minchiotti, L., Galliano, M., and Curti, B. (1982) The primary structure of D-amino acid oxidase from pig kidney. I. Isolation and sequence of the tryptic peptides, J Biol Chem 257, 8817-8823.

[43] Kotaki, A., Harada, M., and Yagi, K. (1967) Structure and function of D-amino acid oxidase. II. Terminal structure and amino acid composition of hog kidney D-amino acid oxidase, J Biochem 61, 598-605.

[44] Yagi, K., Nishikimi, M., Takai, A., and Oishi, N. (1974) Additional evidence for the liberation of substrate alpha-hydrogen prior to reduction of the coenzyme in D-amino acid oxidase reaction, J Biochem 76, 451-454.

[45] Yagi, K., Okamura, K., Naoi, M., and Kotaki, A. (1966) A characterization of a purple intermediate of D-amino acid oxidase, J Biochem 59, 527-530.

[46] Yagi, K., and Ozawa, T. (1989) Crystallization of Michaelis complex of D-amino acid oxidase. 1962, Biochim Biophys Acta 1000, 207-208.

[47] Yagi, K., and Ozawa, T. (1962) Crystallization of Michaelis complex of D-amino acid oxidase, Biochim Biophys Acta 60, 200-201.

[48] Yagi, K., Ozawa, T., and Okada, K. (1959) Mechanism of inhibition of D-amino acid oxidase. II. Inhibitory actions of benzene derivatives, Biochim Biophys Acta 35, 102-110.

[49] Fitzpatrick, P. F., and Massey, V. (1982) Proton release during the reductive half-reaction of D-amino acid oxidase, J Biol Chem 257, 9958-9962.

[50] Krebs, H. A. (1935) Metabolism of amino-acids: Deamination of amino-acids, Biochem J 29, 1620-1644.

[51] Mattevi, A., Vanoni, M. A., Todone, F., Rizzi, M., Teplyakov, A., Coda, A., Bolognesi, M., and Curti, B. (1996) Crystal structure of D-amino acid oxidase: a case of active site mirror-image convergent evolution with flavocytochrome b2, Proc Natl Acad Sci U S A 93, 7496-7501.

[52] Todone, F., Vanoni, M. A., Mozzarelli, A., Bolognesi, M., Coda, A., Curti, B., and Mattevi, A. (1997) Active site plasticity in D-amino acid oxidase: a crystallographic analysis, Biochemistry 36, 5853-5860.

[53] Fitzpatrick, P. F. (2001) Substrate dehydrogenation by flavoproteins, Acc Chem Res 34, 299-307.

[54] Pollegioni, L., Piubelli, L., Sacchi, S., Pilone, M. S., and Molla, G. (2007) Physiological functions of D-amino acid oxidases: from yeast to humans, Cell Mol Life Sci 64, 1373-1394.

[55] Mizutani, H., Miyahara, I., Hirotsu, K., Nishina, Y., Shiga, K., Setoyama, C., and Miura, R. (1996) Three-dimensional structure of porcine kidney D-amino acid oxidase at 3.0 A resolution, J Biochem 120, 14-17.

[56] Dixon, M., and Kleppe, K. (1964) II. Specificity, competitive inhibition and reaction sequence, Biochim Biophys Acta 96, 368-382.

[57] Fitzpatrick, P. F., and Massey, V. (1982) Thiazolidine-2-carboxylic acid, an adduct of cysteamine and glyoxylate, as a substrate for D-amino acid oxidase, J Biol Chem 257, 1166-1171.

[58] Subramanian, K., Gora, A., Spruijt, R., Mitusinska, K., Suarez-Diez, M., Martins Dos Santos, V., and Schaap, P. J. (2018) Modulating D-amino acid oxidase (DAAO) substrate specificity through facilitated solvent access, PLoS One 13, e0198990.

[59] Miyano, M., Fukui, K., Watanabe, F., Takahashi, S., Tada, M., Kanashiro, M., and Miyake, Y. (1991) Studies on Phe-228 and Leu-307 recombinant mutants of porcine kidney D-amino acid oxidase: expression, purification, and characterization, J Biochem 109, 171-177.

[60] Yasukawa, K., Nakano, S., and Asano, Y. (2014) Tailoring D-amino acid oxidase from the pig kidney to R-stereoselective amine oxidase and its use in the deracemization of alpha-methylbenzylamine, Angew Chem Int Ed Engl 53, 4428-4431.

[61] Pollegioni, L., Harris, C. M., Molla, G., Pilone, M. S., and Ghisla, S. (2001) Identification and role of ionizing functional groups at the active center of Rhodotorula gracilis D-amino acids oxidase, FEBS Lett 507, 323-326.

[62] Pollegioni, L., Falbo, A., and Pilone, M. S. (1992) Specificity and kinetics of Rhodotorula gracilis D-amino acid oxidase, Biochim Biophys Acta 1120, 11-16.

[63] Boselli, A., Piubelli, L., Molla, G., Pilone, M. S., Pollegioni, L., and Sacchi, S. (2007) Investigating the role of active site residues of Rhodotorula gracilis D-amino acid oxidase on its substrate specificity, Biochimie 89, 360-368.

[64] Pollegioni, L., Diederichs, K., Molla, G., Umhau, S., Welte, W., Ghisla, S., and Pilone, M. S. (2002) Yeast D-amino acid oxidase: structural basis of its catalytic properties, J Mol Biol 324, 535-546.

[65] Pollegioni, L., Iametti, S., Fessas, D., Caldinelli, L., Piubelli, L., Barbiroli, A., Pilone, M. S., and Bonomi, F. (2003) Contribution of the dimeric state to the thermal stability of the flavoprotein D-amino acid oxidase, Prot Sci 12, 1018-1029.

[66] Pollegioni, L., Caldinelli, L., Molla, G., Sacchi, S., and Pilone, M. S. (2004) Catalytic properties of D-amino acid oxidase in cephalosporin C bioconversion: a comparison between proteins from different sources, Biotechnol Prog 20, 467-473.

[67] Umhau, S., Pollegioni, L., Molla, G., Diederichs, K., Welte, W., Pilone, M. S., and Ghisla, S. (2000) The x-ray structure of D-amino acid oxidase at very high resolution identifies the chemical mechanism of flavin-dependent substrate dehydrogenation, Proc Natl Acad Sci U S A 97, 12463-12468.

[68] Sacchi, S., Lorenzi, S., Molla, G., Pilone, M. S., Rossetti, C., and Pollegioni, L. (2002) Engineering the substrate specificity of D-amino-acid oxidase, J Biol Chem 277, 27510-27516.

[69] Gadda, G., Negri, A., and Pilone, M. S. (1994) Reaction of Phenylglyoxal with Arginine Groups in D-Amino-Acid Oxidase from Rhodotorula-Gracilis, J Biol Chem 269, 17809-17814.

[70] Sacchi, S., Rosini, E., Molla, G., Pilone, M. S., and Pollegioni, L. (2004) Modulating D-amino acid oxidase substrate specificity: production of an enzyme for analytical determination of all D-amino acids by directed evolution, Protein Eng Des Sel 17, 517-525.

[71] Kawazoe, T., Tsuge, H., Pilone, M. S., and Fukui, K. (2006) Crystal structure of human D-amino acid oxidase: context-dependent variability of the backbone conformation of the VAAGL hydrophobic stretch located at the si-face of the flavin ring, Prot Sci 15, 2708-2717.

[72] Sacchi, S., Bernasconi, M., Martineau, M., Mothet, J. P., Ruzzene, M., Pilone, M. S., Pollegioni, L., and Molla, G. (2008) pLG72 modulates intracellular D-serine levels through its interaction with D-amino acid oxidase: effect on schizophrenia susceptibility, J Biol Chem 283, 22244-22256.

[73] Park, H. K., Shishido, Y., Ichise-Shishido, S., Kawazoe, T., Ono, K., Iwana, S., Tomita, Y., Yorita, K., Sakai, T., and Fukui, K. (2006) Potential role for astroglial D-amino acid oxidase in extracellular D-serine metabolism and cytotoxicity, J Biochem 139, 295-304.

[74] Duplantier, A. J., Becker, S. L., Bohanon, M. J., Borzilleri, K. A., Chrunyk, B. A., Downs, J. T., Hu, L. Y., El-Kattan, A., James, L. C., Liu, S., Lu, J., Maklad, N., Mansour, M. N., Mente, S., Piotrowski, M. A., Sakya, S. M., Sheehan, S., Steyn, S. J., Strick, C. A., Williams, V. A., and Zhang, L. (2009) Discovery, SAR, and pharmacokinetics of a novel 3-hydroxyquinolin-2(1H)-one series of potent D-amino acid oxidase (DAAO) inhibitors, J Med Chem 52, 3576-3585.

[75] Sacchi, S., Caldinelli, L., Cappelletti, P., Pollegioni, L., and Molla, G. (2012) Structure-function relationships in human D-amino acid oxidase, Amino Acids 43, 1833-1850.

[76] Sparey, T., Abeywickrema, P., Almond, S., Brandon, N., Byrne, N., Campbell, A., Hutson, P. H., Jacobson, M., Jones, B., Munshi, S., Pascarella, D., Pike, A., Prasad, G. S., Sachs, N., Sakatis, M., Sardana, V., Venkatraman, S., and Young, M. B. (2008) The discovery of fused pyrrole carboxylic acids as novel, potent D-amino acid oxidase (DAO) inhibitors, Bioorg Med Chem Lett 18, 3386-3391.

[77] Cappelletti, P., Piubelli, L., Murtas, G., Caldinelli, L., Valentino, M., Molla, G., Pollegioni, L., and Sacchi, S. (2015) Structure-function relationships in human d-amino acid oxidase variants corresponding to known SNPs, Biochim Biophys Acta 1854, 1150-1159.

[78] Caldinelli, L., Sacchi, S., Molla, G., Nardini, M., and Pollegioni, L. (2013) Characterization of human DAAO variants potentially related to an increased risk of schizophrenia, Biochim Biophys Acta 1832, 400-410.

[79] Yuan, H., Fu, G., Brooks, P. T., Weber, I., and Gadda, G. (2010) Steady-state kinetic mechanism and reductive half-reaction of D-arginine dehydrogenase from Pseudomonas aeruginosa, Biochemistry 49, 9542-9550.

[80] Fu, G., Yuan, H., Wang, S., Gadda, G., and Weber, I. T. (2011) Atomic-resolution structure of an N5 flavin adduct in D-arginine dehydrogenase, Biochemistry 50, 6292-6294.

[81] Ball, J., Bui, Q. V., Gannavaram, S., and Gadda, G. (2015) Importance of glutamate 87 and the substrate alpha-amine for the reaction catalyzed by D-arginine dehydrogenase, Arch Biochem Biophys 568, 56-63.

[82] Gannavaram, S., Sirin, S., Sherman, W., and Gadda, G. (2014) Mechanistic and computational studies of the reductive half-reaction of tyrosine to phenylalanine active site variants of D-arginine dehydrogenase, Biochemistry 53, 6574-6583.

[83] Ouedraogo, D., Ball, J., Iyer, A., Reis, R. A. G., Vodovoz, M., and Gadda, G. (2017) Amine oxidation by d-arginine dehydrogenase in Pseudomonas aeruginosa, Arch Biochem Biophys 632, 192-201.

[84] D'Aniello, A., Vetere, A., and Petrucelli, L. (1993) Further study on the specificity of D-amino acid oxidase and D-aspartate oxidase and time course for complete oxidation of D-amino acids, Comp Biochem Physiol B 105, 731-734.

[85] Negri, A., Massey, V., and Williams, C. H., Jr. (1987) D-aspartate oxidase from beef kidney. Purification and properties, J Biol Chem 262, 10026-10034.

[86] D'Aniello, S., Somorjai, I., Garcia-Fernandez, J., Topo, E., and D'Aniello, A. (2011) D-Aspartic acid is a novel endogenous neurotransmitter, FASEB J 25, 1014-1027.

[87] Setoyama, C., and Miura, R. (1997) Structural and functional characterization of the human brain D-aspartate oxidase, J Biochem 121, 798-803.

[88] Yamamoto, A., Tanaka, H., Ishida, T., and Horiike, K. (2007) Functional and structural characterization of D-aspartate oxidase from porcine kidney: non-Michaelis kinetics due to substrate activation, J Biochem 141, 363-376.

[89] Katane, M., Furuchi, T., Sekine, M., and Homma, H. (2007) Molecular cloning of a cDNA encoding mouse D-aspartate oxidase and functional characterization of its recombinant proteins by site-directed mutagenesis, Amino Acids 32, 69-78.

[90] Tedeschi, G., Negri, A., Ceciliani, F., Ronchi, S., Vetere, A., D'Aniello, G., and D'Aniello, A. (1994) Properties of the flavoenzyme D-aspartate oxidase from Octopus vulgaris, Biochim Biophys Acta 1207, 217-222.

[91] Takahashi, S., Takahashi, T., Kera, Y., Matsunaga, R., Shibuya, H., and Yamada, R. H. (2004) Cloning and expression in Escherichia coli of the D-aspartate oxidase gene from the yeast Cryptococcus humicola and characterization of the recombinant enzyme, J Biochem 135, 533-540.

[92] Errico, F., D'Argenio, V., Sforazzini, F., Iasevoli, F., Squillace, M., Guerri, G., Napolitano, F., Angrisano, T., Di Maio, A., Keller, S., Vitucci, D., Galbusera, A., Chiariotti, L., Bertolino, A., de Bartolomeis, A., Salvatore, F., Gozzi, A., and Usiello, A. (2015) A role for D-aspartate oxidase in schizophrenia and in schizophrenia-related symptoms induced by phencyclidine in mice, Transl Psychiatry 5, e512.

[93] Nuzzo, T., Sacchi, S., Errico, F., Keller, S., Palumbo, O., Florio, E., Punzo, D., Napolitano, F., Copetti, M., Carella, M., Chiariotti, L., Bertolino, A., Pollegioni, L., and Usiello, A. (2017) Decreased free d-aspartate levels are linked to enhanced d-aspartate oxidase activity in the dorsolateral prefrontal cortex of schizophrenia patients, NPJ Schizophr 3, 16.

[94] Sacchi, S., Novellis, V., Paolone, G., Nuzzo, T., Iannotta, M., Belardo, C., Squillace, M., Bolognesi, P., Rosini, E., Motta, Z., Frassineti, M., Bertolino, A., Pollegioni, L., Morari, M., Maione, S., Errico, F., and Usiello, A. (2017) Olanzapine, but not clozapine, increases glutamate release in the prefrontal cortex of freely moving mice by inhibiting D-aspartate oxidase activity, Sci Rep 7, 46288.

[95] Takahashi, S., Kakuichi, T., Fujii, K., Kera, Y., and Yamada, R. H. (2005) Physiological role of D-aspartate oxidase in the assimilation and detoxification of D-aspartate in the yeast Cryptococcus humicola, Yeast 22, 1203-1212.

[96] Katane, M., Saitoh, Y., Maeda, K., Hanai, T., Sekine, M., Furuchi, T., and Homma, H. (2011) Role of the active site residues arginine-216 and arginine-237 in the substrate specificity of mammalian D-aspartate oxidase, Amino Acids 40, 467-476.

[97] Katane, M., Hanai, T., Furuchi, T., Sekine, M., and Homma, H. (2008) Hyperactive mutants of mouse D-aspartate oxidase: mutagenesis of the active site residue serine 308, Amino Acids 35, 75-82.

[98] Takahashi, S., Shimada, K., Nozawa, S., Goto, M., Abe, K., and Kera, Y. (2016) Possible role of a histidine residue in the substrate specificity of yeast d-aspartate oxidase, J Biochem 159, 371-378.

[99] Terry-Lorenzo, R. T., Chun, L. E., Brown, S. P., Heffernan, M. L., Fang, Q. K., Orsini, M. A., Pollegioni, L., Hardy, L. W., Spear, K. L., and Large, T. H. (2014) Novel human D-amino acid oxidase inhibitors stabilize an active-site lid-open conformation, Biosci Rep 34.

[100] Boselli, A., Sacchi, S., Job, V., Pilone, M. S., and Pollegioni, L. (2002) Role of tyrosine 238 in the active site of Rhodotorula gracilis D-amino acid oxidase. A site-directed mutagenesis study, Eur J Biochem 269, 4762-4771.

[101] Takahashi, S., Furukawara, M., Omae, K., Tadokoro, N., Saito, Y., Abe, K., and Kera, Y. (2014) A Highly Stable D-Amino Acid Oxidase of the Thermophilic Bacterium Rubrobacter xylanophilus, Appl Environ Microbiol 80, 7219-7229.

[102] Setoyama, C., Nishina, Y., Mizutani, H., Miyahara, I., Hirotsu, K., Kamiya, N., Shiga, K., and Miura, R. (2006) Engineering the substrate specificity of porcine kidney D-amino acid oxidase by mutagenesis of the "active-site lid", J Biochem 139, 873-879.

[103] Ouedraogo, D., Souffrant, M., Vasquez, S., Hamelberg, D., and Gadda, G. (2017) Importance of Loop L1 Dynamics for Substrate Capture and Catalysis in Pseudomonas aeruginosa d-Arginine Dehydrogenase, Biochemistry 56, 2477-2487.

1.2 Quinone detoxification by flavoenzymes

1.2.1 Quinones

Quinones are six-membered cyclic, unsaturated compounds that contain two carbonyl groups, resulting in a fully conjugated cyclic dione. The carbonyl groups can be adjacent or separated by a vinylene group. The simplest single ring form of a quinone, 1,4-benzoquinone, is shown in **Figure 1.5**. The simplest double ring form of a quinone, 1,4-naphthoquinone, is also shown in **Figure 1.5**. These two classes of 1,4-quinones will be studied as substrates in this dissertation.

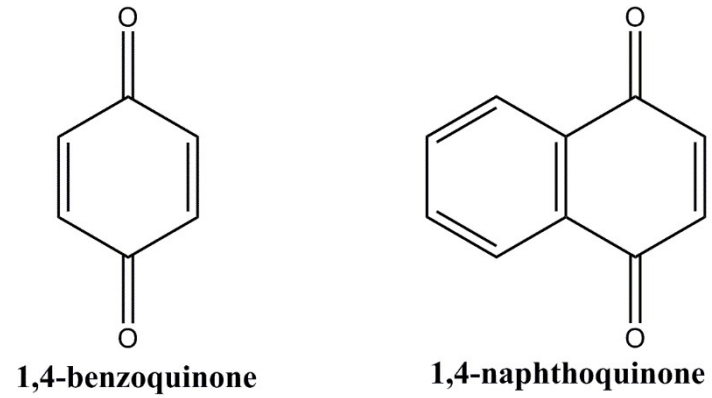

Figure 1.5 1,4-benzoquinone and 1,4-naphthoquinone

Quinones are pervasive in nature and participate in a wide variety of reactions, most notably in the electron transport chain in the form of Coenzyme Q_{10}. As shown in **Scheme 1.2**, quinones can accept one or two electrons to generate the semiquinone or hydroquinone, respectively.

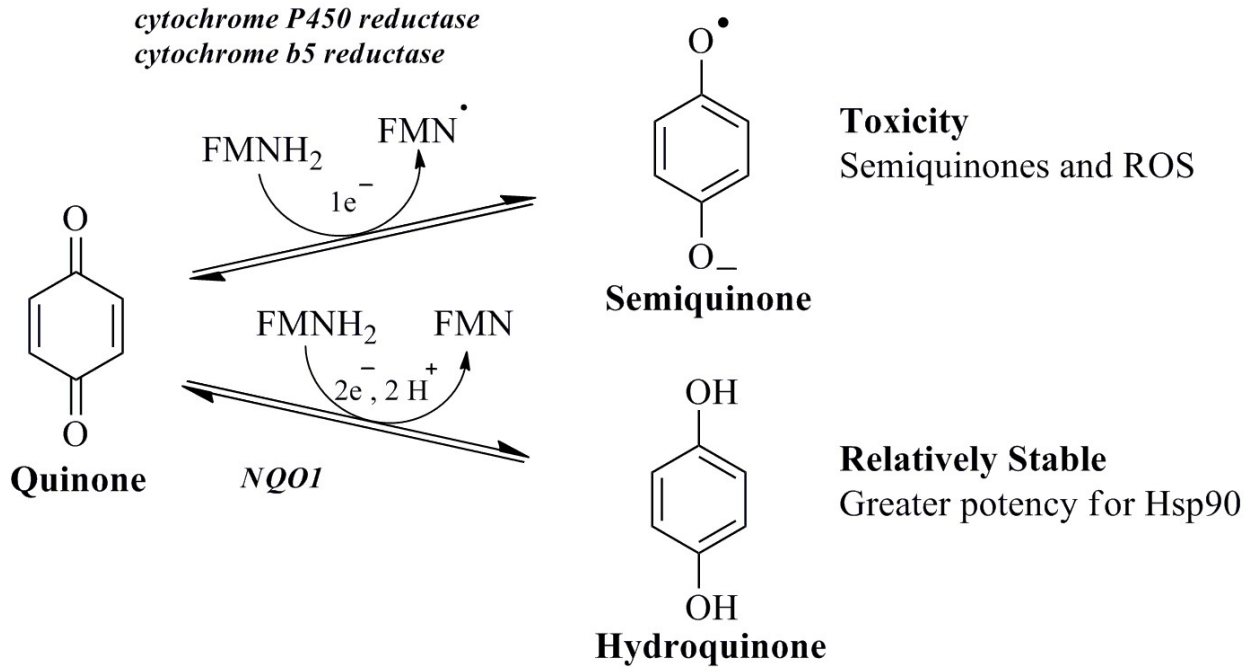

Scheme 1.2 One- and two- electron enzymatic reduction of quinones.
Modified from Piper and Millson.[1]

1.2.2 Two-electron reduction of quinones

The two-electron reduction of quinones is interpreted as a detoxification mechanism employed by organisms to reduce potential oxidative stress.[2, 3] Quinones can be reduced by a single electron by enzymes such as cytochrome p450 reductase to yield a semiquinone radical; however, the semiquinone radical can initiate chain reactions to produce reactive oxygenated species (ROS). Therefore, the prevention of the deleterious one-electron reduction is accomplished by directly reducing by two-electrons to the hydroquinone form. The hydroquinone can be further detoxified through conjugation mechanisms by the organism.

Flavoenzymes can accomplish the two-electron reduction by first receiving two electrons from NADH to form the reduced flavin, and then transferring those two electrons to the quinone. The most well studied flavin-dependent two-electron NADH:quinone oxidoreductase (NQO) is NQO1. This enzyme is found in various sources, including humans, where they have proposed

roles in quinone detoxification and alleviation of oxidative stress.[4] All of the flavin-dependent two-electron NQOs characterized to date are a flavodoxin-like fold.[4] This dissertation will detail the characterization of a novel FMN-dependent two-electron NADH:quinone oxidoreductase from *Pseudomonas aeruginosa* with a TIM-barrel fold.

1.2.3 References

[1] Piper, P. W., and Millson, S. H. (2011) Mechanisms of Resistance to Hsp90 Inhibitor Drugs: A Complex Mosaic Emerges, Pharmaceuticals (Basel) 4, 1400-1422.

[2] Chesis, P. L., Levin, D. E., Smith, M. T., Ernster, L., and Ames, B. N. (1984) Mutagenicity of quinones: pathways of metabolic activation and detoxification, Proc Natl Acad Sci U S A 81, 1696-1700.

[3] Taguchi, K., Fujii, S., Yamano, S., Cho, A. K., Kamisuki, S., Nakai, Y., Sugawara, F., Froines, J. R., and Kumagai, Y. (2007) An approach to evaluate two-electron reduction of 9,10-phenanthraquinone and redox activity of the hydroquinone associated with oxidative stress, Free Radic Biol Med 43, 789-799.

[4] Deller, S., Macheroux, P., and Sollner, S. (2008) Flavin-dependent quinone reductases, Cell Mol Life Sci, 141-160.

1.3 Specific Goals

The first specific goal of this dissertation is to investigate ionizable groups in the active site of *Pa*DADH through site directed mutagenesis in combination with kinetic approaches. H48 is hypothesized to serve as a catalytic base with the aid of two water molecules connected by the hydrogen-bonding network. E87 is hypothesized to be important for binding cationic substrates, a.k.a. amino acid substrates bearing positively-charged side chains. Methods to be employed include a) site-directed mutagenesis of E87 and H48, which are implicated to play roles in catalysis and/or substrate binding and b) pH effects on the kinetic parameters of the variant enzymes with multiple substrates of zwitterionic and cationic nature. The broader impact of this study will determine the identity of the catalytic base, or determine that there is no base functioning in the mechanism. This study will also establish the importance or insignificance of E87 and H48 for binding substrates through kinetic approaches. The factors controlling substrate specificity in *Pa*DADH can provide valuable information to investigators interested in protein engineering efforts, particularly those focused on a single biosensor capable of detecting all types of amino acids.

The second specific goal of this dissertation is to characterize the gene product of *pa*1024 to improve the gene prediction of thousands of misannotated genes. Many of the genes annotated as Nitronate monooxygenases (NMOs) are likely not NMOs, specifically *pa*1024. Based on the genomic context of PA1024, the enzyme most likely is involved in β-oxidation, not nitronate detoxification. PA1024 may serve as a mechanism to regenerate NAD^+ for use by a 3-hydroxy-acyl Coa dehydrogenase present in the operon. Methods to be employed include testing of the potential substrates/non-substrates for the enzyme. A comprehensive spectral and kinetic characterization of PA1024 will be pursued. Refinement of the bioinformatic analysis of PA1024

will be carried out to more accurately assess the patterns or motifs in the amino acid sequence critical to the specific reaction catalyzed by the enzyme. This study will characterize the enzyme through pH and kinetic solvent viscosity approaches and X-ray crystallography, which will provide valuable insights on the function of ionizable groups in the mechanism, rate-limiting steps operative in the mechanism, and substrate binding modes. Finally, this study will aim to establish a new class of enzymes and remedy the annotations of more than one thousand hypothetical proteins in the database.

2 AMINE OXIDATION BY D-ARGININE DEHYDROGENASE IN *Pseudomonas aeruginosa*

(This chapter has been published *verbatim* in Ouedraogo D., Ball J., Iyer A., Reis R.A.G., Vodovoz M., and Gadda G. (2017) Arch Biochem Biophys, 632, 192-201; the author contributed the substrate specificity and steady-state kinetic mechanism sections in addition to help with editing the final manuscript.)

2.1 Abstract

*Pa*DADH is a flavin-dependent oxidoreductase with a noncovalently linked FAD that exhibits broad substrate specificity towards D-amino acids. Various biochemical studies have established the structure and the mechanistic properties of the enzyme. The enzyme effectively catalyzes the oxidation of positively charged and hydrophobic D-amino acids to their respective imino acids. It is a true dehydrogenase, since it displays no reactivity towards oxygen. As established through solvent and multiple kinetic isotope studies, *Pa*DADH catalyzes the asynchronous CH and NH bond cleavage via a hydride transfer mechanism. The Steady-state kinetic studies with D-arginine and D-histidine are consistent with the enzyme following a ping-pong bi-bi mechanism. As shown by a combination of crystallography, kinetic and computational data the shape and flexibility of the active site, in particular loop L1 in *Pa*DADH, plays a significant role in its ability to oxidize a diverse range of D-amino acids.

2.2 Introduction

In 1848 Louis Pasteur made the groundbreaking discovery of molecular chirality[1]. Pasteur was also one of the first to observe enantioselectivity in a biochemical process, which is now a well-established concept[1-3]. Numerous investigations were launched concerning D-amino acids and their roles in nature[4, 5]. Later in 1935, Hans Krebs discovered D-amino acid oxidase

(DAAO) through the observation that D-amino acids undergo selective deamination by homogenates derived from pig kidney[6].

D-amino acid oxidase is a ubiquitous flavin-dependent enzyme found in various species of bacteria, fungi, and mammals and remains the most extensively studied enzyme that oxidizes D-amino acids, with more than 30 structures deposited in the Protein Data Bank[7]. D-amino acid oxidase from pig kidney (pDAAO) remains the most studied orthologue of the D-amino acid oxidase structural family, which also contains D-amino acid oxidases from other organisms, sarcosine oxidases, glycine oxidase and dimethylglycine oxidase[8-11].The enzyme has become a model for stereospecific flavin-dependent oxidoreductases that oxidize D-amino acids into their corresponding imino acids. Flavin-dependent enzymes that also oxidize D-amino acids include D-glutamate oxidase, D-amino acid dehydrogenase, and D-arginine dehydrogenase, among others[12-16].

The function of DAAO in microorganisms is to utilize D-amino acids as a nutrient source, although the functions of the enzyme in eukaryotes are still under investigation[8, 17]. DAAO has been reported to function in maintaining critical concentrations of D-serine that acts as a neuromodulator in mammals[18-20]. To gain an in-depth understanding of D-amino acid oxidizing enzymes, the readers are referred to recent reviews on DAAO and D-aspartate oxidase[7, 19, 21, 22].

The present review highlights the mechanistic and structural findings on D-arginine dehydrogenase from *Pseudomonas aeruginosa* which is a member of the DAAO structural family. D-arginine dehydrogenase is an FAD-dependent enzyme that catalyzes the oxidative deamination of D-amino acids to their respective imino acids, which nonenzymatically hydrolyze to α-keto acids and ammonia[23, 24]. The enzyme plays a pivotal role in utilizing D-arginine as a

primary source of carbon and nitrogen[16]. *Pa*DADH oxidizes the CN bond between the αC and the amine group of the D-amino acid converting it to an imino acid[25]. The enzyme does not display any reactivity towards molecular oxygen, which could potentially be a preventative mechanism to avoid production of harmful reactive oxygen species in host cells.

2.3 D-amino acids and their metabolism

D-amino acids occur in free-form naturally in soil, plants, and are utilized by microorganisms commonly found in soil i.e., *P. aeruginosa*[26]. Racemization of amino acids depends on various abiotic factors like temperature, ionizing radiation, metal ions and pH, including several biotic factors like enzymes[4]. Environmental pressures and increased D-amino acid content in soil and waterways have forced bacteria to evolve in order to not only metabolize, but utilize and synthesize D-amino acids[4].

Higher organisms lack extensive machinery in place to degrade D-amino acids**.** Indeed, high levels of D-isomers are not tolerated and have a toxic effect on plants and fungi growth[27, 28]. In humans, D-amino acids have specialized roles such as D-Serine and D-aspartate which are agonists for N-methyl-D-aspartate receptors and D-aspartate is also associated with ageing in tissues[18, 29-32]. D-amino acids in most eukaryotes are racemized via a one-enzyme racemase, most of which are PLP-dependent[19, 32, 33].

In bacteria, however, several cases of the utilization of D-amino acids in peptidoglycan layers have been reported[34]. Bacteria, in most cases, have the required machinery in place to metabolize and utilize D-amino acids[34]. D-alanine and D-glutamate are among the D-amino acids that are most prevalent in bacteria, making alanine and glutamate racemases essential in microorganisms[35]. Tsukada in 1966 demonstrated that *Pseudomonas fluorescens* had two distinct D-amino acid dehydrogenases expressed in D-tryptophan treated cells. Both enzymes use FAD

as a cofactor and do not use molecular oxygen as an electron acceptor. One of the D-amino acid dehydrogenases specifically reacted with Dichlorophenolindophenol as an electron acceptor, while the other with methylene blue and were named D-amino acid:2,6-dichloroindophenol oxidoreductase and D-amino acid :methylene blue oxidoreductase, respectively[15].

Li & Lu in 2009 discovered a novel two-enzyme system that functions to convert D-arginine to L-arginine in *P. aeruginosa*. Further analysis of the two gene products revealed that the two-enzyme system is composed of an FAD-dependent D-arginine dehydrogenase and an NAD(P)H-dependent L-arginine dehydrogenase as described in Scheme 2.1[23]. Although Haas & associates in 1988 did provide evidence for an arginine racemase in *P. aeruginosa* by demonstrating utilization of D-arginine by Arginine auxotrophs, they were not able to demonstrate arginine racemase activity *in vitro*[24]. The two enzymes are products of the dauBAR operon, which can be induced by D-arginine and D-Lysine. The gene products DauA and DauB provide a unique coupled anabolic and catabolic system that enables PAO1 to utilize D-arginine as the only source of carbon and nitrogen. Li & Lu also reported that the DauBAR operon is conserved among several other bacterial species[16, 23, 36].

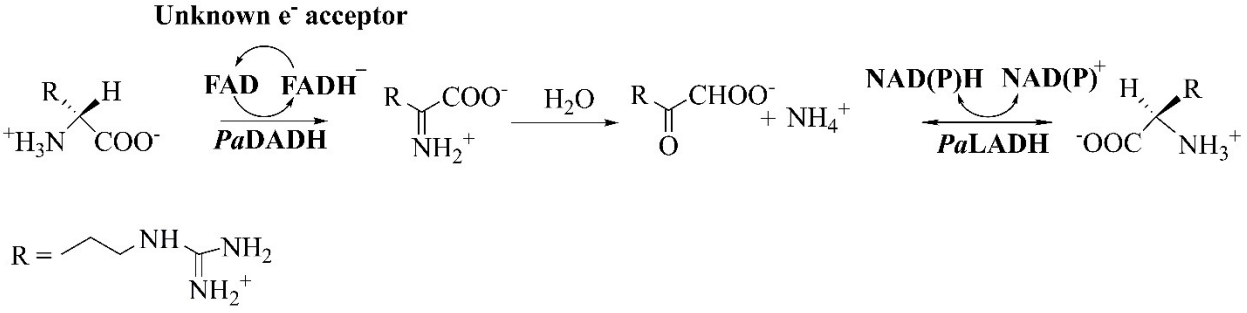

Scheme 2.1 D-Arginine racemization with the two-enzyme racemic system in *Pseudomonas aeruginosa*.

2.4 Structural features of *Pa*DADH

2.4.1 Overall fold of PaDADH

The three-dimensional structure of *Pa*DADH was determined by X-ray crystallography at high resolution without added D-amino acids (~ 1.06 Å, PDB ID: 3NYC)[36]. However, extra density for a low occupancy iminoarginine was found in the active site. Ligand-free and bound forms were obtained, the latter of which was probably due to the product of the enzymatic reaction being trapped during the expression of the enzyme by *E. coli*.[36] The *Pa*DADH crystal structures were also determined for crystals grown in presence of D-arginine and D-histidine thereby yielding a *Pa*DADH/iminoarginine (PDB ID 3NYE)[36] and PaDADH/iminohistidine (PDB ID 3NYF)[36] complexes. Additionally, a covalent N5 flavin adduct was obtained at atomic-resolution in the enzyme co-crystallized with D-leucine instead of the expected iminoleucine (PDB ID 3SM8)[37]. **Table 2.1** summarizes the crystal structures of *Pa*DADH available in the PDB. The four structures of hexahistidine-tagged *Pa*DADH are highly similar, with RMS deviations of less than 0.14 Å for 381 αC atoms, and display a non-covalently bound FAD as the cofactor[36]. All 375 residues of *Pa*DADH were well defined in the electron density map and organized in two domains. The FAD-binding domain is formed by a central six-stranded β-sheet surrounded by three-stranded antiparallel β-sheets with two α-helices on one side and five α-helices on the other side (Figure 1A). The substrate binding domain is composed of eight-stranded β-sheets and two short antiparallel β-strands that constitute a sandwich surrounded by four α-helices and four loops (L1 to L4)[36] (**Figure 2.1A**).

Table 2.1 Crystal structures of PaDADH deposited in PDB

PDB ID	Resolution (Å)	Redox state of flavin	Ligand
3NYC	1.06	Mixed*	Iminoarginine
3NYE	1.30	Reduced	Iminoarginine
3NYF	1.30	Reduced	Iminohistidine
3SM8	1.07	Reduced	D-leucine N5 flavin adduct

*Ligand-free and product-bound conformations for *Pa*DADH. The crystal structures of *Pa*DADH exhibit all the same space group $P2_12_12_1$.

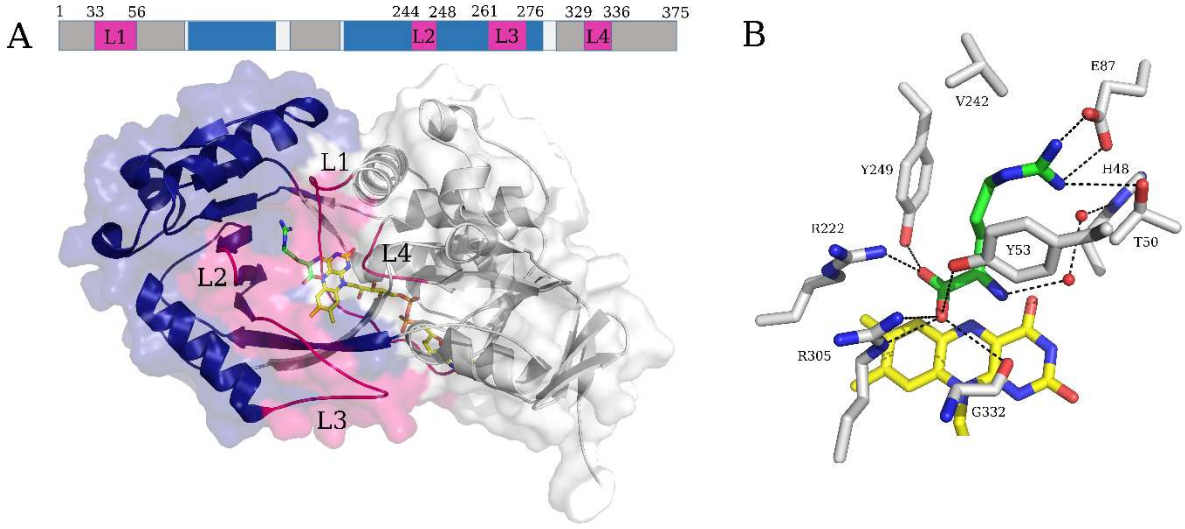

Figure 2.1 Overall structure and active site of *Pa*DADH in complex with iminoarginine. (A) The *Pa*DADH structure is shown in cartoon diagram and surface representation. Carbon atoms are colored blue for the FAD-binding domain and gray for the substrate-binding domain. Iminoarginine and FAD stick representations are illustrated in green and yellow, respectively. Loops that contribute to the active site are highlighted in magenta. (B) Close up view of the active site showing the substrate interactions of the active site residues and FAD with the iminoarginine product. Protein side chains are displayed in sticks.

2.4.2 FAD-binding domain

The crystal structures of *Pa*DADH show a noncovalently bound FAD as the cofactor[36]. The flavin adopts an elongated conformation with the isoalloxazine moiety located at the interface of the substrate-binding domain and the FAD-binding domain. The adenosine portion of the FAD moiety is buried deep within the FAD-binding domain[36] (**Figure 2.1A**). The major

interactions involved in the flavin-apoprotein complex are shown in Figure 2. The ribose ring moiety has hydrogen bond interactions with the main-chain of R33 and A171, water molecules and the side chain of E32. The pyrimidine portion of the isoalloxazine moiety interacts through hydrogen bonds with backbone atoms of the I335, Q336, His48 and a water molecule while the benzene portion forms van der Waals contacts with R44, R222, W301, G303 and R305 (**Figure 2.1B**)[36]. Crystallographic data of *Pa*DADH demonstrate that the isoalloxazine moiety of the FAD is in a non-planar conformation with a ring puckering angle of 15° along the N5 – N10 axis, defining two planes containing the benzene and pyrimidine moieties[36]. The bent conformation is in agreement with other flavin-dependent enzymes structures containing flavin in the reduced state[38, 39].

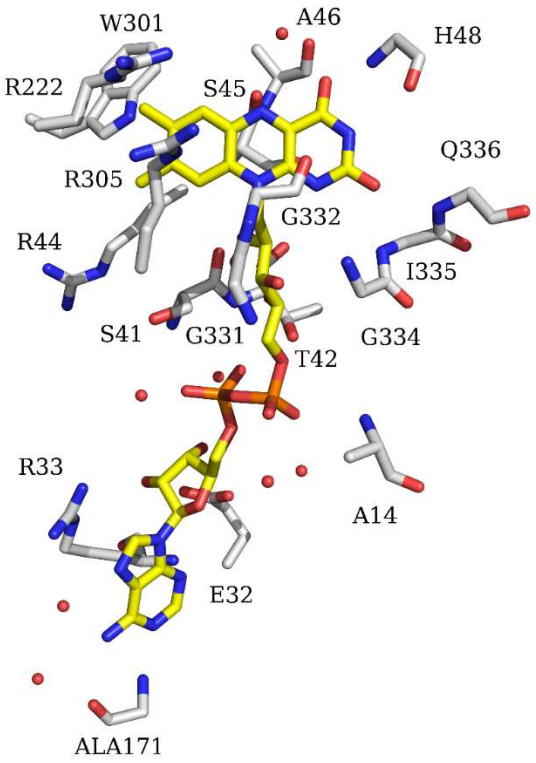

Figure 2.2 Interactions of FAD with apoprotein.
Apoprotein carbons in *Pa*DADH are in grey and FAD moiety carbons are in yellow. The red spheres represent water molecules.

2.4.3 Substrate binding-domain

The substrate-binding domain of *Pa*DADH is formed by a small entrance that extends at the bottom near the isoalloxazine moiety of the FAD, adopting a triangular cross section shape with ~10 Å deep from the αC of G54 to the FAD O2 atom[36]. The carboxylate group of the iminoarginine product occupies the same plane as the isoalloxazine moiety of the FAD, while its side chain is almost perpendicular to the FAD (**Figure 2.1B**)[36]. The side chain atoms of Y53, R222, Y249, R305 and main-chain of G332 form polar interactions with the iminoproduct carboxylate group (**Figure 2.1B**)[36]. The side chain of the iminoarginine product has hydrophobic interactions with V242 and Y53 side chain, hydrogen bond interaction with T50 and ionic interaction with E87 side chain[36](**Figure 2.1B**). Two water molecules are located near the imino group of the product and form a hydrogen bond network extending to the side chain of H48[36]. The entrance of the active site is controlled by a flexible loop L1, which is formed by residues 33-56. The loop L1 has two different peptidyl regions including residues 45-47 and residues 50-56 adopting two conformations depending on whether the substrate is present or not in the active site[36].

2.4.4 Structural Comparison of PaDADH with D-amino Acid Oxidase (DAAO)

Previous crystallographic analysis showed that *Pa*DADH has a high three-dimensional structural similarity compared to DAAO[36]. The crystal structure of *Pa*DADH (PDB ID 3NYE) and pDAAO (PDB ID 1DDO) were used for an in-depth comparison of the overall structure and the active site[36, 40, 41]. pDAAO and *Pa*DADH share 17.2 % sequence identity with a RMS deviation value of 2.4 Å for 270 αC atoms [36]. *Pa*DADH and DAAO were chosen since both enzymes catalyze the same chemical reaction except that DAAO utilizes molecular oxygen as its electron acceptor. As shown in Figure 3A, the overall structure of *Pa*DADH is similar to

pDAAO. The isoalloxazine moiety of the FAD is located at the interface between the FAD-binding domain and the substrate-binding domain in both enzymes[36]. The main difference between the two structures is observed in the FAD-binding domain as indicated in Figure 3A where three antiparallel β-sheets in *Pa*DADH are replaced by an α-helix in DAAO[36]. The substrate binding-domain in both *Pa*DADH and pDAAO is characterized by the presence of a large β-sheets[36] (**Figure 2.3A**).

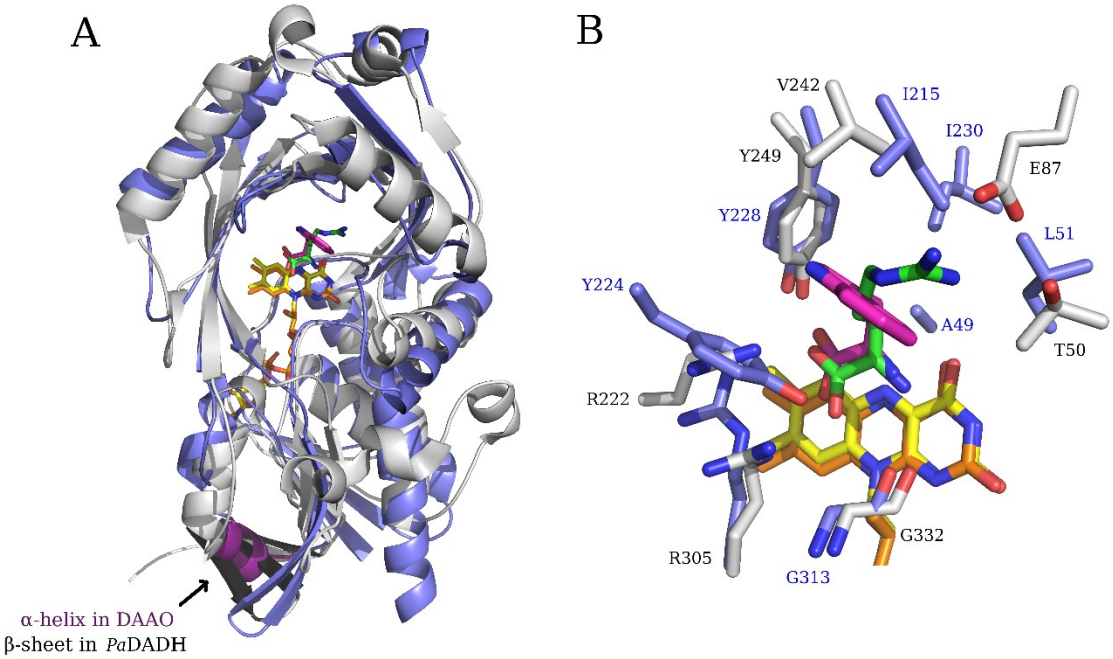

Figure 2.3 Comparison of the three-dimensional structure of pDAAO (light-blue, PDB ID 1DDO) with PaDADH (gray, PDB ID 3NYE).
(A) represents the overall structure of the two enzymes and (B) represents the active sites of the enzymes. For clarity, Y53 from *Pa*DADH was omitted. Iminoacid carbons in *Pa*DADH are in green, iminotryptophan carbons in pDAAO are in magenta and FAD moiety carbons are in yellow and orange in *Pa*DADH and pDAAO, respectively.

The active site of *Pa*DADH in complex with iminoarginine and pDAAO in complex with imonotryptophan showed that the ligands in both enzymes bind at the *re* face of the isoalloxazine ring of the FAD moiety[36, 40] (**Figure 2.3B**). The carboxylate groups of the iminoproducts in both enzymes lie almost on the same plane and parallel to the isoalloxazine moiety (**Figure 2.3B**). On

the contrary, the side chains of the iminoproducts are quasi-perpendicular to the isoalloxazine moiety of the FAD (**Figure 2.3B**). In pDAAO only one arginine side chain residue, R283, interacts with the iminoproduct carboxylate group whereas in *Pa*DADH two arginine residues, R222 and R305, participate in the interaction (**Figure 2.3B)**[36]. pDAAO has polar interactions with the iminotryptophan product formed by the side chain residues of Y224, Y228, and the main chain oxygen atom of G313, which are similar to the interaction in *Pa*DADH formed by the side chains of Y53,Y249 and main chain oxygen of G332 (**Figure 2.3B**). The side chains of the A49, L51, I215, I230 and Y224 in pDAAO form a hydrophobic cage interacts with the iminotryptophan product. *Pa*DADH has a similar hydrophobic cage, but a key difference being the presence of E87 and T50 in *Pa*DADH in place of I230 and L51 in pDAAO, respectively[36, 40] (**Figure 2.3B**).

2.5 Substrate specificity of PaDADH

*Pa*DADH exhibits broad substrate scope, being most active with large basic and hydrophobic substrates, and demonstrates the highest activity with D-arginine and D-lysine[42] (**Table 2.2**). *Pa*DADH is strictly stereospecific and L-amino acids are not substrates[36]. *Pa*DADH cannot oxidize the anionic amino acids aspartate and glutamate. The anionic amino acids are oxidized by specific D-aspartate and D-glutamate oxidases[12, 21]. The portion of the *Pa*DADH active site that binds the main chain follows intuition for the most part by providing a protein positive charge(s) from R222 and R305 to bind the carboxylate of the substrate, and hydrogen-bonds from Y53 and the main chain O atom of G332 to bind the amino group. The portion of the active site that binds the side chain of the substrate is fine-tuned to bind arginine with E87 positioned to form an electrostatic interaction at a distance of 2.5 Å with the guanidinium head-group of arginine (Figure 1B)[36]. The relatively large active site volume and the presence of a

hydrophobic cage comprised of residues Y53, Y254, M240, and V242 grants *Pa*DADH the ability to oxidize large hydrophobic amino acids as well[43]. The large active site of *Pa*DADH and lack of a handle on glycine is likely the reason glycine cannot find an optimal configuration to be oxidized and smaller hydrophobic substrates are oxidized slowly by *Pa*DADH[36]. Based on crystallographic and computational evidence *Pa*DADH is proposed to be further modulated by a flexible loop to enhance the substrate scope by providing active site plasticity[36].

Table 2.2 Steady-state kinetic parameters for *Pa*DADH with various D-amino acids.

Substrate	k_{cat}/K_m, M^{-1} s^{-1}	k_{cat}, s^{-1}	K_m, mM
D-arginine	(3.4 ± 0.3) x 10^6	204 ± 3	0.06 ± 0.01
D-lysine	(5.3 ± 0.2) x 10^5	141 ± 3	0.26 ± 0.01
D-tyrosine	27600 ± 3800	23 ± 1	0.8 ± 0.1
D-methionine	14800 ± 600	154 ± 3	10 ± 1
D-phenylalanine	6900 ± 300	75 ± 3	11 ± 1
D-histidine	3140 ± 30	35 ± 1	11 ± 1
D-leucine	515 ± 60	6.4 ± 0.3	12 ± 1
D-proline	420 ± 10	-[a]	-
D-tryptophan	245 ± 3	-	-
D-isoleucine	195 ± 3	-	-
D-glutamine	186 ± 3	-	-
D-valine	47 ± 1	-	-
D-alanine	41 ± 1	-	-
D-asparagine	16 ± 1	-	-
D-serine	3.8 ± 0.1	-	-
D-threonine	0.75 ± 0.01	-	-
D-glutamate	-	-	-
D-aspartate	-	-	-
L-arginine	-	-	-
glycine	-	-	-
D-cysteine	nd[b]	nd	nd

Enzyme activity was measured varying concentrations of the desired amino acid and 1 Mm PMS in 20 mM Tris-HCl, pH 8.7, at 25 °C. [b]Cannot be saturated with substrate thereby k_{cat} and K_m values are not reported. [c]Not determined. PMS was reduced nonenzymatically by cysteine.

2.5.1 E87 dictates substrate specificity

D-Arginine and D-lysine are the best substrates for *Pa*DADH as gauged by their large k_{cat}/K_m values in the 10^6 M^{-1} s^{-1} range[36]. The kinetic parameter k_{cat}/K_m defines the ability of the enzyme for capturing the substrate to form the enzyme-substrate complex that proceeds to catalysis. D-Arginine exhibits the largest k_{cat}/K_m value at pH 8.7 of 3.4 x 10^6 M^{-1} s^{-1}, about 7-fold higher than the next closest k_{cat}/K_m value belonging to D-lysine[36]. The bi-dentate electrostatic interaction that arginine engages with E87 is likely more energetically favorable than the mono-dentate interaction involved with D-lysine and may account for the differences in kinetic parameters. Replacement of E87 with leucine resulted in a 20-fold decrease in the k_{cat}/K_m value with D-arginine, yet the value is still in the 10^5 M^{-1} s^{-1} range, hence the contributions of the hydrophobic cage and other H-bonds to bind the D-arginine side-chain, such as T50 shown in Figure 4, may be underestimated[42].

The k_{cat}/K_m value with D-histidine as a substrate may suffer simply because it cannot interact with E87 due to distance requirements[42]. In the crystal structure of the iminohistidine complex as shown in Figure 4, the iminohistidine product is present in two distinct conformations, one of which does not point towards E87 and may partially explain the 1000-fold lower k_{cat}/K_m values with D-histidine as compared to D-arginine[36]. Further evidence of a distinct binding behavior for D-histidine comes from the inverse solvent viscosity effect on the k_{cat}/K_m value, Such a solvent effect is not seen with D-arginine as a substrate[36].

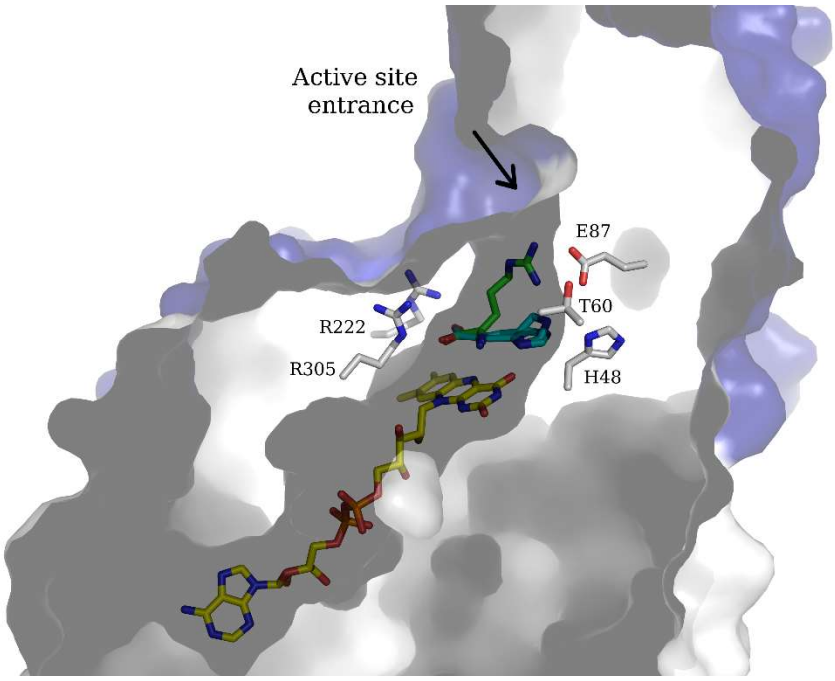

Figure 2.4 Overlay of the crystal structures of *Pa*DADH in complex with iminoarginine and iminohistidine.
*Pa*DADH residues line the interior of the substrate binding pocket. (Some residues were omitted for clarity). Iminoarginine and iminohistidine bind in two distinct conformations. The surface of the substrate binding pocket is in blue and the surface of the FAD binding domain is in white. Iminoacid carbons are in green, FAD carbons are in yellow, and side chain carbons are in grey. The arrow indicates the entrance to the active site.

2.5.2 A hydrophobic cage and a flexible loop extends substrate scope

In addition to exceptional kinetic parameters for amino acids bearing positively charged side chains, *Pa*DADH can efficiently oxidize the bulky aromatic substrates tyrosine and phenylalanine, and the sulfur-containing methionine (**Table 2.2**)[36]. The ability of *Pa*DADH to accommodate hydrophobic amino acid substrates is rooted in the presence of a hydrophobic cage as mentioned above (**Figure 2.3B**). The D-phenylalanine and D-tyrosine substrates most likely form π-π stacking interactions with either or both of Y53 and Y249[36]. D-Tyrosine can also potentially form hydrogen bonds with one or both of the Y53 and Y249 residues. D-Methionine is also a good substrate, making it likely that the sulfur of methionine engages in favorable

sulfur-π interactions with the aromatic rings of Y53 and Y249[42, 44]. The flexible loop L1 of *Pa*DADH is present in two alternate conformations and is proposed to act as a gate to control substrate entry/exit and substrate accommodation[36]. A similar loop is found in pDAAO composed of residues 216-228[40]. Loop L1 in *Pa*DADH may help lock small substrates in place by closing tightly, whereas in the case of large substrates like D-tyrosine and D-tryptophan the loop may protrude outward[36].

2.5.3 Substrate specificity comparison to D-amino acid Oxidases

The specificity of *Pa*DADH for large and basic substrates is in contrast to the *p*DAAO and human DAAO enzymes which show a preference for smaller hydrophobic substrates i.e., D-alanine, and likewise possess small active site volumes of 160 and 220 $Å^3$, respectively[7]. The substrate specificity of the yeast enzymes, *Rg*DAAO and *Tv*DAAO, demonstrate a preference for amino acids bearing large and bulky hydrophobic side-chains such as valine, phenylalanine and tryptophan[45]. Naturally, the key factors that determine the specificity of each of the enzymes seem to lie within the interactions of the substrate side-chain with the active site residues and the relative sizes of the active site pockets.

2.6 Steady-state kinetic mechanism of *Pa*DADH

The steady-state kinetic mechanism of *Pa*DADH is consistent with the minimal ping-pong bi-bi kinetic mechanism depicted in Scheme 2[46]. Evidence for a ping-pong mechanism stems from the occurrence of parallel lines in the double reciprocal plots of the enzymatic rates versus varied concentrations of D-arginine or D-histidine at different fixed concentrations of PMS as electron acceptor. The artificial electron acceptor PMS was utilized because the physiological oxidizing substrate is unknown. As shown in Scheme 2, the irreversible release of the iminoacid product (k_5) must occur before the second substrate, PMS, binds to enzyme (k_7)[46].

In agreement with a ping-pong mechanism, the binding of PMS was not significantly altered when either D-arginine or D-histidine was used as the reducing substrate, yielding a K_m of around 10 μM in both cases. Flavin reduction (k_3) was demonstrated to be irreversible with D-histidine as substrate using rapid kinetics approaches[46]. This conclusion can be extended to the faster substrate D-arginine, since it was shown that 85% of the reduction of the flavin occurs within the dead time of the instrument (2.2 ms)[46]. The reoxidation of the flavin (k_9) is also presumed to be irreversible after examination of the reduction potentials of PMS/$PMSH_2$ > FAD/$FADH_2$, with values of +80 and -200 mV respectively[47]. However, it is worth noting that the reduction potentials could potentially be far different when buried within the enzyme environment.

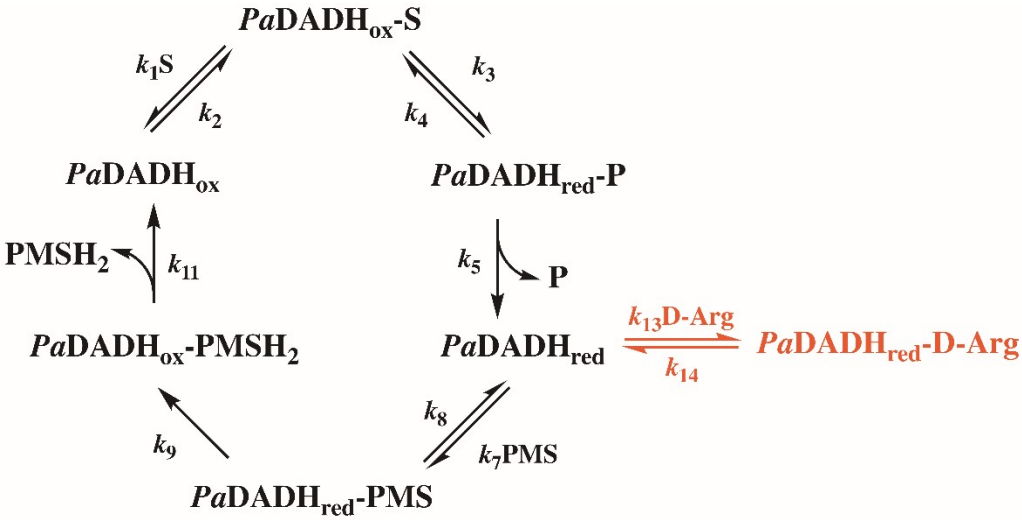

Scheme 2.2 Steady-state kinetic mechanism of PaDADH.
Pa$DADH_{ox}$, oxidized D-arginine dehydrogenase; S, amino acid substrate; *Pa*$DADH_{red}$, reduced D-arginine dehydrogenase; P, iminoacid product; PMS, phenazine methosulfate. $k5$ and k_{11} are shown as irreversible because products are assumed to be close to zero during the determination of the initial rates of reaction; k_4 is shown although it is close to zero based on stopped-flow data[46].

2.6.1 Product release

The release of the iminoacid product (k_5) is partially rate determining for overall turnover with D-arginine as substrate. Evidence for this conclusion comes from the effect of increasing solvent viscosity on the normalized rate constant for overall turnover when the enzyme is saturated with substrates[21.] Product release is the only diffusion-controlled step present in the proposed steady-state kinetic mechanism of *Pa*DADH[46]. The k_{cat} value for D-arginine exhibits a linear dependence on increasing viscosity yielding a positive slope of 0.14, consistent with product release being partially rate-determining, or about 14% responsible for the rate[46]. Furthermore, the k_{red} value for D-arginine is not measurable using stopped-flow reaction techniques due to the reduction occurring within the dead-time of the instrument, consistent with an estimated value for flavin reduction > 800 s^{-1} [48]. Thus, another step other than product release may also be contributing to the overall rate of turnover with D-arginine but has yet to be elucidated. In the case of D-histidine, increasing solvent viscosity elicited no effect on k_{cat}, indicating product release was not limiting for turnover[48]. Comparison of the k_{red} value of 60 s^{-1} with D-histidine and its corresponding k_{cat} of 35 s^{-1} implies that flavin reduction is at least partially rate-limiting with D-histidine as substrate[46]. Yet this also implies there is another step that occurs prior to product release and after substrate binding, such as an internal isomerization of the enzyme, that contributes to the overall turnover with D-histidine as well.

2.6.2 Substrate inhibition via a dead-end complex

At sufficiently high concentrations of D-arginine (> 0.5 mM) during steady-state turnover, substrate inhibition of *Pa*DADH occurs[46]. The excess D-arginine binds to the free reduced enzyme to form a dead-end complex *Pa*$DADH_{red}$-D-Arg as shown in Scheme 2. The accumulation of the dead-end complex leads to a lower overall rate of turnover. Substrate

inhibition due to the formation of dead-end complexes between the reduced enzyme and substrate has been observed in other flavoproteins such as nitroalkane oxidase, flavocytochrome b2, thymidylate synthase, aldehyde oxidase, and cellobiose dehydrogenase[49-53].

2.7 Catalytic mechanism

2.7.1 Mechanism CN bond cleavage

The reductive-half reaction of *Pa*DADH was investigated to gain insight on the mechanism of CN bond cleavage. During flavin reduction with either D-leucine or D-histidine, C4a or flavin N5 adducts were not observed, which is consistent with a hydride transfer mechanism (**Scheme 3**). pH-profile and computational studies showed that the hydride transfer in *Pa*DADH is triggered by the abstraction of the substrate α-NH_3^+ group proton (**Scheme 2.3**). Moreover, substrate, solvent and multiple kinetic isotope effects studies on wild-type *Pa*DADH were consistent with the NH and CH bond cleavage of the substrate occurring asynchronously with irreversible flavin reduction (**refs**). In order to investigate on the status of the base that abstracts the substrate α-NH_3^+ group proton (**Scheme 2.3**), Y53F and Y249F variant enzymes were generated through site-directed mutagenesis. Indeed, the crystal structure of *Pa*DADH showed that the hydroxyl groups of Y53 and Y249 residues are at a distance ≤ 4 Å from the substrate amino group consistent with the Y53 and Y249 residues to act as a base[25, 36]. The pH-profile studies on the reductive-half reaction of the Y53F and Y249F variant enzymes, and subsequent steady-state kinetic studies on E87L and H48F enzymes, established that Y53, Y249, E87 or H48 residues were not the base[25, 42]. Thus, it was proposed that the α-NH_3^+ group of the substrate loses its proton to the solvent to trigger amine oxidation in *Pa*DADH[25, 42, 48].

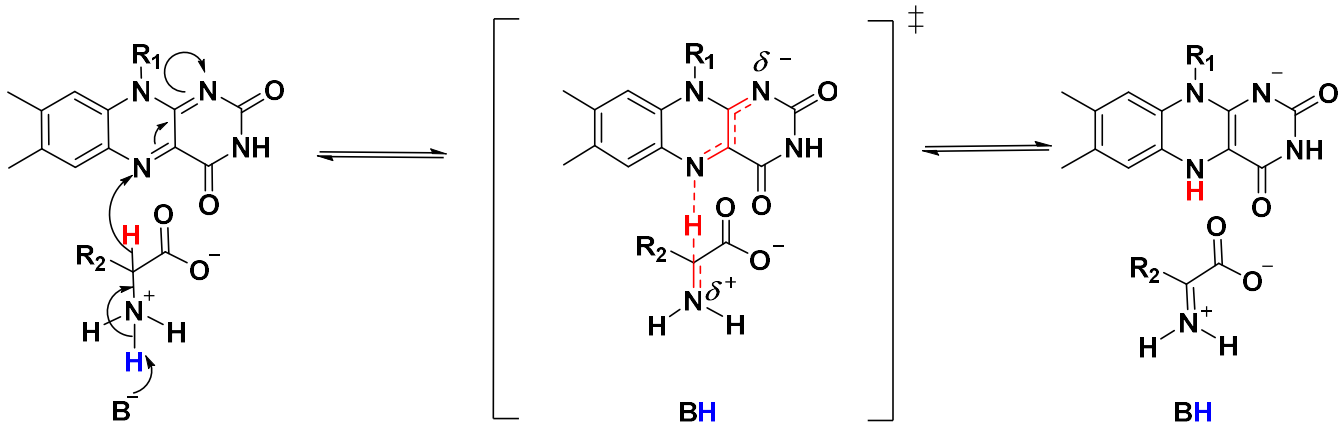

Scheme 2.3 Hydride transfer mechanism in *Pa*DADH.
B^- is a catalytic base, currently assumed to be a solvent molecule.

Similar to the wild-type *Pa*DADH, no flavin intermediates were observed in the Y53F and Y249F variants, consistent with a hydride transfer mechanism. On the contrary, flavin reduction was reversible in both the Y53F and Y249F variants. Moreover, the solvent and multiple kinetic isotope effect studies on the Y53F and Y249F variants demonstrate a synchronous CH and NH bond cleavage, consistent with a hydride transfer, and an alteration in the relative timing of the two bond cleavages as compared to the wild-type enzyme[25]. Based on this observation, it was concluded that the two tyrosine residues are involved in the stabilization of the transition state in *Pa*DADH to facilitate the hydride transfer from the substrate αC to the N5 atom of the isoalloxazine moiety of the FAD[25].

2.7.2 Restricted proton transfer

The pH-profile studies on the substrate affinity value, $K_{d,}$ and computational studies indicate that *Pa*DADH prefers to bind the protonated form of the substrate (i.e., α-NH_3^+)[48]. As shown in Scheme 4, after formation of the ESH^+ complex the substrate then loses a proton to

form the ES complex that proceeds to catalysis. A prominent hollow observed in the k_{cat} pH-profiles with D-lysine as a substrate with the wild-type *Pa*DADH provides evidence that the equilibration of the proton within the enzyme-substrate complex (i.e., k_{16}/k_{15}) is slower than other relevant kinetic steps[42] (**Scheme 2.4**). Moreover, a requirement for the hollow is usually observed with sticky substrates, which have a very high capacity to proceed to catalysis (i.e., k_3) after the formation of the enzyme-substrate complex in comparison to its dissociation (i.e., k_2) to free enzyme and substrate[54-56].

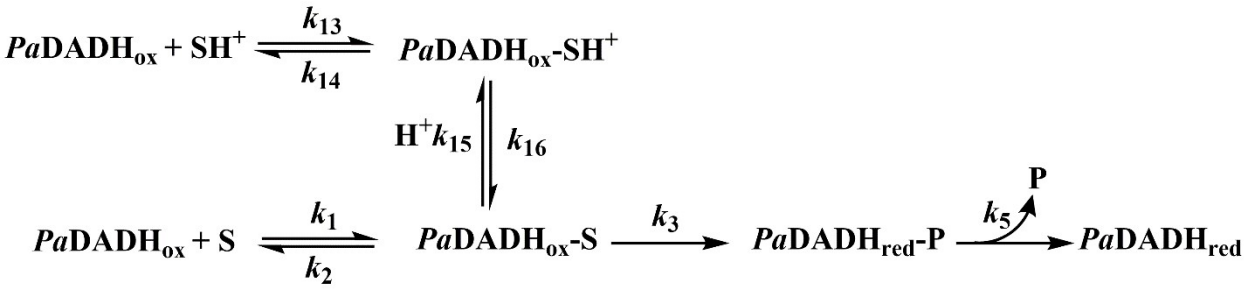

Scheme 2.4 Reductive half-reaction of PaDADH accounting for a slow proton equilibrium in the Michaelis complex.
S is the D-amino acid substrate. P is the iminoacid product.

The pH-profiles on the variant enzymes H48F and E87L provide further evidence that the hollow is related to a sub-optimal binding of the substrate in the active site of the enzyme[42]. The E87 residue stabilizes D-arginine by engaging in an ionic interaction with the substrate guanido group, thereby replacement of the E87 side chain to leucine impaired the optimal binding of the substrate, resulting in a slow proton release to the solvent[42]. It was shown that the hollowed pH-profile of the H48F variant, which is not in direct contact with the substrate, is likely due to the disruption of the H-bond network between the water molecules, H48 residue and the amino group of the substrate (**Figure 2.5**)[36, 42]. The H-bond network is important to optimize substrate binding and to prevent a slow proton release from the enzyme-substrate complex[42] (**Figure 2.5**). As shown in the crystal structure, E87 residue has an ionic interaction with the substrate guanido

group, while H48 residue interacts indirectly with the substrate via two water molecules (**Figure 2.5**)[36]. Thus, it was concluded that both H48 and E87 residues participate in the optimal orientation of the substrate to prevent a slow proton exchange between the ESH^+ complex and the solvent[42] (**Figure 2.5**).

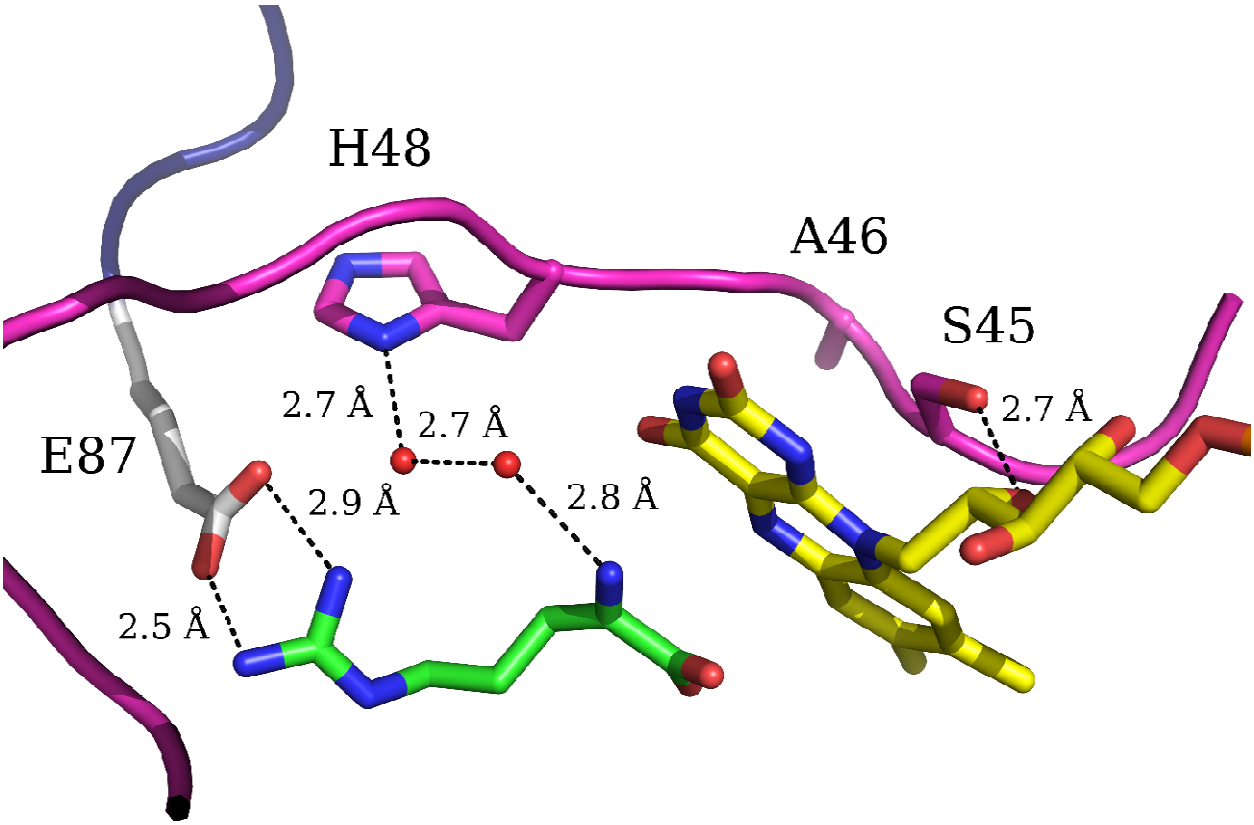

Figure 2.5 *Pa*DADH loop L1 with S45, A46 and H48 residues.
The isoalloxazine moiety of the FAD is in yellow, and the iminoarginine product is in green. Loop L1 is in magenta with H48 interacting with the iminoarginine product through two water molecules.

2.8 Role of loop L1 dynamics in PaDADH

The crystallographic data showed that *Pa*DADH has an active site loop L1 with two flexible segments that span the FAD-binding domain and the substrate-binding domain[36]. Loop L1 was also shown to occupy two distinct conformations corresponding to an open, competent

substrate binding conformation, and a catalytic ligand-bound closed conformation[36] (**Figure 2.6**). Y53 residue in loop L1, located at the entrance of active site, was proposed to act as a gate to control the access to the active site[36]. In the FAD-binding domain the side chains of S45 and A46 residues in loop L1, which do not interact directly with the substrate, adopt two alternate conformations depending on whether the ligand is present in the active site or not (**Figure 2.6**)[36]. Thus, the alternating conformations of S45 and A46, known as the S45/A46 switch was also considered to participate in the catalytic function of *Pa*DADH[36].

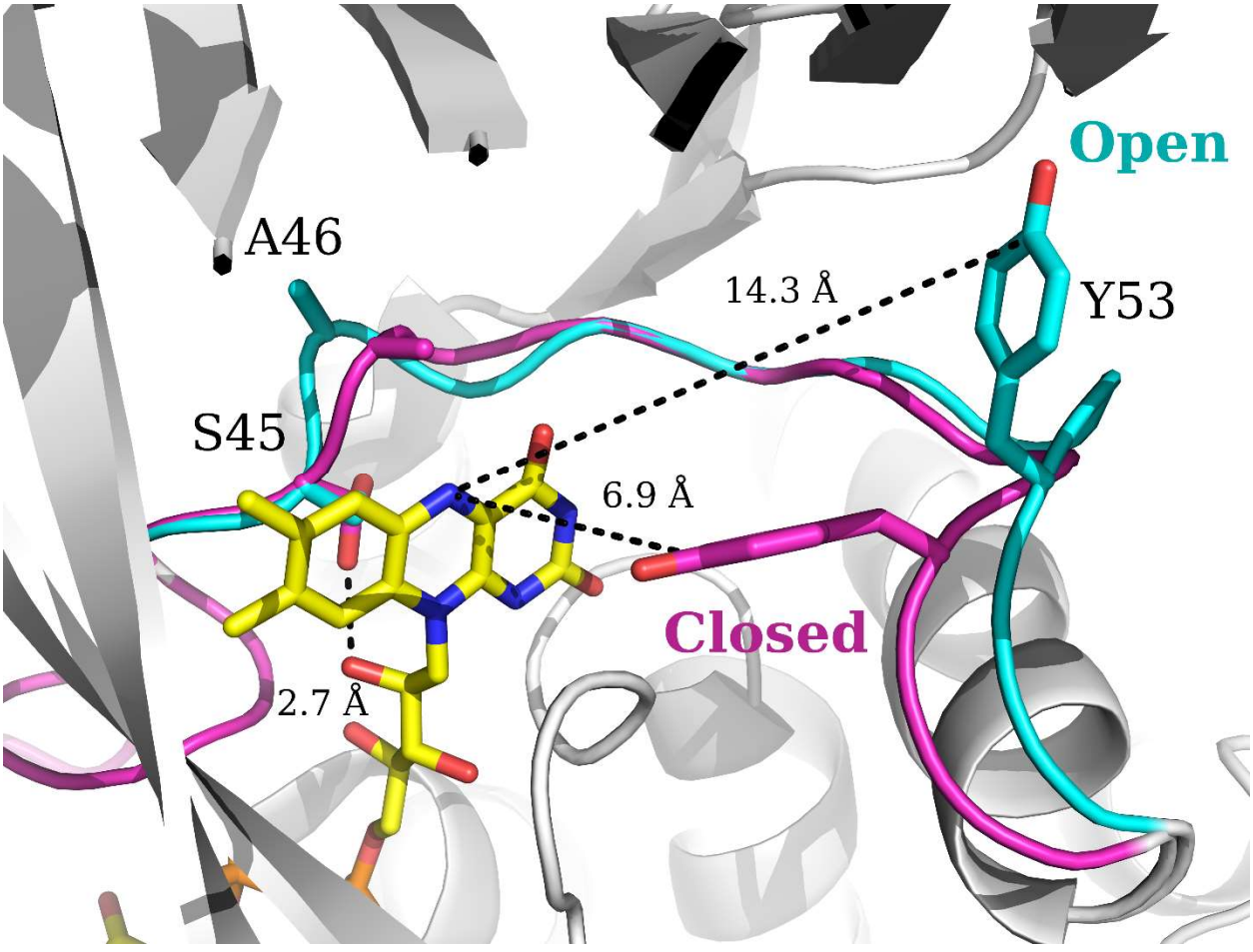

Figure 2.6 Open-closed conformations of loop L1.
The open conformation is shown in blue and the closed conformation in magenta. The carbons in the isoalloxazine ring of the FAD are shown in yellow.

2.8.1 S45/A46 switch and the Y53 gate

In the open conformation, as shown by the crystal structure, both the side chains of S45 and A46 located at the FAD-binding domain point away from the isoalloxazine moiety, while the side chain of Y53 points away from the active site pocket toward the bulk solvent (**Figure 2.6**)[36]. In the closed conformation, S45 and A46 side chains move closer to the isoalloxazine moiety and the side chain of Y53 gate swings back into the active site pocket to interact with the carboxylate group of the iminoarginine product [36]. S45 and A46 residues were mutated individually to alanine and glycine, respectively, to investigate the dynamics of loop L1 [57]. The molecular dynamics data indicate that in both S45A and A46G variants the Y53 gate has a higher probability to be in the open conformation as compared to the wild-type, where the gate has almost equal probability to be in the open and closed conformations during the simulation time[57]. Thus, it was concluded that the conformations of the S45/A46 switch and the Y53 gate are coupled[57]. Moreover, the intensity of the fluorescence spectroscopy showed an increase of ~ 2-fold in the S45A and A46G variant enzymes compared to the wild-type when the flavin was excited at its lower energy peak in the enzyme bound-flavin[57]. The emission peak of the flavin fluorescence of the enzyme-bound flavin was red-shifted from 513 nm in the wild-type to 522 nm in both the variant enzymes (**Figure 2.7**). It was concluded that the active site in the S45A and the A46G variant is more exposed to the solvent due to the higher probability of Y53 gate to stay in the open conformation with respect to wild-type *Pa*DADH[57].

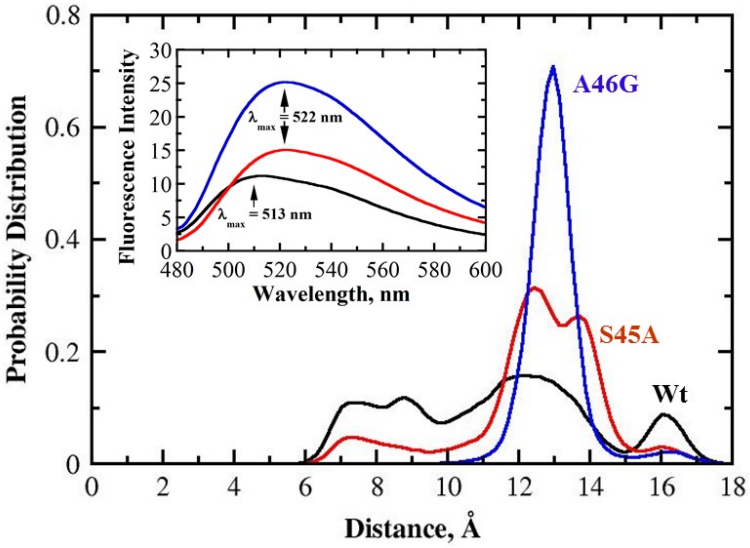

Figure 2.7 Probability distribution of the S45A, A46G variant enzymes and the wild-type. S45A variant is colored in blue, A46G variant in read and the wild-type in black. The inset represents the flavin fluorescence of the variants and the wild-type enzyme.

2.8.2 Dynamics of loop L1 in substrate capture and catalysis

The dynamics of loop L1 participate in the optimal orientation of the enzyme-substrate complex, as evidenced by molecular dynamics simulations and steady-state kinetic approaches[57]. The pH-independent k_{cat}/K_m values were lowered by 11- to 13-fold in the S45A and A46G variants compared to the wild-type[42, 57]. Based on the decreased k_{cat}/K_m values observed in the S45A and A46G variants, it was proposed that the likelihood of substrate capture in the variants is impaired due to the higher probability of the Y53 gate to be in the open conformation as compared to the wild-type enzyme[57]. A hollow was observed in the k_{cat} pH-profiles for both the S45A and A46G variants, consistent with a restricted proton transfer from the enzyme-substrate complex to the solvent[57]. To gain insight on the effect of loop L1 dynamics on the rate of flavin reduction, the reductive half-reaction of both variants was investigated. No conclusions could be gained on the status of flavin reduction since both variants could not be saturated with the slow substrate D-leucine[57].

The movement of side chain residues in mobile loops has been shown to participate in the catalytic function of several enzymes[58]. In *Rg*DAAO, Y238 was proposed to act as a gate that may control substrate entrance and product exit from the active site, and the corresponding residue in pDAAO, Y224, was proposed to contribute to the active site plasticity responsible for the binding of various substrates[40, 59]. Y215 in lactate oxidase and E89 in phosphoenolpyruvate carboxykinase, which are not in direct contact with the substrate, help to optimize substrate binding[60, 61]. Residues on flexible loop portions located at the entrance of enzymes not only act as gates but have been shown to shield the active site from the solvent upon binding of the substrate[58, 62-64].

2.9 Open questions

Although the mechanistic and structural features of *Pa*DADH have been established, the physiological electron acceptor of the enzyme has yet to be identified. *In vitro*, PMS has been used as an artificial electron acceptor. Based on the abundance of quinones in nature and their participation in many electron transport systems, quinones could possibly act as potential physiological electron acceptors. Oxygen reactivity could be useful in exploiting the enzyme function in industrial use to separate racemic mixtures. Engineering flavoprotein dehydrogenases to react with molecular oxygen to this day remains a challenging endeavor. Previous studies have established that there is no catalytic base in *Pa*DADH and the proton is simply transferred from the substrate amino group to the solvent in the active site of the enzyme. Investigation into identifying if there is a catalytic base functioning in *Pa*DADH is still under work. *Pa*DADH is part of a novel two-enzyme racemic system involved in D- to L-arginine racemization, since most of the racemization is catalyzed by a single enzyme. The presence of two enzymes instead of one could potentially serve as a regulatory mechanism. Further investigation of *Pa*DADH and

engineering variants that display oxygen reactivity can be utilized for enzymatic synthesis of various α-keto acids and the separation of racemic amino acid mixtures which are of potential interest to the industry.

2.10 References

[1] Gal, J. (2008) The discovery of biological enantioselectivity: Louis Pasteur and the fermentation of tartaric acid, 1857--a review and analysis 150 yr later, Chirality 20, 5-19.

[2] Pasteur, L. (1848) Mémoire sur la relation qui peut exister entre la forme cristalline et la composition chimique, et sur la cause de la polarisation rotatoire, Comptes rendus de l'Académie des sciences 26, 535–538.

[3] Pasteur, L. (1848) Sur les relations qui peuvent exister entre la forme cristalline, la composition chimique et le sens de la polarisation rotatoire, Annales de Chimie et de Physique 24, 442–459.

[4] Friedman, M. (1999) Chemistry, nutrition, and microbiology of D-amino acids, J. Agric. Food Chem. 47, 3457-3479.

[5] Fujii, N. (2002) D-amino acids in living higher organisms, Orig Life Evol Biosph 32, 103-127.

[6] Krebs, H. A. (1935) Metabolism of amino-acids: Deamination of amino-acids, Biochem J 29, 1620-1644.

[7] Pollegioni, L., Piubelli, L., Sacchi, S., Pilone, M. S., and Molla, G. (2007) Physiological functions of D-amino acid oxidases: from yeast to humans, Cell Mol. Life Sci. 64, 1373-1394.

[8] Pilone, M. S. (2000) D-Amino acid oxidase: new findings, Cell Mol Life Sci 57, 1732-1747.

[9] Job, V., Marcone, G. L., Pilone, M. S., and Pollegioni, L. (2002) Glycine oxidase from Bacillus subtilis. Characterization of a new flavoprotein, J. Biol. Chem. 277, 6985-6993.

[10] Trickey, P., Wagner, M. A., Jorns, M. S., and Mathews, F. S. (1999) Monomeric sarcosine oxidase: structure of a covalently flavinylated amine oxidizing enzyme, Structure 7, 331-345.

[11] Leys, D., Basran, J., and Scrutton, N. S. (2003) Channelling and formation of 'active' formaldehyde in dimethylglycine oxidase, EMBO J. 22, 4038-4048.

[12] Urich, K. (1968) [D-Glutamate oxidase from the antennal gland of the crayfish Oronectes limosus: purification and characterization], Z Naturforsch B 23, 1508-1511.

[13] Olsiewski, P. J., Kaczorowski, G. J., and Walsh, C. (1980) Purification and properties of D-amino acid dehydrogenase, an inducible membrane-bound iron-sulfur flavoenzyme from Escherichia coli B, J Biol Chem 255, 4487-4494.

[14] Satomura, T., Ishikura, M., Koyanagi, T., Sakuraba, H., Ohshima, T., and Suye, S. (2015) Dye-linked D-amino acid dehydrogenase from the thermophilic bacterium Rhodothermus marinus JCM9785: characteristics and role in trans-4-hydroxy-L-proline catabolism, Appl Microbiol Biotechnol 99, 4265-4275.

[15] Tsukada, K. (1966) D-amino acid dehydrogenases of Pseudomonas fluorescens, J Biol Chem 241, 4522-4528.

[16] Li, C., Yao, X., and Lu, C. D. (2010) Regulation of the dauBAR operon and characterization of D-amino acid dehydrogenase DauA in arginine and lysine catabolism of Pseudomonas aeruginosa PAO1, Microbiology 156, 60-71.

[17] Fischer, L., Gabler, M., Horner, R., and Wagner, F. (1996) Microbial D-amino acid oxidases (EC .4.3.3), Ann N Y Acad Sci 799, 683-688.

[18] Rodriguez-Crespo, I. (2008) D-amino acids in the brain: pyridoxal phosphate-dependent amino acid racemases and the physiology of D-serine, FEBS J 275, 3513.

[19] D'Aniello, A., D'Onofrio, G., Pischetola, M., D'Aniello, G., Vetere, A., Petrucelli, L., and Fisher, G. H. (1993) Biological role of D-amino acid oxidase and D-aspartate oxidase. Effects of D-amino acids, J Biol Chem 268, 26941-26949.

[20] Pollegioni, L., and Sacchi, S. (2010) Metabolism of the neuromodulator D-serine, Cell Mol Life Sci 67, 2387-2404.

[21] Negri, A., Massey, V., and Williams, C. H., Jr. (1987) D-aspartate oxidase from beef kidney. Purification and properties, J Biol Chem 262, 10026-10034.

[22] Tishkov, V. I., and Khoronenkova, S. V. (2005) D-Amino acid oxidase: structure, catalytic mechanism, and practical application, Biochemistry (Mosc) 70, 40-54.

[23] Li, C., and Lu, C. D. (2009) Arginine racemization by coupled catabolic and anabolic dehydrogenases, Proc Natl Acad Sci U S A 106, 906-911.

[24] Jann, A., Matsumoto, H., and Haas, D. (1988) The fourth arginine catabolic pathway of Pseudomonas aeruginosa, J Gen Microbiol 134, 1043-1053.

[25] Gannavaram, S., Sirin, S., Sherman, W., and Gadda, G. (2014) Mechanistic and computational studies of the reductive half-reaction of tyrosine to phenylalanine active site variants of D-arginine dehydrogenase, Biochemistry 53, 6574-6583.

[26] Rejsek, K., Formanek, P., and Vranova, V. (2010) The soil amino acids : quality, distribution, and site ecology, Nova Science Publishers, Hauppauge, N.Y.

[27] Erikson, O., Hertzberg, M., and Nasholm, T. (2004) A conditional marker gene allowing both positive and negative selection in plants, Nat. Biotechnol. 22, 455-458.

[28] Aldag, R. W., and Young, J. L. (1970) Aspects of D-leucine and D-lysine metabolism in maize and ryegrass seedlings, Planta 95, 187-201.

[29] Errico, F., Napolitano, F., Nistico, R., and Usiello, A. (2012) New insights on the role of free D-aspartate in the mammalian brain, Amino Acids 43, 1861-1871.

[30] Sacchi, S. (2013) D-Serine metabolism: new insights into the modulation of D-amino acid oxidase activity, Biochem Soc Trans 41, 1551-1556.

[31] Snyder, S. H., and Kim, P. M. (2000) D-amino acids as putative neurotransmitters: focus on D-serine, Neurochem Res 25, 553-560.

[32] Yoshimura, T., and Goto, M. (2008) D-amino acids in the brain: structure and function of pyridoxal phosphate-dependent amino acid racemases, FEBS J 275, 3527-3537.

[33] Yoshimura, T., and Esak, N. (2003) Amino acid racemases: functions and mechanisms, J Biosci Bioeng 96, 103-109.

[34] Cava, F., Lam, H., de Pedro, M. A., and Waldor, M. K. (2011) Emerging knowledge of regulatory roles of D-amino acids in bacteria, Cell Mol Life Sci 68, 817-831.

[35] Radkov, A. D., and Moe, L. A. (2014) Bacterial synthesis of D-amino acids, Appl. Microbiol. Biotechnol. 98, 5363-5374.

[36] Fu, G., Yuan, H., Li, C., Lu, C. D., Gadda, G., and Weber, I. T. (2010) Conformational changes and substrate recognition in Pseudomonas aeruginosa D-arginine dehydrogenase, Biochemistry 49, 8535-8545.

[37] Fu, G., Yuan, H., Wang, S., Gadda, G., and Weber, I. T. (2011) Atomic-resolution structure of an N5 flavin adduct in D-arginine dehydrogenase, Biochemistry 50, 6292-6294.

[38] Dixon, D. A., Lindner, D. L., Branchaud, B., and Lipscomb, W. N. (1979) Conformations and electronic structures of oxidized and reduced isoalloxazine, Biochemistry 18, 5770-5775.

[39] Kao, Y. T., Saxena, C., He, T. F., Guo, L., Wang, L., Sancar, A., and Zhong, D. (2008) Ultrafast dynamics of flavins in five redox states, J Am Chem Soc 130, 13132-13139.

[40] Todone, F., Vanoni, M. A., Mozzarelli, A., Bolognesi, M., Coda, A., Curti, B., and Mattevi, A. (1997) Active site plasticity in D-amino acid oxidase: a crystallographic analysis, Biochemistry 36, 5853-5860.

[41] Mattevi, A., Vanoni, M. A., Todone, F., Rizzi, M., Teplyakov, A., Coda, A., Bolognesi, M., and Curti, B. (1996) Crystal structure of D-amino acid oxidase: a case of active site mirror-image convergent evolution with flavocytochrome b2, Proc Natl Acad Sci U S A 93, 7496-7501.

[42] Ball, J., Bui, Q. V., Gannavaram, S., and Gadda, G. (2015) Importance of glutamate 87 and the substrate alpha-amine for the reaction catalyzed by D-arginine dehydrogenase, Arch Biochem Biophys 568, 56-63.

[43] Pollegioni, L., Diederichs, K., Molla, G., Umhau, S., Welte, W., Ghisla, S., and Pilone, M. S. (2002) Yeast D-amino acid oxidase: structural basis of its catalytic properties, J Mol Biol 324, 535-546.

[44] Meyer, E. A., Castellano, R. K., and Diederich, F. (2003) Interactions with aromatic rings in chemical and biological recognition, Angew Chem Int Ed Engl 42, 1210-1250.

[45] Komarova, N. V., Golubev, I. V., Khoronenkova, S. V., Chubar, T. A., and Tishkov, V. I. (2012) Engineering of substrate specificity of D-amino acid oxidase from the yeast

Trigonopsis variabilis: directed mutagenesis of Phe258 residue, Biochemistry (Mosc) 77, 1181-1189.

[46] Yuan, H., Fu, G., Brooks, P. T., Weber, I., and Gadda, G. (2010) Steady-state kinetic mechanism and reductive half-reaction of D-arginine dehydrogenase from Pseudomonas aeruginosa, Biochemistry 49, 9542-9550.

[47] Pudek, M. R., and Bragg, P. D. (1976) Redox potentials of the cytochromes in the respiratory chain of aerobically grown Escherichia coli, Arch Biochem Biophys 174, 546-552.

[48] Yuan, H., Xin, Y., Hamelberg, D., and Gadda, G. (2011) Insights on the mechanism of amine oxidation catalyzed by D-arginine dehydrogenase through pH and kinetic isotope effects, J. Am. Chem. Soc. 133, 18957-18965.

[49] Gadda, G., and Fitzpatrick, P. F. (2000) Iso-mechanism of nitroalkane oxidase: 1. Inhibition studies and activation by imidazole, Biochemistry 39, 1400-1405.

[50] Rouviere, N., Mayer, M., Tegoni, M., Capeillere-Blandin, C., and Lederer, F. (1997) Molecular interpretation of inhibition by excess substrate in flavocytochrome b2: a study with wild-type and Y143F mutant enzymes, Biochemistry 36, 7126-7135.

[51] Wang, Z., Chernyshev, A., Koehn, E. M., Manuel, T. D., Lesley, S. A., and Kohen, A. (2009) Oxidase activity of a flavin-dependent thymidylate synthase, FEBS J 276, 2801-2810.

[52] Itoh, K., Asakawa, T., Hoshino, K., Adachi, M., Fukiya, K., Watanabe, N., and Tanaka, Y. (2009) Functional analysis of aldehyde oxidase using expressed chimeric enzyme between monkey and rat, Biol Pharm Bull 32, 31-35.

[53] Igarashi, K., Momohara, I., Nishino, T., and Samejima, M. (2002) Kinetics of inter-domain electron transfer in flavocytochrome cellobiose dehydrogenase from the white-rot fungus Phanerochaete chrysosporium, Biochem J 365, 521-526.

[54] Cook, P. F., Kenyon, G. L., and Cleland, W. W. (1981) Use of pH studies to elucidate the catalytic mechanism of rabbit muscle creatine kinase, Biochemistry 20, 1204-1210.

[55] Ralph, E. C., Anderson, M. A., Cleland, W. W., and Fitzpatrick, P. F. (2006) Mechanistic studies of the flavoenzyme tryptophan 2-monooxygenase: deuterium and 15N kinetic isotope effects on alanine oxidation by an L-amino acid oxidase, Biochemistry 45, 15844-15852.

[56] Emanuele, J. J., and Fitzpatrick, P. F. (1995) Mechanistic studies of the flavoprotein tryptophan 2-monooxygenase. 2. pH and kinetic isotope effects, Biochemistry 34, 3716-3723.

[57] Ouedraogo, D., Souffrant, M., Vasquez, S., Hamelberg, D., and Gadda, G. (2017) Importance of Loop L1 Dynamics for Substrate Capture and Catalysis in Pseudomonas aeruginosa D-Arginine Dehydrogenase, Biochemistry.

[58] Gora, A., Brezovsky, J., and Damborsky, J. (2013) Gates of enzymes, Chem Rev 113, 5871-5923.

[59] Boselli, A., Sacchi, S., Job, V., Pilone, M. S., and Pollegioni, L. (2002) Role of tyrosine 238 in the active site of Rhodotorula gracilis D-amino acid oxidase. A site-directed mutagenesis study, Eur. J. Biochem. 269, 4762-4771.

[60] Stoisser, T., Brunsteiner, M., Wilson, D. K., and Nidetzky, B. (2016) Conformational flexibility related to enzyme activity: evidence for a dynamic active-site gatekeeper function of Tyr(215) in Aerococcus viridans lactate oxidase, Sci Rep 6, 27892.

[61] Johnson, T. A., McLeod, M. J., and Holyoak, T. (2016) Utilization of Substrate Intrinsic Binding Energy for Conformational Change and Catalytic Function in Phosphoenolpyruvate Carboxykinase, Biochemistry 55, 575-587.

[62] Sampson, N. S., and Knowles, J. R. (1992) Segmental movement: definition of the structural requirements for loop closure in catalysis by triosephosphate isomerase, Biochemistry 31, 8482-8487.

[63] Schnell, J. R., Dyson, H. J., and Wright, P. E. (2004) Structure, dynamics, and catalytic function of dihydrofolate reductase, Annu. Rev. Biophys. Biomol. Struct. 33, 119-140.

[64] Newby, Z., Lee, T. T., Morse, R. J., Liu, Y., Liu, L., Venkatraman, P., Santi, D. V., Finer-Moore, J. S., and Stroud, R. M. (2006) The role of protein dynamics in thymidylate synthase catalysis: variants of conserved 2'-deoxyuridine 5'-monophosphate (dUMP)-binding Tyr-261, Biochemistry 45, 7415-7428.

3 IMPORTANCE OF GLUTAMATE 87 AND THE SUBSTRATE α-AMINE IN THE REACTION CATALYZED BY D-ARGININE DEHYDROGENASE

(This chapter has been published *verbatim* in Ball J., Bui Q.V., Gannavaram S., and Gadda G. (2015), Arch Biochem Biophys, 568, 56-63; the author contributed the pH effects with D-arginine and D-Lys, and the pH effects with the H48F variant.)

3.1 Abstract

Pseudomonas aeruginosa D-arginine dehydrogenase (*Pa*DADH) catalyzes the oxidation of D-arginine to iminoarginine, which is non-enzymatically hydrolyzed to 2-ketoarginine and ammonia. Here, site-directed mutagenesis and pH effects were used to investigate binding and catalysis of zwitterionic and cationic substrates for the enzyme. An unprotonated group with apparent pK_a value ≥7.9 is required for binding D-arginine or D-lysine, but not D-methionine or D-leucine. This group is E87, as suggested by its replacement with leucine. An unprotonated group with pK_a of 9.5, which persists in the H48F and E87L variants, is required for amine oxidation with all substrates. Since Y53 and Y249 were previously ruled out, the pK_a is assigned to the substrate α-NH_3^+ group, which previous QM/MM and K_d pH-profile demonstrated to be protonated for preferred binding to the enzyme. Lack of pH effects on the $^Dk_{red}$ with D-leucine established 9.5 as the intrinsic pK_a, and D-leucine as a non-sticky substrate. D-Arginine, D-lysine and D-methionine and their corresponding iminoproducts were significantly stickier than D-leucine, as indicated by apparent pK_a values <9.5 in both k_{cat}/K_m and k_{cat}. Restricted proton movements in catalysis were established from hollowed k_{cat} pH profiles in wild-type PaDADH with D-lysine and in the H48F and E87L enzymes with D-arginine.

3.2 Introduction

Pseudomonas aeruginosa D-arginine dehydrogenase (*Pa*DADH) catalyzes the flavin-mediated, oxidative deamination of D-arginine to iminoarginine, followed by the non-enzymatic hydrolysis in solution of the imino product to give 2-ketoarginine and ammonia (**Scheme 3.1**).[1]

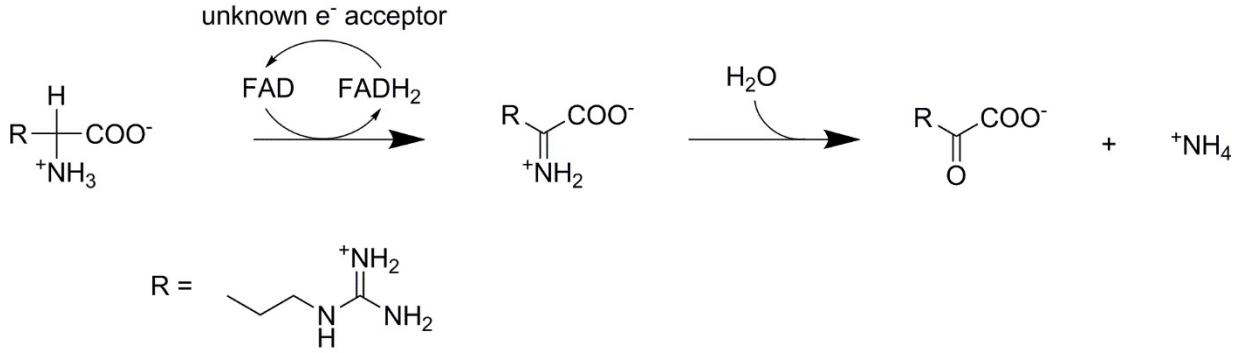

Scheme 3.1 Oxidation of D-Arginine by *Pa*DADH.

All the standard D-amino acids except D-glutamate, D-aspartate, and glycine are oxidized by the enzyme,[1, 2] with D-arginine and D-lysine displaying the highest rate constants for substrate capture, k_{cat}/K_m, of 10^5-10^6 $M^{-1}s^{-1}$.[2] *Pa*DADH is one of the few known enzymes that can oxidize cationic D-amino acids with great efficiency, sharing strikingly similar substrate specificity to D-amino acid oxidase (DAAO) from *Arthrobacter protophormiae*.[3] Acidic D-amino acids are oxidized by the highly selective D-aspartate oxidases.[4, 5] L-Amino acids are not substrates for *Pa*DADH.[2] *Pa*DADH is a strict dehydrogenase because during turnover it reacts with an electron acceptor other than molecular oxygen, presumably ubiquinone *in vivo*.[6] The enzyme follows a Ping-Pong Bi-Bi steady-state kinetic mechanism, as demonstrated with D-arginine or D-histidine as substrate and phenazine methosulfate (PMS) as electron acceptor.[6] In the reductive half-reaction the enzyme-bound flavin (*Pa*DADH$_{ox}$) is reduced to hydroquinone with concomitant oxidation of the amino acid to the imino acid (*Pa*DADH$_{ox}$-P), as shown in

Scheme 3.2. In the oxidative half-reaction, the reduced flavin is oxidized (*in vitro*) by PMS (**Scheme 3.3**).

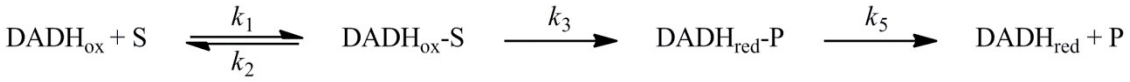

Scheme 3.2 Reductive half-reaction of *Pa*DADH.

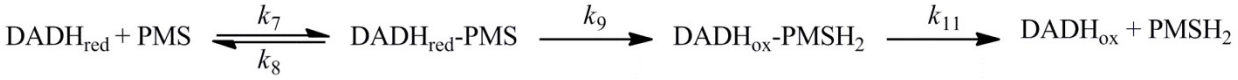

Scheme 3.3 Oxidative half-reaction of *Pa*DADH.

Flavin reduction is irreversible with D-histidine or D-leucine as substrate, as established by a zero intercept value in a plot of the observed rate constant for flavin reduction as a function of substrate concentration.[6] With D-arginine, however, the reaction is too fast and cannot be studied in a stopped-flow spectrophotometer due to >80% of the flavin being completely reduced within the mixing time of the instrument (i.e., 2.2 ms), as previously reported.[6] Amine oxidation has been studied with D-leucine, which is amenable to mechanistic investigation using a stopped-flow spectrophotometer, with pH, substrate and solvent kinetic isotope effects, as well as computational studies.[7] Free energy calculations and the pH profile for K_d are consistent with the enzyme binding preferentially the zwitterionic form of D-leucine.[7] After isomerization of the enzyme-substrate complex, amine deprotonation triggers the oxidation reaction, with cleavages of the NH and CH bonds of D-leucine occurring asynchronously, as suggested by multiple deuterium kinetic isotope effects on the rate constant for flavin reduction.[7] In this respect *Pa*DADH is similar to proline dehydrogenase,[8] but different from other flavin-dependent amine oxidases, such as DAAO or monomeric sarcosine oxidase, for which amine oxidation occurs from the anionic substrate.[9]

The three-dimensional structures of *Pa*DADH in complex with iminoarginine or iminohistidine, or in the unliganded form, have been previously solved at high resolution (1.06-1.3 Å), along with an atomic-resolution structure of a 4-methyl-2-pentanone-FAD adduct in the enzyme co-crystallized with D-leucine.[2, 10] The structure of the enzyme in complex with iminoarginine underlines the importance of the side chain carboxylate of E87 for binding the cation of the iminoarginine side chain, as shown in **Figure 3.1**.[10]

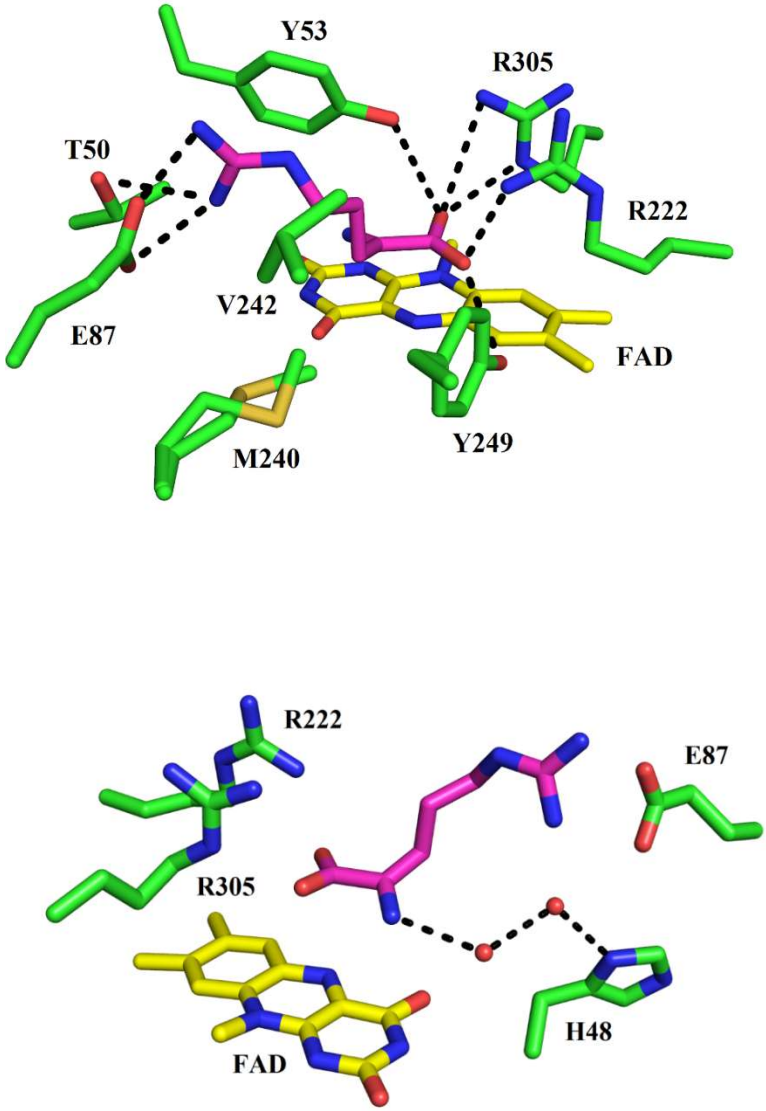

Figure 3.1 Interactions of iminoarginine with active site residues of *Pa*DADH.
Carbon atoms are colored green for each of the *Pa*DADH active site residues and magenta for iminoarginine. FAD is represented by its isoalloxazine ring with the C atoms colored yellow. H-bond and ionic interactions are shown as dashed lines. Two water molecules in the binding site are shown as red spheres. For clarity, panels A and B focus on different interactions. Note that the side chain of M240 is present in two alternate conformations.

Two tyrosine residues, i.e., Y53 and Y249, with the aid of M240 and V242 arrange into a hydrophobic pocket that surrounds the central part of the iminoarginine side chain. The imine of the imino-product is connected to H48 through two intervening water molecules (**Figure 3.1B**). The imino-product Cα atom is close to the flavin N(5) atom, presumably indicating where the Cα atom of the amino acid substrate resides during catalysis. The structure of the enzyme in complex with iminohistidine demonstrates that the imidazole of the ligand is present in two alternate conformations, with H-bonding interactions with the side chains of H48, T50, and either E87 or Q336. A mobile loop, composed of residues 50-56, is present in two alternate conformations in the unliganded and product-bound enzyme structures.[2] This flexible loop forms an active site lid and is proposed to play an important role for substrate specificity and recognition, allowing the enzyme to accommodate bulky substrates like phenylalanine or tryptophan.[2]

In this study, we have used mechanistic approaches to investigate further the reaction of amine oxidation catalyzed by *Pa*DADH. Effects of pH were determined on the steady-state kinetic parameters with selected substrates and on the kinetic isotope effects associated with flavin reduction using D-leucine. Mutagenesis of specific residues hypothesized to be important for catalysis or binding has been carried out to facilitate in the assignment of the observed pK_a values. The results shed light on the ionization states of groups that are relevant to amine oxidation and provide further mechanistic insight on the catalytic mechanism for amine oxidation by *Pa*DADH.

3.3 Experimental Procedures

3.3.1 Materials

D-Methionine and D-leucine were purchased from Sigma-Aldrich (St. Louis, MO). D-Arginine and D-lysine were obtained from Alfa-Aesar (Ward Hill, MA). D-Leucine$_{d10}$ was obtained from CDN Isotopes (Pointe-Claire, Canada). PaDADH-wt was prepared as described previously.[2, 6] All other reagents used were of the highest purity commercially available.

3.3.2 Steady-state kinetics

The steady-state kinetic parameters for D-arginine, D-lysine, or D-methionine were measured polarographically on a computer-interfaced O_2 electrode by using the method of initial rates. The enzyme does not react with O_2, hence as electron acceptor we used PMS, which spontaneously reacts in its reduced form with molecular oxygen.[11] The reaction was initiated by the addition of the enzyme, with final concentrations ranging from 5 nM to 2 μM depending on pH and the substrate used, yielding a reaction volume of 1 mL. Substrate concentrations ranged from 0.01-100 mM for D-arginine, 0.25-250 mM for D-lysine, 1-186 mM for D-methionine, and 0.5-50 mM for D-leucine, ensuring that the K_m values determined were within the range of substrate concentrations used at any given pH. The same concentrations of D-arginine were used as substrate for the H48F and E87L enzyme variants. The assays were carried out at 25 ^{o}C in 20 mM sodium pyrophosphate (pH 8.5-10.0), 20 mM sodium phosphate (pH 6.0-8.5) or 20 mM piperazine (pH 4.75-6.0). The same buffers, substrate concentrations, and enzyme concentrations were used for the assays performed at 6 ^{o}C. Substrate solutions were prepared in buffer and the pH values were adjusted prior to addition to the reaction mixtures. The concentration of PMS was kept fixed at 1 mM to ensure full saturation of the enzyme. Data for D-leucine with the wild-type were taken from Yuan *et al*.[7]

3.3.3 Kinetic isotope effects

The reductive half-reaction of PaDADH with D-leucine was monitored using an SF-61DX2 Hi-Tech KinetAsyst high performance stopped-flow spectrophotometer thermostated at 25 ^{o}C. The observed first-order rate constants for flavin reduction (k_{obs}) were determined at varying concentrations of D-leucine or D-leucine$_{d10}$ between 0.5 and 50 mM under pseudo first-order conditions using the buffer system described above at pH 7.0, 8.5, and 10.0. Multiple measurements typically differed by ≤5%.

3.3.4 Mutagenesis

Mutagenesis to prepare the H48F or E87L variants of the enzyme was performed following the QuikChange protocol using the cloned wild-type gene pET20b(+)/PA3863 as template. The forward primer for H48F was 5'-GCTCCGCCGCGTTCTACACGGTGGCCTA-3', while that for E87L was 5'-AGCCCGCGTCCGCTGATGGTGGTCGACTTC-3' The underlined portions represent the mutated sites. Oligonucleotide primers were purchased from Sigma Genosys (The Woodlands, TX). Plasmids were purified using kits from Qiagen, Inc (Valencia, CA). Sequencing was performed by the GSU Biology Core Facility using an Applied Biosystems Big Dye Kit on an Applied Biosystems model ABI377 DNA sequencer. The expression and purification of H48F and E87L mutant enzymes followed the same protocol as the wild-type enzyme.[2, 6]

3.3.5 Data analysis

Kinetic data were analyzed with KaleidaGraph software (Synergy Software, Reading, PA) and the Kinetic Studio Software Suite (Hi-Tech Scientific, Bradford on Avon, U.K.). Stopped-flow traces were fit to eq 1, which describes a single exponential process where k_{obs} represents the observed first-order rate constant for flavin reduction at any given concentration of

substrate, t is time, A is the absorbance at 446 nm at any given time, B is the amplitude of the absorbance change, and C is the absorbance at infinite time, which in this case is the non-zero absorbance of the fully reduced enzyme. Kinetic parameters for the reductive half-reactions were determined by using eq 2, where k_{obs} is the observed first-order rate constant for the reduction of the enzyme-bound flavin at any given concentration of substrate (S), k_{red} is the limiting first-order rate constant for flavin reduction at saturating concentrations of substrate, and ${}^{app}K_d$ is the apparent dissociation constant for binding of the substrate to the enzyme.

The apparent steady-state kinetic parameters at varying substrate concentrations were determined by using the Michaelis-Menten equation for a single substrate. Previous results demonstrated a Ping Pong Bi–Bi steady-state kinetic mechanism for PaDADH for both the fast substrate arginine and the slow substrate histidine, with a K_m value for PMS of ~10 μM.[6] Consequently, and after considering the results of the pH effect obtained in this study, when the steady-state kinetic parameters were determined at a fixed concentration of 1 mM PMS they approximate well the true k_{cat}, K_m, and k_{cat}/K_m values for the amino acid substrate.

The pH profiles of the k_{cat} values for D-arginine and k_{cat} and k_{cat}/K_m values for D-methionine were fit to eq 3, which describes a curve that increases at increasing pH with slope of +1 and a limiting value (C) at high pH. The pH profiles of the k_{cat}/K_m values for D-arginine and D-lysine were fit to eq 4, which describes a curve that increases at increasing pH with slope of +2, a limiting value (C) at high pH and two indistinguishable pK_a values. The pH profiles of the k_{cat} values for D-lysine with the wild-type enzyme and D-arginine with the H48F and E87L enzymes were fit to eq 5, which describes a curve that increases with increasing pH to a limiting value (C) to yield three pH dependent terms containing a hollow that is defined by $\beta = 1 + k_3/k_2$ and $K_\alpha = (k_1/k_7)(1+k_8/k_5)K_1$. Here, p$K_e$ is the intrinsic pK_a value for k_{cat}, β reflects the stickiness

of the substrate (k_3/k_2), and K_α describes the relative rates of the kinetic steps involved in the equilibration of ESH+ complex. [12]

$$A = Be^{-k_{obs}t} + C \quad (1)$$

$$k_{obs} = \frac{k_{red}S}{{}^{app}K_d + S} \quad (2)$$

$$\log(k_{cat}, k_{cat}/K_m) = \log\left(\frac{C}{1+10^{(pK_a - pH)}}\right) \quad (3)$$

$$\log(k_{cat}/K_m) = \log\left(\frac{C}{1+10^{(pK_a - pH)^2}}\right) \quad (4)$$

$$\log(k_{cat}) = \log\left(\frac{C*(1+10^{(pK_\alpha - p\ )})}{(1+10^{(pK_e - pH)})(1+10^{(\beta pK_\alpha - pH)})}\right) \quad (5)$$

Standard errors were obtained from KaleidaGraph's "General curve fit", which uses the Levenburg-Marquardt algorithm.[13]

3.4 Results

3.4.1 Steady-state kinetics with D-leucine at variable concentration of PMS

The steady-state kinetic parameters for D-leucine as substrate for PaDADH were measured at two concentrations of PMS (0.1 and 1 mM) at pH 6.0 and 10.0, in order to ensure full saturation of PMS was achieved across the pH range used. As shown in **Table 3.1**, the kinetic parameters were indistinguishable at both pH values, consistent with the enzyme being fully saturated at 1 mM PMS. In agreement with these results, previous data with D-arginine and D-histidine at pH 8.7 established a $K_m \leq 10$ μM for PMS.[6] Since the enzyme follows a Ping Pong Bi–Bi steady-state kinetic mechanism,[6] it is concluded that 1 mM PMS saturates the enzyme irrespective of the substrate used within the pH range used in this study.

Table 3.1 Apparent steady-state kinetic parameters at saturating PMS

[PMS] (mM)	pH	k_{cat} (s^{-1})	K_m (mM)	k_{cat}/K_m ($M^{-1}s^{-1}$)	$(R^2)^a$
0.1	6.0	0.061 (±0.002)	1.8 (±0.2)	33 (±3)	0.994
1.0	6.0	0.059 (±0.002)	1.6 (±0.1)	36 (±3)	0.995
0.1	10.0	55 (±1)	4.6 (±0.3)	12,000 (±1,000)	0.998
1.0	10.0	53 (±1)	4.4 (±0.3)	12,000 (±1,000)	0.997

Experimental conditions: 20 mM sodium pyrophosphate in H_2O at 25 °C. Data were acquired at varying concentrations of D-leucine and fixed PMS concentrations of 0.1 and 1.0 mM yielding overlapping saturation curves.

[a] Coefficient of determination, which in the algorithm used in KaleidaGraph is: $R^2 = 1 - \frac{\chi^2}{\sum_i \sigma_i (y_i - \bar{y})^2}$, where χ^2 is defined as Chi Square, σ_i is the weight, y_i is the actual value, and $\bar{y}$ is the mean of actual values.

3.4.2 k_{cat}/K_m and k_{cat} pH-profiles with cationic substrates

The pH-dependences of the steady-state kinetic parameters k_{cat}/K_m and k_{cat} were determined with D-arginine or D-lysine as substrate to establish relevant ionizations of groups involved in binding or catalysis with substrates carrying a positive charge on the side chain. As shown in **Figure 3.2**, the k_{cat} pH-profile with D-arginine increased to a limiting value at high pH, defining the requirement for an unprotonated group for catalysis. With D-lysine as substrate a similar pattern was seen at low pH, with an unprotonated group required for catalysis having a pK_a similar to that seen with D-arginine, although the enzyme could not be saturated with D-lysine below pH 6.0 (**Figure 3.2**). Despite similar k_{cat} values with the two substrates up to pH 7.5, turnover with D-lysine was significantly faster than with D-arginine at high pH, and the curve demonstrated a hollow that yielded three pK_a values. Both D-lysine and D-arginine had k_{cat}/K_m pH-profiles increasing to limiting values with increasing pH (**Figure 3.2**). However, the ascending limbs clearly showed the presence of two unprotonated groups rather than the single one seen in the k_{cat} pH-profiles. The apparent pK_a values and the pH-independent, limiting values of k_{cat}/K_m and k_{cat} determined with D-arginine and D-lysine are summarized in **Table 3.2**.

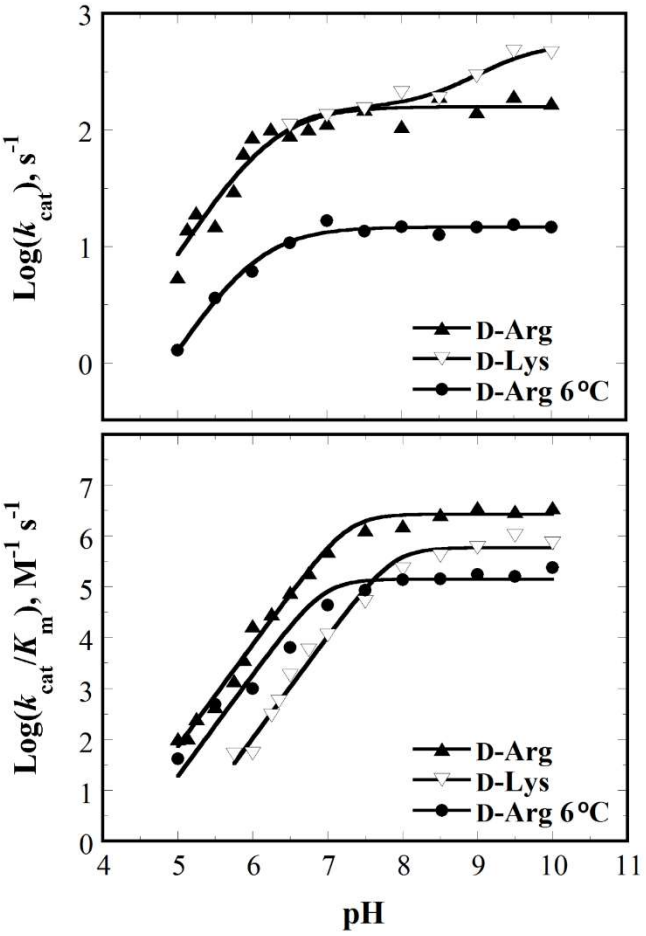

Figure 3.2 pH-profiles of k_{cat} (A) and k_{cat}/K_m (B) with D-arginine (▲), D-lysine (∇), and D-arginine (●) at 6 ^{o} C.
*Pa*DADH activity was measured at varying concentrations of D-arginine or D-lysine and 1 mM PMS at 25 ^{o}C, unless otherwise stated. Curves represent fits of the data to eqs 3-5.

Table 3.2 pH Effects on k_{cat}/K_m and k_{cat} of *Pa*DADH

	k_{cat}/K_m			k_{cat}			
	pK_{a1}	pK_{a2}	$(k_{cat}/K_m)_H$[a] ($M^{-1}s^{-1}$)	pK_a	pK_α	pK_e	$(k_{cat})_H$[a] (s^{-1})
cationic substrates							
D-arginine	7.2[b,c]	7.2[b,c]	2,600,000 (±500,000)	6.3[b,d]	–	–	160 (±20)
D-lysine	7.9[b,c]	7.9[b,c]	580,000 (±150,000)	~6.2[e,f,g,h]	8.7[f,g]	9.2[f,g]	~550[j]
D-arginine 6 °C	6.9[b]	6.9[b,c]	140,000 (±40,000)	6.0[b,d]	–	–	
zwitterionic substrates							
D-methionine	7.7[b,d]	–	36,000 (±6,000)	6.9[b,d]	–	–	190 (±20)
D-leucine[i]	~9.5[d,j]	–	~11,000[j]	~9.5[d,j]	–	–	~100[j]

[a] pH-independent limiting value at high pH.
[b] (±0.1).
[c] Determined by using eq 4.
[d] Determined by using eq 3.
[e] Inferred by visual inspection of Figure 2A.
[f] (±0.3).
[g] Determined by using eq 5.
[h] βpK_α
[i] From Yuan *et al.[7]*
[j] Approximate value, due to plateau being not well defined.

3.4.3 k_{cat}/K_m and k_{cat} pH-profiles with D-arginine at 6 °C

Previous studies on creatine kinase by Cook *et al.* demonstrated that altering temperature may induce hollowed pH profiles of steady-state kinetic parameters.[14] In an effort to evaluate if this could be the case for *Pa*DADH with D-arginine, the pH profiles of the steady-state kinetic parameters were determined at 6 °C. As shown in Figure 2A, no hollow was detected for the pH profile of the k_{cat}, which qualitatively looked similar to that obtained at 25 °C. **Table 3.2** summarizes the apparent pK_a values and the pH-independent, limiting values of k_{cat}/K_m and k_{cat} determined with D-arginine at 6 °C.

3.4.4 k_{cat}/K_m and k_{cat} pH-profiles with zwitterionic substrates

The pH-dependences of the steady-state kinetic parameters k_{cat}/K_m and k_{cat} were determined with D-methionine or D-leucine as substrate to establish relevant ionizations of

groups involved in binding or catalysis with substrates not carrying a positive charge on the side chain. With both D-methionine and D-leucine, the pH-profiles of the k_{cat} and k_{cat}/K_m values increased with increasing pH, reaching limiting values at high pH, and demonstrating the requirement for a single unprotonated group for catalysis (**Figure 3.3**).

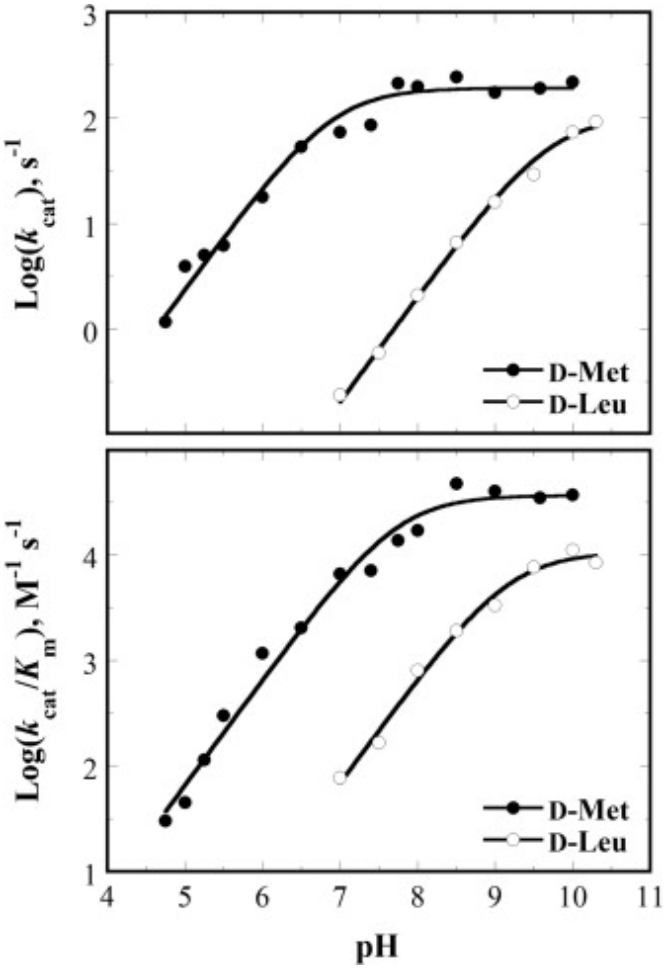

Figure 3.3 pH-profiles of k_{cat} and k_{cat}/K_m with D-methionine (●) and D-leucine (○). PaDADH activity was measured at varying concentrations of d-methionine or d-leucine and 1 mM PMS at 25 °C. Curves represent fits of the data to Eq. 3.

3.4.5 k_{cat}/K_m and k_{cat} pH-profiles with H48F variant

The pH-dependences of the steady-state kinetic parameters k_{cat}/K_m and k_{cat} were determined with D-arginine in the H48F variant to investigate if H48 acts as a catalytic base in amine oxidation. The k_{cat}/K_m pH profiles of the H48F enzyme resembled that obtained with the

wild-type enzyme; however, the k_{cat} pH profile did not exhibit a pronounced hollow describing three pK_a values (**Figure 3.4**), as for the case of D-lysine with wild-type PaDADH. Thus, H48 was not responsible for the pK_a values seen in the wild-type enzyme. **Table 3.3** summarizes the apparent pK_a values and the pH-independent, limiting values of k_{cat}/K_m and k_{cat}.

Table 3.3 pH Effects on k_{cat}/K_m and k_{cat} of PaDADH Variants with D-Arginine as Substrate.

	k_{cat}/K_m				k_{cat}		
	pK_{a1}	pK_{a2}	$(k_{cat}/K_m)_H$[a]($M^{-1}s^{-1}$)	βpK_α	pK_α	pK_e	$(k_{cat})_H$[a](s^{-1})
PaDADH Variant							
H48F	7.1[b,c]	7.1[b,c]	1,100,000 (±240,000)	6.1[b,d]	8.9[b,d]	9.4[d,e]	~150[f]
E87L	8.2[g,h]	–	150,000 (±50,000)	~5.5[i]	9.0[b,d]	9.7[d,h]	~150[f]

[a] pH-independent limiting value at high pH.
[b] (±0.1).
[c] Determined by using eq 4.
[d] Determined by using eq 5.
[e] (±0.3).
[f] Approximate value, due to plateau being not well defined.
[g] Determined by using eq 3.
[h] (±0.2).
[i] Approximate value, not able to populate limb because of increasing K_m at acidic pH.

3.4.6 k_{cat}/K_m and k_{cat} pH-profiles with E87L variant

The pH-dependences of the steady-state kinetic parameters k_{cat}/K_m and k_{cat} were determined with D-arginine in the E87L variant to investigate the role of E87 in amine oxidation. The k_{cat} pH profile of the E87L variant increased with increasing pH to reach a limiting value at high pH, exhibiting three pH dependent terms (**Figure 3.4**). In contrast to the wild-type k_{cat}/K_m, the E87L variant demonstrated the requirement for only a single unprotonated group for maximal activity. **Table 3.3** summarizes the apparent pK_a values and the pH-independent, limiting values of k_{cat}/K_m and k_{cat}.

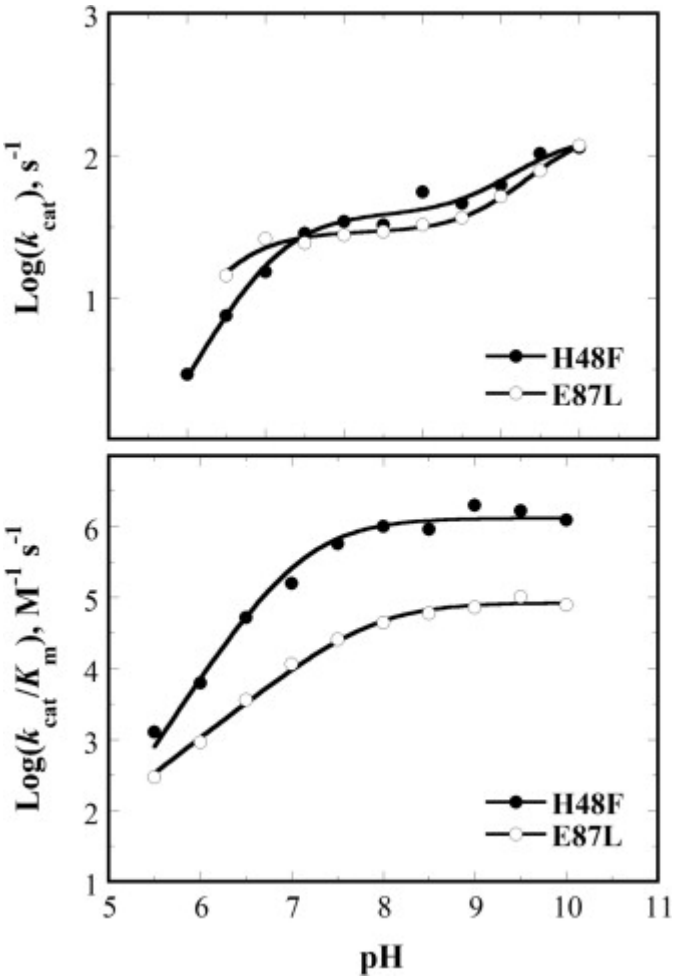

Figure 3.4 pH-profiles of k_{cat} and k_{cat}/K_m with PaDADH variants H48F (●) and E87L (○). PaDADH activity was measured at varying concentrations of D-arginine and 1 mM PMS at 25 °C. Curves represent fits of the data to Eqs. (3)–(5).

3.4.7 $^{D}k_{red}$ pH-profile with D-leucine

The pH-dependence of the kinetic isotope effects on the rate constant for flavin reduction at saturating substrate (k_{red}) was determined with D-leucine to establish if the latter is a slow substrate for PaDADH for which apparent and intrinsic pK_a values are identical. Since the reaction is too fast with D-arginine, it could not be studied in a stopped-flow spectrophotometer, as previously reported.[6] Flavin reduction was followed at 446 nm upon mixing the enzyme with varying concentrations of D-leucine in a stopped-flow spectrophotometer, yielding monophasic traces (**Figure 3.5** shows the case of pH 8.5, with pH 7.0 and 10.3 being similar).

The $^{D}k_{red}$ values were computed from the ratio of the k_{red} values with D-leucine and D-leucine$_{d10}$ determined by plotting the observed rate constants for flavin reduction as a function of substrate concentration. As illustrated in **Table 3.4**, the $^{D}k_{red}$ had similar values in the pH range from 7.0 to 10.3.

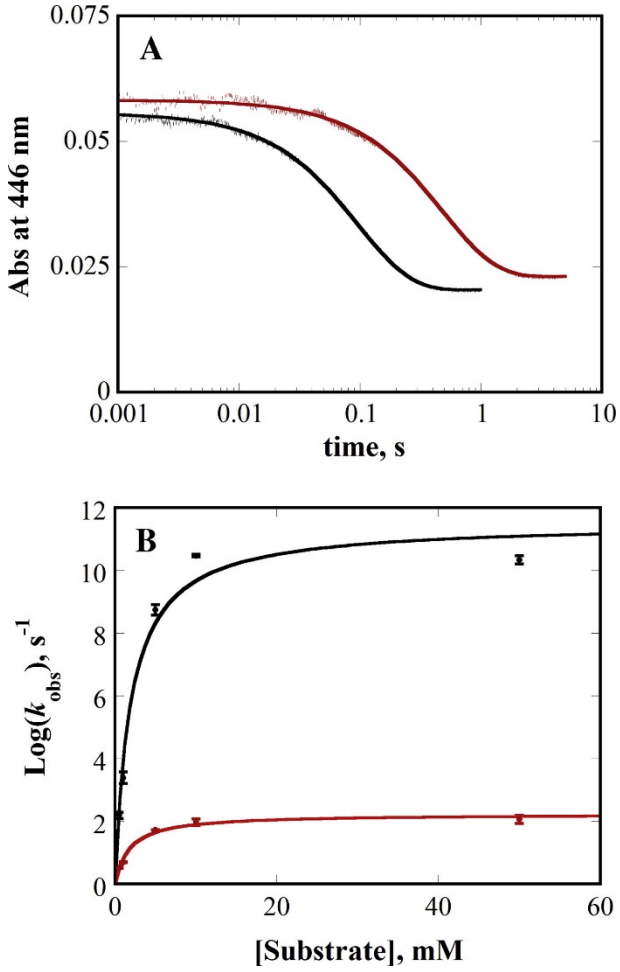

Figure 3.5 Kinetic isotope effects on k_{red} at pH 8.5 with D-leucine (black) and D-leucine$_{d10}$ in (red).
Panel A shows representative time courses for the light and heavy substrate at 50 mM substrate concentration; the traces were fit to Eq. (1). Panel B shows the concentration dependences of the observed rate constants for flavin reduction at different substrate concentrations of protiated and deuterated leucine.

Table 3.4 pH effects on kinetic isotope effects with D-leucine.

pH	$^{D}k_{red}$
7.0[a]	4.6 (±0.9)
8.5[b]	5.2 (±0.4)
10.3[c]	5.1 (±0.1)

Experimental conditions: 20 mM [a]sodium phosphate and [b]sodium pyrophosphate in H_2O at 25 °C with between 0.5 to 50 mM D-leucine and D-leucine-d_{10}.
[c] From Yuan *et al.[7]*

3.5 Discussion

The substrates of PaDADH, which displays broad specificity being able to oxidize most of the D-amino acids except D-aspartate, D-glutamate, and glycine,[2] can be classified as cationic or zwitterionic, depending on the presence of a charge on the side chain. In this study, we have used D-arginine, D-lysine, D-methionine and D-leucine to investigate mechanistically how cationic and zwitterionic substrates bind to and are oxidized by PaDADH. Insights on the roles played by several functional groups in the active site of the enzyme have emerged from the investigation of wild-type and selected active site variants of the enzyme, as discussed below.

The unprotonated side chain of E87 is important for binding cationic substrates through an electrostatic interaction with the substrate side chain. This conclusion is supported by pH profiles of the steady-state kinetic parameters, site-directed mutagenesis and previously published X-ray structures of the enzyme in complex with the iminoarginine product.[2] While a single unprotonated group is required to achieve maximal k_{cat}/K_m values at high pH with the zwitterionic substrates D-methionine and D-leucine, two groups are seen in the k_{cat}/K_m pH-profiles with the cationic substrates D-arginine and D-lysine. The extra unprotonated group must be involved in substrate binding rather than catalysis, since it is not seen in the k_{cat} pH-profiles, which show the requirement for a single unprotonated group for catalysis with both cationic and

zwitterionic substrates. The k_{cat}/K_m pH-profile of the E87L mutant indicates only a single group is required for maximal activity with D-arginine, providing unequivocal evidence that E87 is the unprotonated group on the enzyme that binds cationic substrates. Further support for E87 interacting with the side chain of the cationic substrates comes from the X-ray structures of the enzyme in complex with iminoarginine and one of the two alternate conformations of iminohistidine,[2] showing the carboxylate chain of E87 at ≤2.8 Å away from the guanido and ε-amino groups of the cationic products of the reaction. Interestingly, the pK_a of E87 is perturbed to a value ≥7.9, as suggested by the k_{cat}/K_m pH-profiles with the cationic substrates D-arginine and D-lysine. This may be due to E87 being close to the hydrophobic side chains of M240 and V242. Large upward perturbations of pK_a values for aspartate and glutamate attributed to a hydrophobic environment have been previously reported for bacteriorhodopsin and bacterial thioredoxin, respectively.[15-18] Upward shifts in pK_a values of anionic residues have also been reported to occur when other negatively-charged residues are in close proximity to the group in question, such as E72 in *Bacillus circulans* xylanase.[19] In the case of PaDADH, while there is no other anionic group close to E87 a hydrogen bond interaction of the side chain of E87 with the O atom of T50 may also contribute to the elevation of the pK_a value, similar to human thioredoxin, in which a hydrogen bond to a neighboring serine elevates the pK_a of an aspartate residue.[20] An intrinsic value for the pK_a for E87 in the active site of PaDADH, however, cannot be estimated because different pK_a values were determined with D-arginine and D-lysine. pK_a values determined from k_{cat}/K_m pH-profiles refer to ionizations of the free enzyme or substrate, but not of enzyme-substrate complexes.[21] Thus, the different values determined with D-arginine and D-lysine reflect the stickiness of these substrates, i.e., the propensity of the enzyme-substrate complex to catalyze amine oxidation rather than releasing the substrate to bulk

solvent (k_3/k_2 in **Scheme 3.2**). Due to substrate stickiness perturbing apparent pK_a values outward in k_{cat}/K_m pH-profiles,[21] D-arginine, with a pK_a value of 7.2, is stickier than D-lysine, with pK_a value of 7.9. However, no conclusion on the stickiness of D-lysine can be drawn with the data available, preventing the determination of the intrinsic pK_a value of E87[1]. In the case of DAAO, Denu and Fitzpatrick observed outward perturbation of the pK_a values with D-alanine, establishing it as a sticky substrate.[22]

An unprotonated group with an intrinsic pK_a value of ~9.5, which is assigned to the α-NH_3^+ group of the amino acid substrate, is required for catalysis with both cationic and zwitterionic substrates. Evidence for this conclusion comes from the pH profiles of the steady-state kinetic parameters and site-directed mutagenesis. The k_{cat} and k_{cat}/K_m values increased to limiting values with increasing pH with all substrates. This establishes the requirement for an unprotonated group acting in the chemical step of amine oxidation rather than in substrate binding, since k_{cat} excludes binding steps because the enzyme is saturated with the substrate.[23] The linear decrease with decreasing pH in both k_{cat} and k_{cat}/K_m with all tested substrates is consistent with the unprotonated group not acting as an electrostatic catalyst, in which case the kinetic parameters would approach a limiting, lower value at low pH. The apparent pK_a values determined in the k_{cat} and k_{cat}/K_m pH profiles with D-leucine approximate well the intrinsic pK_a value, since D-leucine is a slow, non-sticky substrate for PaDADH. This conclusion comes from the pH-independence of the $^Dk_{red}$ value for the reduction of the enzyme-bound flavin with D-leucine between pH 7.0 and 10.3, where both k_{cat} and k_{cat}/K_m depend on pH, which establishes that the enzyme-substrate complex is not committed to catalysis and that D-leucine is not a

[1] Since E87 does not interact with the side chain of D-leucine, the perturbations of the apparent pK_a of E87 and of the unprotonated group participating in catalysis, which is instead common to all substrates oxidized by PaDADH, are not the same. For this reason, while the ΔpK_a values attributed to the chemical step of catalysis allows the determination of the intrinsic pK_a value on k_{cat} (*vide infra*), the same cannot be done to establish the intrinsic pK_a value of E87.

sticky substrate.[24] Independent support for D-leucine being a slow substrate is provided by the comparison of the pK_a of ~9.5 determined for k_{cat}/K_m with the pK_a of 9.6 recently reported for the k_{red} pH-profile with D-leucine.[7] The active site of the enzyme has several side chains that could potentially act as catalytic base for the deprotonation of the α-NH_3^+ group of the amino acid substrate, including H48, Y53, Y249 and, although less likely due to its location and participation in binding the side chain of cationic substrate, E87. The pH profiles of the k_{cat} and k_{cat}/K_m values for the H48F variant with D-arginine still show the requirement for the unprotonated group in the catalytic step, thereby eliminating H48 as being responsible for the observed pK_a value. A similar conclusion is drawn for E87, since the unprotonated group involved in catalysis is still present in the pH profiles for the E87L variant. Previous site-directed mutagenesis and rapid reaction studies established that neither Y53 nor Y249 is the catalytic group required for flavin reduction.[25] Instead, Y53 may exert a similar role to the analogous Y238 in DAAO from *Rhodotorula gracilis* by modulating the substrate entry and exit.[26] Thus, despite the presence of several candidates in the active site of PaDADH the unprotonated group required for catalysis cannot be attributed to any of the protein residues with potential to act as base in the active site of the enzyme. Consequently, the pK_a value of 9.5 for the unprotonated group involved in catalysis is assigned to the α-NH_3^+ group of the amino acid substrate.

D-Arginine is considerably stickier than D-leucine, followed by D-methionine and D-lysine, as suggested by the perturbations of the apparent pK_a values in the k_{cat}/K_m pH-profiles from the intrinsic value of ~9.5 determined with D-leucine. Substrate stickiness can be computed by using eq 6, where ΔpK_a is the difference between the apparent and intrinsic pK_a values. As expected from the k_{cat}/K_m of 10^6 $M^{-1}s^{-1}$, D-arginine is the stickiest substrate, with k_3/k_2 of ~200, likely due to the optimization of the active site with key residues involved in binding, such as

Y53, Y249, R222, R305 and, most importantly, E87. Interestingly, k_3/k_2 ratios of similar magnitude are computed with D-methionine (~60) and D-lysine (~40), despite lack of interaction of the side chain of methionine with E87, which instead is present with D-lysine. The stickiness of D-methionine is possibly due to its S atom establishing S-π interactions[27] with the phenols of either Y53, Y249 or both.

$$\Delta \mathrm{p}K_\mathrm{a} = \log\left(1 + \frac{k_3}{k_2}\right) \quad (6)$$

The cationic side chains of the iminoarginine and iminolysine products contribute to their stickiness compared to products lacking a positive charge. This conclusion is supported by the pH-profiles of the k_{cat} values, showing apparent pK_a values with D-arginine and D-lysine ~3 pH units lower than the intrinsic value of 9.5 determined with D-leucine. Perturbations of pK_a values in k_{cat} pH-profiles are symptomatic of a kinetic step other than the chemical step of catalysis being at least partially rate-determining for the overall turnover of an enzyme saturated with substrates.[21] Since PaDADH operates through a Ping-Pong Bi-Bi kinetic mechanism in steady-state and previous studies established that the oxidative half-reaction with PMS as electron acceptor is fast,[7] the only first-order kinetic step other than amine oxidation in the reductive half-reaction of the enzyme is product release (k_5 in **Scheme 3.2**). Most likely product stickiness with cationic substrates is due to an interaction of the positive charge present on the side chain of the ligand with the carboxylate of E87, as suggested by the structures of the enzyme in complex with iminoarginine.[2] The similar pK_a perturbations seen with D-arginine and D-lysine suggest that the interaction of the carboxylate of E87 with the side chain of the ligand has similar effects on the rate of turnover of PaDADH irrespective of the presence of an ε-amino or guanido group on the product side chain. The increase in k_{cat} from ~150 s^{-1} to ~550 s^{-1} seen in the pH-profile with D-lysine above pH 9.2 is consistent with a difference in the rate-limiting kinetic step

between the two substrates, potentially product release. Interestingly, iminomethionine is also considerably stickier than iminoleucine, as suggested by the apparent pK_a of 6.9 compared to the intrinsic pK_a ~9.5. Since both lack a cationic side chain, the stickiness of iminomethionine cannot be due to electrostatic interactions with E87. Rather, potential S-π interactions of the ligand S atom with the aromatic rings of Y53 or Y249 are likely responsible for the stickiness of iminomethionine,[27] as also proposed for D-methionine.

Previous QM/MM computations and the pH profile of the K_d value determined in the reductive half-reaction of wild-type PaDADH with D-leucine as substrate demonstrated that the enzyme preferentially binds the zwitterionic form of the substrate rather than the anionic form.[7] Solvent and substrate deuterium kinetic isotope effects on the rate constant for flavin reduction with D-leucine further indicated that flavin reduction occurs through the asynchronous cleavage of the substrate NH and CH bonds.[7] Thus, an accurate representation of the reductive half-reaction that accounts for the effects of pH on the ionization state of the substrate is given by **Scheme 3.4**, in which the substrate α-amino group is either protonated or unprotonated before binding to form the enzyme-substrate complex.

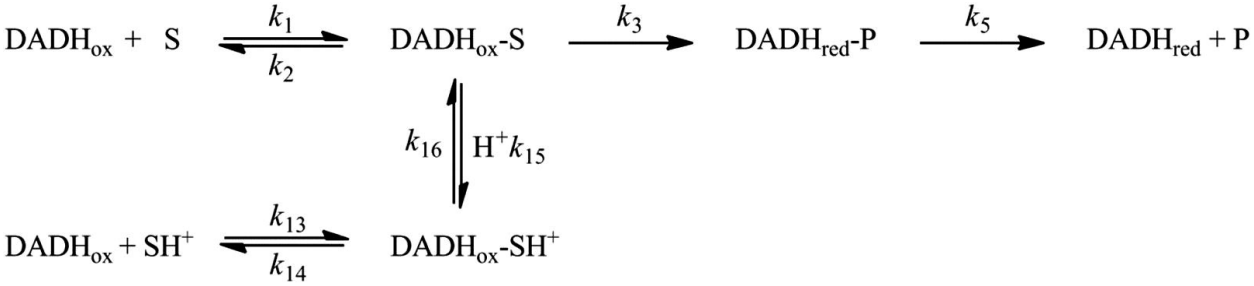

Scheme 3.4 Reductive half-reaction of *Pa*DADH accounting for pH effects on substrate ionization.

Cook *et al.* demonstrated earlier with creatine kinase that a "hollowed" pH profile is obtained with sticky substrates when the equilibration of a proton within an enzyme-substrate complex is

not rapid with respect to other relevant kinetic steps.[14] This yields three apparent pK_a values, which corresponds to the intrinsic pK_a value for the ionization of the relevant group involved in catalysis and two apparent pK_a values from which the stickiness of both the substrate and the proton with restricted movement can be extracted.[14] Alternatively, the hollow will not be present when the proton rapidly equilibrates within the complex, as is the case for most enzymatic reactions, or when the substrate/product is non-sticky.[14] With wild-type PaDADH in turnover with cationic substrates the pH profile of the k_{cat} value clearly demonstrates the presence of a hollow with D-lysine, but not with D-arginine irrespective of temperature. Thus, despite both substrates are sticky (*see above*) and share long, cationic side-chains that interact with E87, they must have (slightly) different arrangements within their respective enzyme complexes that result in different rates of proton release to the solvent. This may arise from a sub-optimal orientation of the α-NH_3^+ group of D-lysine as compared to D-arginine, which would impair the unrestricted release of the proton to solvent within the active site of the enzyme. In the three dimensional structure of the enzyme in complex with iminoarginine two well-defined water molecules are present in the active site of the enzyme-product complex, which are arranged to connect the α-NH_3^+ group of the ligand with the side chain of H48 and likely contribute to deprotonation of the substrate α-NH_3^+ group in turnover. Such an optimal arrangement may be missing in the complex with D-lysine and is likely to be disrupted upon mutation of H48 or of the neighboring residue E87, as suggested by the appearance of hollowed k_{cat} pH profiles in the H48F and E87L variants with D-arginine as substrate. Lack of an interaction between E87 and the side chain of D-methionine likely arranges the substrate α-NH_3^+ group so that proton release to solvent is also unrestricted, resulting in a k_{cat} pH profile not being hollowed. Similarly, the k_{cat} pH profile with D-leucine is not hollowed due to the latter being a

non-sticky substrate (*see above).* In this context, previous results with tryptophan 2-monooxygenase showed hollowed k_{cat}/K_m pH profiles with methionine or alanine, which were associated with proton related isomerizations of the enzyme-substrate complex.[28, 29] Although hollowed pH profiles were reported for the rate constant for anerobic flavin reduction of *Rhodotorula gracislis* DAAO with alanine or asparagine as substrate, a different interpretation was offered based on these substrates being nonsticky.[30]

In summary, we have used pH profiles, kinetic isotope effects, and site-directed mutagenesis to investigate further the steady-state mechanism of amine oxidation in PaDADH with a number of amino acid substrates. From a structural-functional standpoint, the results presented herein have established the importance of E87 in the active site of the enzyme for binding cationic substrates that carry a positive charge on the side chain, i.e., D-arginine and D-lysine. Despite the presence of several groups in the active site of the enzyme with the potential to act as base, substrate deprotonation occurs through the direct release of the substrate α-amino proton to the solvent without involvement of protein residues. In this respect, PaDADH is similar to other well-characterized flavoproteins that catalyze the oxidation of amino acids, i.e., L-amino acid oxidase, DAAO, and monomeric sarcosine oxidase, which lack in their active sites catalytic bases.[9, 30-32] From a mechanistic standpoint, D-arginine, D-lysine and D-methionine, as well as their respective imino-products, are sticky, resulting in steady-state turnover being primarily populated of enzyme complexes with substrates and products rather than the free enzyme. Among the pool of sticky substrates, proton release from the substrate α-amino group to solvent is restricted with D-lysine as substrate due, most likely, to a non-optimal configuration of the enzyme-substrate complex. The side chains of both H48 and E87 also contribute to optimal orientation of the D-arginine substrate and its α-amino group and the solvent in the active site of

the enzyme. This study demonstrated restricted movements of protons that are relevant to catalysis have been observed in a flavoenzyme that oxidizes α-amino acids, both in the wild-type species with a non-preferred substrate and in mutated variants with the physiological substrate.

3.6 Acknowledgements

The authors thank Irene T. Weber and Yuan-Fang Wang for valuable discussions.

3.7 References

[1] Li, C., Lu, C.D. (2009) Arginine racemization by coupled catabolic and anabolic dehydrogenases, Proc Natl Acad Sci U S A 106, 906-911.

[2] Fu, G., Yuan, H., Li, C., Lu, C. D., Gadda, G., Weber, I.T. (2010) Conformational changes and substrate recognition in Pseudomonas aeruginosa D-arginine dehydrogenase, Biochemistry 49, 8535-8545.

[3] Geueke, B., Weckbecker, A., Hummel, W. (2007) Overproduction and characterization of a recombinant D-amino acid oxidase from Arthrobacter protophormiae, Appl Microbiol Biotechnol 74, 1240-1247.

[4] Negri, A., Massey, V., Williams Jr., C.H. (1987) D-aspartate oxidase from beef kidney. Purification and properties, J Biol Chem 262, 10026-10034.

[5] D'Aniello, A., D'Onofrio, G., Pischetola, M., D'Aniello, G., Vetere, A., Petrucelli, L., Fisher, G.H. (1993) Biological role of D-amino acid oxidase and D-aspartate oxidase. Effects of D-amino acids, J Biol Chem 268, 26941-26949.

[6] Yuan, H., Fu, G., Brooks, P. T., Weber, I.T., Gadda, G. (2010) Steady-state kinetic mechanism and reductive half-reaction of D-arginine dehydrogenase from Pseudomonas aeruginosa Biochemistry 49, 9542-9550.

[7] Yuan, H., Xin, Y., Hamelberg, D., Gadda, G. (2011) Insights on the mechanism of amine oxidation catalyzed by D-arginine dehydrogenase through pH and kinetic isotope effects, J Am Chem Soc 133, 18957-18965.

[8] Serrano, H., Blanchard, J.S. (2013) Kinetic and isotopic characterization of L-proline dehydrogenase from Mycobacterium tuberculosis, Biochemistry 52(29), 5009-15

[9] P.F. Fitzpatrick, (2010) Oxidation of amines by flavoproteins, Arch Biochem Biophys 493, 13-25.

[10] Fu, G., Yuan, H., Wang, S., Gadda, G., Weber, I.T. (2011) Atomic-resolution structure of an N5 flavin adduct in D-arginine dehydrogenase, Biochemistry 50, 6292-6294.

[11] Gadda, G., McAllister-Wilkins, E.E. (2003) Cloning, Expression, and Purification of Choline Dehydrogenase from the Moderate Halophile Halomonas elongata, Appl Environ Microbiol 69, 2126-2132.

[12] Cook, P.F., Cleland, W.W. Enzyme kinetics and mechanism, Garland Science, London ; New York, 2007.

[13] W.H. Press, Teukolsky, S.A., Vetterling, W.T., Flannery, B.P., Numerical recipes in C (2nd ed.): the art of scientific computing, Cambridge University Press, 1992.

[14] Cook, P.F., Kenyon, G.L., Cleland, W.W. (1981) Use of pH studies to elucidate the catalytic mechanism of rabbit muscle creatine kinase Biochemistry 20, 1204-1210.

[15] Richter, H.T., Brown, L.S., Needleman, R., Lanyi, J.K. (1996) A linkage of the pKa's of asp-85 and glu-204 forms part of the reprotonation switch of bacteriorhodopsin, Biochemistry 35, 4054-4062.

[16] Szaraz, S., Oesterhelt, D., Ormos, P. (1994) pH-induced structural changes in bacteriorhodopsin studied by Fourier transform infrared spectroscopy, Biophys J 67, 1706-1712.

[17] Zscherp, C., Schlesinger, R., Tittor, J., Oesterhelt, D., Heberle, J. (1999) In situ determination of transient pKa changes of internal amino acids of bacteriorhodopsin by using time-resolved attenuated total reflection Fourier-transform infrared spectroscopy Proc Natl Acad Sci U S A 96, 5498-5503.

[18] Jeng, M.F., Dyson, H.J. (1996) Direct measurement of the aspartic acid 26 pKa for reduced Escherichia coli thioredoxin by 13C NMR, Biochemistry 35, 1-6.

[19] McIntosh, L.P., Hand, G., Johnson, P.E., M.D. Joshi, M.D., Korner, M., Plesniak, L.A., Ziser, L., Wakarchuk, W.W., Withers, S.G. (1996) The pKa of the general acid/base carboxyl group of a glycosidase cycles during catalysis: a 13C-NMR study of bacillus circulans xylanase Biochemistry 35, 9958-9966.

[20] Qin, J., Clore, G.M., Gronenborn, A.M. (1996) Ionization equilibria for side-chain carboxyl groups in oxidized and reduced human thioredoxin and in the complex with its target peptide from the transcription factor NF kappa B, Biochemistry 35, 7-13.

[21] Cleland, W.W. Methods Enzymol 87 (1982) 390-405.

[22] Denu, J.M., Fitzpatrick, P.F. (1992) pH and kinetic isotope effects on the reductive half-reaction of D-amino acid oxidase, Biochemistry 31, 8207-8215.

[23] Cleland, W.W. (1963) The kinetics of enzyme-catalyzed reactions with two or more substrates or productsBiochim Biophys Acta 67, 104-137.

[24] Cleland, W.W. (1982) Use of isotope effects to elucidate enzyme mechanisms, CRC Crit Rev Biochem 13, 385-428.

[25] Gannavaram, S., Sirin, S., Sherman, W., Gadda, G. (2014) Mechanistic and computational studies of the reductive half-reaction of tyrosine to phenylalanine active site variants of D-arginine dehydrogenase, Biochemistry 53, 6574-6583.

[26] Boselli, A., Sacchi, S., Job, V., Pilone, M.S., Pollegioni, L. (2002) Role of tyrosine 238 in the active site of Rhodotorula gracilisd-amino acid oxidase, Eur J Biochem 269, 4762-4771.

[27] Meyer, E.A., Castellano, R.K., Diederich, F. (2003) Interactions with aromatic rings in chemical and biological recognition.Angew Chem Int Ed Engl 42, 1210-1250.

[28] Emanuele, J.J., Fitzpatrick, P.F. (1995) Mechanistic studies of the flavoprotein tryptophan 2-monooxygenase. 2. pH and kinetic isotope effects, Biochemistry 34, 3716-3723.

[29] Ralph, E.C., Anderson, M.A., Cleland, W.W., Fitzpatrick, P.F., (2006) Mechanistic studies of the flavoenzyme tryptophan 2-monooxygenase: deuterium and 15N kinetic isotope effects on alanine oxidation by an L-amino acid oxidase, Biochemistry 45, 15844-15852.

[30] Harris, C.M., Pollegioni, L., Ghisla, S. Eur J Biochem 268 (2001) 5504-5520.

[31] Porter, D.J., Bright, H.J. (1980) Interpretation of the pH Dependence of Flavin Reduction in the L-amino acid oxidase Reaction, J Biol Chem 255, 2969-2975.

[32] Zhao, G., Jorns, M.S. (2005) Ionization of Zwitterionic Amine Substrates Bound to Monomeric Sarcosine OxidaseBiochemistry 44, 16866-16874.

4 FUNCTIONAL ANNOTATION OF A PRESUMED NITRONATE MONOOXYGENASE REVEALS A NEW CLASS OF NADH:QUINONE REDUCTASES

(This chapter has been published *verbatim* in Ball J., Salvi F., and Gadda G., (2016), J Biol Chem, 291(40), 21160-21170)

4.1 Abstract

The protein PA1024 from *Pseudomonas aeruginosa* PAO1 is currently classified as 2-nitropropane dioxygenase, the previous name for nitronate monooxygenase in the GenBank™ and PDB databases, but the enzyme was not kinetically characterized. In this study, PA1024 was purified to high levels and the enzymatic activity was investigated by spectroscopic and polarographic techniques. Purified PA1024 did not exhibit nitronate monooxygenase activity; however, it displayed NADH:quinone reductase and a small NADH:oxidase activity. The enzyme preferred NADH to NADPH as a reducing substrate. PA1024 could reduce a broad spectrum of quinone substrates via a Ping Pong Bi-Bi steady-state kinetic mechanism, generating the corresponding hydroquinones. The reductive half reaction with NADH showed a k_{red} value of 24 s^{-1} and an apparent K_d value estimated in the low μM range. The enzyme was not able to reduce the azo dye methyl red, routinely used in the kinetic characterization of azoreductases. Finally, we revisited and modified the existing six conserved motifs of PA1024, which define a new class of NADH:quinone reductases and are present in more than 490 hypothetical proteins in the GenBank™, the vast majority of which are currently misannotated as nitronate monooxygenase.

4.2 Introduction

The discrepancy between the rapid increase in the number of sequenced genomes of

prokaryotes and the slower experimental determination of protein function has resulted in the presence of a large number of hypothetical proteins in the databases, with gene function prediction oftentimes unreliable (1,2). One case of an enzyme family consisting mainly of hypothetical proteins is represented by the nitronate monooxygenases (NMOs, E.C. 1.13.12.16), which includes >5000 genes in the GenBank™. NMOs are FMN-dependent enzymes that catalyze the detoxification of propionate 3-nitronate (P3N), a metabolic poison produced by plants and fungi as a defense mechanism against herbivores (3). The kinetic mechanism of NMO has been investigated in previous studies on the fungal enzymes from *Neurospora crassa* (4) and *Cyberlindnera saturnus* (previously known as *Williopsis saturnus*) (5). The recent structural and kinetic characterization of the gene product PA4202 from *Pseudomonas aeruginosa* PAO1 as PaNMO identified four motifs that establish Class I NMO, with 500 sequences from bacteria, fungi, one insect and one animal (6). Class I NMO oxidizes the anionic nitronate form of the substrate, whereas Class II NMO can oxidize both the neutral and anionic forms of P3N (6). *P. aeruginosa* PAO1 possesses two other genes coding for hypothetical NMOs, namely *pa0660* and *pa1024*; however, these proteins do not carry the four motifs characteristic of Class I NMO nor any of the motifs signature of Class II NMO, raising the possibility that they code for enzymes with different function. While there is no experimental evidence at transcript or protein levels for the gene product PA0660, a crystal structure for the hypothetical protein PA1024 is available for the enzyme in free form and in complex with 2-nitropropane (PDB codes 2GJL and 2GJN) at 2.0 and 2.3 Å resolution, respectively (7). The protein PA1024 is currently classified as 2-nitropropane dioxygenase, a previous name for NMOs, based on the gene function prediction (~32% sequence identity) and a qualitative enzymatic assay performed with 20 mM 2-nitropropane at pH 6.5 (7). Nonetheless, the kinetic parameters with 2-nitropropane were not

determined, and the physiological substrate P3N was not tested, because it was unknown at the time of the study. The structural characterization of PA1024 previously highlighted six motifs conserved in other hypothetical proteins similar to PA1024 (7), which are different from the four motifs described for Class 1 NMO (6).

In the present study, we have cloned from genomic DNA the gene *pa1024*, purified the His-tagged recombinant PA1024, and characterized the spectral and kinetic properties of the enzyme. We demonstrated that purified PA1024 does not exhibit NMO activity. The enzyme belongs to an operon that contains two acyl-CoA dehydrogenases, an acyl-CoA hydratase/isomerase, a short chain dehydrogenase, and a porin (all hypothetical). All of these enzymes together imply the operon plays a role in β-oxidation. Based on the genomic context of PA1024, we hypothesized the enzyme oxidizes NAD(P)H to $NAD(P)^+$ to maintain a favorable $[NADH]/[NAD^+]$ ratio, since it has been observed that a low ratio stimulates β-oxidation (8,9). The connection between the $[NADH]/[NAD^+]$ ratio and β-oxidation is assumed to be due to the cofactor requirement of NAD^+ for 3-hydroxyacyl-CoA dehydrogenases, which catalyze the third step in β-oxidation (10). We also hypothesized the reduced enzyme is oxidized by quinones since they are prevalent redox agents in nature (11,12). To investigate this hypothesis, we experimentally tested NADH, NADPH, and various quinones for catalytic activity. Furthermore, we reanalyzed and modified the conserved motifs identified by Ha *et al.* in the protein sequence of PA1024 (7), and showed that they are present in more than 490 sequences in the non-redundant protein database. The results reinforce the need for accurate experimental data on select hypothetical proteins to work in concert with computational methods for improved gene function prediction.

4.3 Results

4.3.1 Protein purification

The gene *pa1024* was cloned from the genomic DNA of *P. aeruginosa* PAO1 in the expression vector pET20b(+), with the addition of a His-tag at the C terminus of the recombinant protein. The recombinant protein PA1024 was expressed in *Escherichia coli* and purified to high yield by affinity chromatography. The presence of 200 mM NaCl in a storage buffer composed of 20 mM TRIS-Cl, pH 8.0, 10 % v/v glycerol, was necessary for the *in vitro* stability of purified PA1024. SDS-PAGE analysis of the purified protein estimated a high level of purity.

4.3.2 Spectral properties

The UV-visible absorption spectrum of purified PA1024 shows maxima at 370 and 461 nm (**Figure 4.1**), which are consistent with the presence of FMN as a cofactor, as previously demonstrated in the crystal structure of PA1024 (PDB code 2GJL) (7) (**Figure 4.2**). The flavin cofactor extracted by heat denaturation was released to the bulk solvent, indicative of a non-covalent attachment of FMN to the protein, which is also in agreement with the crystal structure of the enzyme. The molar ratio FMN/enzyme was ~0.9, consistent with a 1:1 stoichiometry per monomer of protein. The enzyme-bound flavin emitted light at 545 nm when excited at 461 nm, with an intensity equivalent to ~10% that of an equimolar concentration of FMN in solution (**Figure 4.1**).

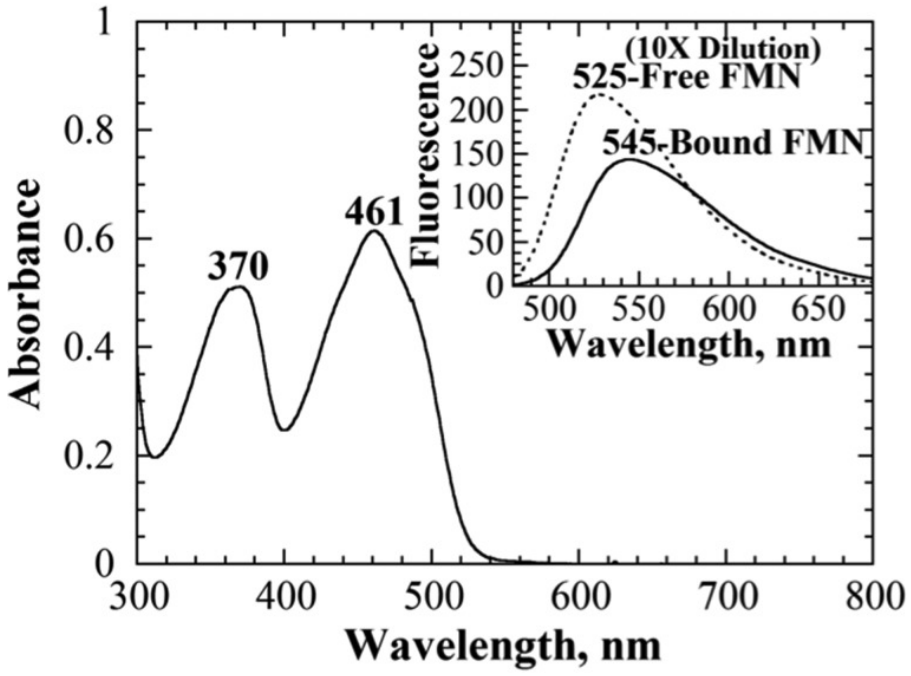

Figure 4.1 UV-visible absorption spectrum of the gene product PA1024.
Inset, solid line, fluorescence emission spectrum when the low energy band of the FMN-bound to PA1024 is excited; *dashed line*, fluorescence emission spectrum when the low energy band of the free FMN is excited.
Buffer conditions: 20 mm Tris-Cl, pH 8.0, 200 mm NaCl, 10% v/v glycerol, at 25 °C.

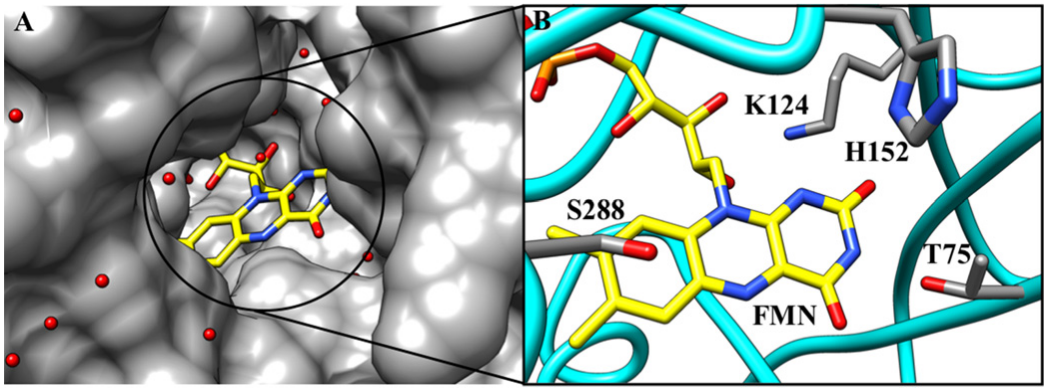

Figure 4.2 Surface depiction and active site of PA1024.
A, surface depiction of the three-dimensional structure of PA1024. FMN is shown as yellow sticks. Water molecules are represented by red circles. B, FMN locus of PA104 with select residues.

4.3.3 Lack of nitronate monooxygenase activity

Nitronate monooxygenase activity was tested at pH 7.5 and atmospheric oxygen, *i.e.* 230 μM, as previously described (5,6,13), to determine the validity of the previous classification of PA1024 as an NMO. No enzymatic activity was detected with 1 mM P3N or 3-NPA. No enzymatic activity was detected with 20 mM nitroethane, 1-nitropropane, 2-nitropropane, nor the anionic forms ethylnitronate, propyl-1-nitronate, and propyl-2-nitronate. In the case of propyl-2-nitronate and ethylnitronate, velocities of 16 and 5 μM oxygen consumed per minute were detected, which would correspond to enzymatic rates of 1 and 0.5 s^{-1} with 180 nM enzyme. However, the same velocities were detected by incubating propyl-2-nitronate or ethylnitronate in the reaction buffer without PA1024, and they therefore represent non-enzymatic reactions. The activity reported by Ha et al was thus likely due to the non-enzymatic reaction of propyl-2-nitronate with oxygen.

4.3.4 Reducing substrate

The operon where PA1024 is found suggests that PA1024 could serve to regenerate $NAD(P)^+$ for use by fatty acid oxidizing enzyme(s) also found in the operon. To evaluate the reduction of PA1024 by NAD(P)H, the reduction of the FMN cofactor was followed by monitoring the decrease in absorbance at 461 nm under anaerobic conditions at pH 7.0 and 25 °C, with the use of a stopped-flow spectrophotometer. The enzyme was fully reduced with NADH in a biphasic pattern (**Figure 4.3**).

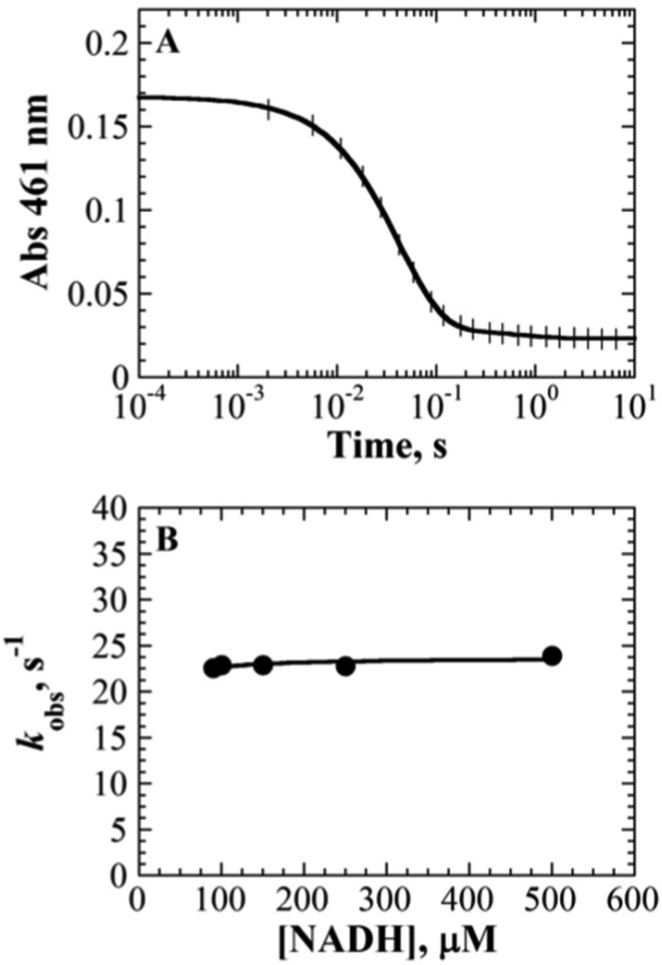

Figure 4.3 Reduction of PA1024 by NADH.
A, anaerobic reduction with 500 μm NADH of PA1024 in 20 mm potassium phosphate, 200 mm NaCl, pH 7.0, at 25 °C. B, observed rate constants of the first phase as a function
Note the log time scale on the x axis. The dead-time of the instrument was 2.2 ms.

The fast phase, which accounts for more than 95% of the total change in absorbance at 461 nm, was assigned to flavin reduction. A slow phase accounting for less than 5% of the total change in absorbance at 461 nm was seen, with a substrate concentration-independent k_{obs} value of 1 s^{-1}. The latter phase, which was considerably slower than the k_{cat} values determined with various quinone substrates (see below), could be due to a fraction of the enzyme being damaged. The fast phase of flavin reduction was analyzed with Eq. 2, demonstrating that the enzyme was fully saturated with NADH from 90 to 500 μM, with a k_{red} value of 24 ± 1 s^{-1}. An accurate K_d value

was not determined because it was not possible to lower NADH below 90 μM in order to maintain pseudo first-order conditions. However, the observation that the enzyme was fully saturated with 90 μM NADH suggests a K_d value in the 5 μM range or lower. When the enzyme was anaerobically mixed with 500 μM NADPH, there was slow reduction of the enzyme-bound flavin over 10 min, with an estimated rate constant of 0.0074 ± 0.0006 s^{-1}. Thus, NADH is the preferred reducing substrate of PA1024.

4.3.5 Oxidizing substrates

Quinones were selected as potential oxidizing substrates based on their powerful oxidizing ability and pervasive nature in the cell. Turnover of PA1024 was monitored with a quinone as the oxidizing substrate and NADH as the reducing substrate at pH 7.0 and 25 °C. PA1024 turned over with a number of different quinones and the apparent steady-state kinetic parameters were determined at a fixed, saturating concentration of 100 μM NADH. As shown in **Table 4.1**, benzoquinone and 5,8-dihydroxy-1,4-naphthoquinone were the best substrates for the enzyme based on the k_{cat}/K_m value. Naphthoquinone substrates with hydroxyl groups on the aromatic ring of the naphthoquinone showed the highest k_{cat}/K_m values for the bi-cyclic series. The k_{cat}/K_m values plotted against the one-electron reduction potentials did not show a linear relationship (data not shown).

Table 4.1 Apparent steady-state kinetic parameters of PA1024 with various electron acceptors.

Electron acceptor	$^{app}k_{cat}/K_m$ (M^{-1} s^{-1})	$^{app}k_{cat}$ (s^{-1})	$^{app}K_m$ (μM)
1,4-Naphthoquinones			
5,8-dihydroxy-	1,500,000 ± 100,000	14 ± 1	10 ± 1
5-hydroxy-	1,200,000 ± 100,000	17 ± 1	14 ± 2
2-methyl-5-hydroxy-	920,000 ± 120,000	16 ± 1	18 ± 3
2-methyl-	270,000 ± 10,000	16 ± 1	60 ± 5
2-methoxy-	30,000 ± 3,000	6 ± 1	185 ± 40
2-hydroxy-	nd[a]	nd[a]	nd[a]
1,4-Benzoquinones			
benzoquinone	1,900,000 ± 130,000	27 ± 1	15 ± 1
2-methyl-5,6-dimethoxy- (Q_0)	350,000 ± 30,000	24 ± 1	70 ± 10
2,6-dimethoxy-	100,000 ± 20,000	nd[b]	nd[b]
2,3,4,6-tetramethyl-	80,000 ± 10,000	28 ± 3	355 ± 75

The kinetic parameters were determined with 100 μM NADH in 20 mM potassium phosphate, 200 mM NaCl, pH 7.0, at 25 °C. [a]Enzymatic activity not detected; [b]k_{cat} or K_m not determined because unable to saturate with substrate

4.3.6 Steady-state kinetic mechanism with 5-Hydroxy-1,4-naphthoquinone

The traditional approach to obtain the steady-state kinetic mechanism of varying both NADH and quinone concentrations yielded overlapping lines in a double reciprocal plot (data not shown), likely due to NADH being saturating at all concentrations used. Consequently, the product inhibition pattern using NAD^+ and 5-hydroxy-1,4-naphthoquinone as a substrate was used to establish the steady-state kinetic mechanism of PA1024. 5-Hydroxy-1,4-naphthoquinone was chosen for its occurrence and importance in nature (14), and because of its high k_{cat}/K_m value (Table 1). A double reciprocal plot of the initial rate of reaction versus the substrate concentration yielded lines converging on the y-axis (**Figure 4.4**), consistent with 5-hydroxy-1,4-naphthoquinone and NAD^+ binding to the same form of enzyme. This, in turn, is in line with a Ping-Pong Bi-Bi steady-state kinetic mechanism, as illustrated in **Scheme 4.1**. The K_{is} for NAD^+ was determined to be 2.2 mM.

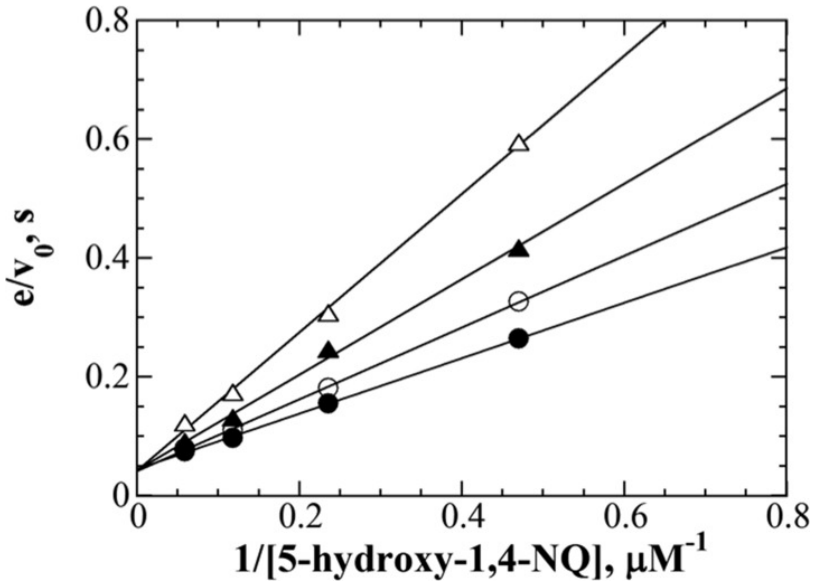

Figure 4.4 Lineweaver-Burk plots of product inhibition of PA1024 by NAD^+.
Buffer conditions: 20 mM potassium phosphate, 200 mM NaCl, pH 7.0, at 25 °C. NADH was kept at a fixed, saturating concentration of 100 μM, and 5-hydroxy-1,4-NQ varied from 2 to 17 μM. Each *line* represents a different concentration of NAD^+: ●, 0 mM; ○, 0.4 mM; ▲, 1.2 mM; and △, 3 mM.

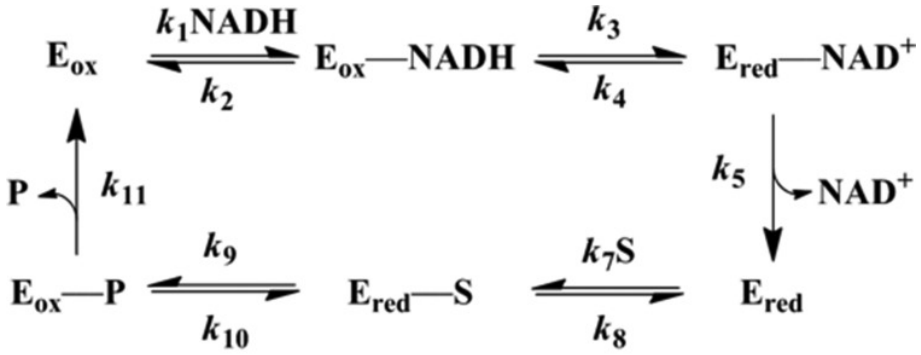

Scheme 4.1 Steady-state kinetic mechanism of PA1024 with 5-hydroxy-1,4-napthoquinone as substrate.

4.3.7 Quinone mode of reduction

To assess if the reduction of the quinones catalyzed by PA1024 occurs through a single- or two-electron transfer from the enzyme-bound flavin, the obligatory one-electron transferring

protein Cyt *c* was employed as a reporter. A single-electron flux, as defined by Iyanagi (15), is the coupled Cyt c reduction rate (v) divided by the doubled NADH oxidation rate ($2v$). The single-electron flux can have a value of 1 or lower, depending upon whether the reaction of PA1024 with the quinone occurs via a single- or a two-electron transfer. As shown in **Figure 4.5**, all quinones tested had single-electron fluxes considerably lower than unity, ruling out a pure single-electron reduction of the quinone being catalyzed by PA1024.

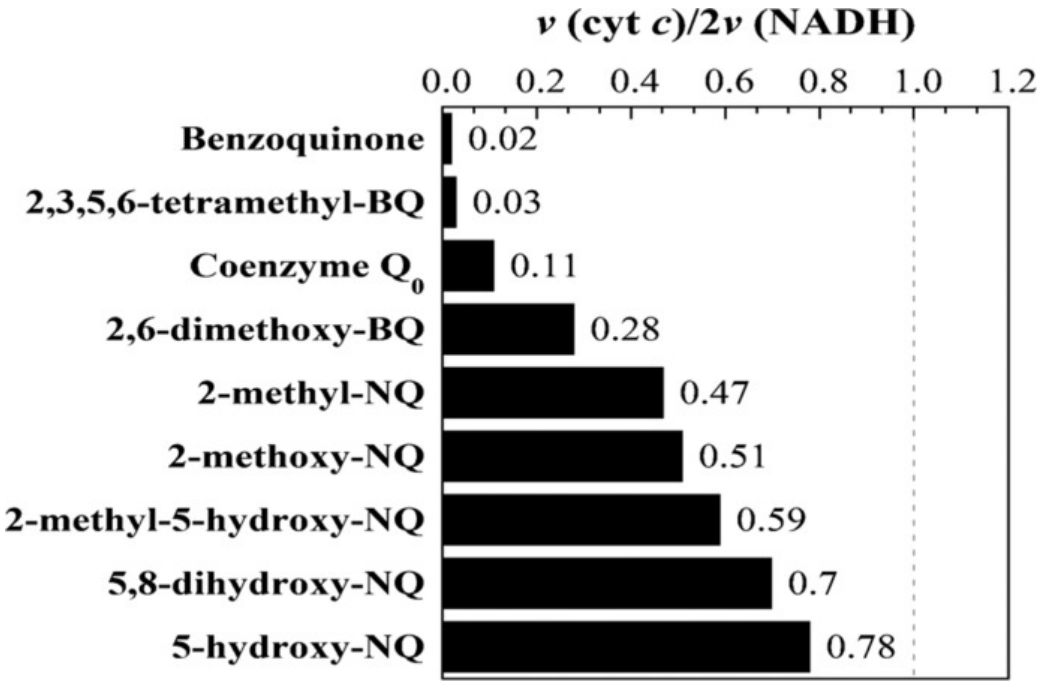

Figure 4.5 Single electron flux for quinone reduction by PA1024.
Values are expressed as the ratio of coupled Cyt *c* reduction rate divided by the doubled NADH oxidation rate. The *dashed line* represents the theoretical limit for a one-electron quinone reductase. Experiments were performed in 20 mM potassium phosphate, 200 mM NaCl, pH 7.0, at 25 °C. The concentration of each quinone was saturating (if possible), and NADH was held at a fixed, saturating concentration of 100 μM. *BQ,* benzoquinone; *NQ,* naphthoquinone.

In an independent experiment, the initial rates of the coupled Cyt *c* reduction were measured in the absence and presence of SOD, since in the latter case a roughly 50% decrease in the rate of reaction would be expected if quinone reduction by PA1024 occurred through a single-electron reaction. As illustrated in **Table 4.2**, in all cases except 2,6-dimethoxy-1,4-

benzoquinone[2], the initial rates for the coupled Cyt *c* reduction catalyzed by PA1024 were equal or lower than 50% in the presence of SOD, further ruling out a single-electron reaction of PA1024 with the quinone substrates.

Table 4.2 Rate constants for the coupled Cyt c reduction by PA1024 with various quinones in the presence or absence of SOD.

Electron acceptor	Coupled Cyt *c* reduction (s^{-1})	Coupled Cyt *c* reduction + SOD (s^{-1})
1,4-Naphthoquinones		
2-methyl-5-hydroxy-	20.0 ± 1.5	7.5 ± 0.3
5-hydroxy-	22.1 ± 1.1	11.1 ± 1.2
2-methyl-	13.0 ± 0.3	4.6 ± 0.1
5,8-dihydroxy-	14.5 ± 0.3	7.0 ± 0.3
2-methoxy-	4.6 ± 0.2	2.1 ± 0.1
1,4-Benzoquinones		
benzoquinone	0.9 ± 0.1	nd
2,6-dimethoxy-	9.3 ± 0.9	6.7 ± 0.2
2-methyl-5,6-dimethoxy- (Q_0)	3.8 ± 0.2	1.4 ± 0.1
2,3,5,6-tetramethyl-	0.9 ± 0.2	nd

nd: enzymatic activity not detected. The kinetic parameters were determined with 100 μM NADH in 20 mM potassium phosphate, 200 mM NaCl, pH 7.0, 25 °C, at a saturating (if possible) concentration of the quinone substrate with or without the addition of superoxide dismutase.

4.3.8 NADH:oxidase activity

PA1024 displayed an NADH oxidase activity of ~1.0 s^{-1} at atmospheric oxygen, pH 7.0 and 25 °C. Addition of catalase to the reaction mixture decreased the rates of oxygen consumption by half (data not shown), providing evidence for the production of hydrogen peroxide, consistent with PA1024 displaying a small oxidase activity.

[2]The product of this substrate may reduce Cyt *c* primarily through the hydroquinone form of the product and the autoxidation products are a minor reduction pathway, thus SOD exerts less of an inhibitory effect.

4.3.9 Lack of azoreductase activity

In order to determine if PA1024 could perform azoreductase reactions, which is a common activity shared among most quinone reductases, turnover of PA1024 was monitored with the azo dye methyl red at saturating NADH concentration at pH 7.0, 25 °C. No significant enzymatic reduction of methyl red was observed over 10 min, indicating PA1024 is not an azoreductase.

4.3.10 Bioinformatics

In a previous study, Ha *et al.* identified six consensus motifs in the amino acid sequence of PA1024 (7) and annotated PA1024 as 2-nitropropane dioxygenase, the former official name of NMO. That study was carried out before the crystal structure of Pa-NMO (PA4202) was available (6), which established Class I NMO. A reanalysis of the conserved motifs of PA1024 based on the comparison of the active site residues of the two enzymes, PA1024 and Pa-NMO, in addition to a comprehensive PHI-BLAST search was carried out here, identifying small changes in the six motifs originally reported (**Table 4.3**). A PHI-BLAST search of the six consensus motifs of PA1024 recognized ~500 (erroneously annotated) hypothetical proteins that share these motifs, the bulk of which come from bacterial sources and are currently annotated as NMOs. The complete list of the genes and the PHI-BLAST search parameters can be found in the supplemental data at http://www.jbc.org/content/291/40/21160/suppl/DC1.

Table 4.3 Conserved motifs in the protein sequence of PA1024.

Motif	Consensus sequence
I[b]	^{17}P-[I/V]-*h*-Q-G-G-M-Q-W-[V/I]^{26}
II[a]	^{66}T-D-[K/R]-P-F-G-V-N-L-T-*h*-[L/F]-P^{78}
III[b]	^{121}[V/I]-*h*-H-K-C-T-X-[V/I]-R-H-A^{131}
IV[b]	^{144}I-D-G-F-E-C-[A/G]-G-H-P-G-E-X-D-X-[P/G/T]^{159}
V[b]	^{177}A-S-G-G-*h*-[A/G]-[D/E]-[A/G]-R-G-L-*h*-A-A-[L/F]-A-L-G-A-[D/E]-[G/A]-*h*-X-M-G-T-R-F^{204}
VI[b]	^{225}E-X-X-[T/S]-X-L-*h*-X-R-X-[L/M/W]-[R/H/K]-N-T-[S/A/V]-R-V^{241}
VII	^{85}Y-A-E-Y-R-X-[A/V]-I-[I/V]-E-X-G-*h*-X-[I/V]-V-E-T-A-G-X-X-P-X-[E/D]-H^{110}

The numbering of the residues refers to the protein sequence of PA1024; the brackets identify alternative residues that can be present in that position, *h* represents a position occupied by a hydrophobic residue, while X represents a position where any amino acid is accepted. [a]Motif was identified in a previous study by Ha *et al.* (7). [b]Motif was identified in a previous study by Ha et al. (7) and modified in this study. The modifications to the consensus sequence are underlined.

4.4 Discussion

Recent advances in the efficiency and speed of gene sequencing coupled to a comparatively much slower pace of acquiring experimental evidence for protein function has given rise to a large number of hypothetical or erroneously annotated proteins in the databases (1,2). An example of a family of enzymes with a sizable amount of hypothetical proteins in the database is the nitronate monooxygenases (NMOs), with over 5000 genes in the GenBank™ currently annotated as NMO. The present study aimed to characterize PA1024, one of the three genes encoding a hypothetical NMO in *Pseudomonas aeruginosa* PAO1. The current classification of PA1024 is based on a 2006 study (7), but the enzyme does not carry the consensus motifs characteristic of the recently defined Class I and Class II NMOs (6). The biochemical and kinetic characterization of PA1024 presented herein show that the enzyme indeed is not an NMO, as indicated by the lack of oxygen consumption with propionate-3-nitronate and other nitronates. The enzyme, instead, uses NADH and quinones as reducing and oxidizing substrates, respectively. Thus, PA1024 should be reclassified as an NADH:quinone Reductase (E.C. 1.6.99.5), along with ~500 genes that contain the consensus motifs identified in PA1024.

PA1024 efficiently uses NADH as a reducing substrate; the enzyme was fully reduced by NADH with a k_{red} value of 24 s^{-1} and a K_d value estimated in the low μM range (**Figure 4.3**). PA1024 displayed a marked preference for NADH over NADPH, as indicated by the fact that flavin reduction with 500 μM NADPH is ~3,500 times slower than with an equivalent concentration of NADH. Preference for NADH as a substrate was previously reported for some flavin-dependent monooxygenases (16), FMN-dependent quinone reductases in bacteria, such as tryptophan [W] repressor-binding protein (WrbA) (17), and the FMN-dependent azoreductases

AzoA (18), AcpD (19), and AzoR (20). In the case of PA1024, the structural determinants for NADH specificity are currently unknown, and future crystallographic studies of the enzyme in complex with the product NAD^+ will be required for their elucidation.

PA1024 catalyzes the reduction of various quinone substrates as shown in **Table 4.1**. The enzyme prefers benzoquinone, but naphthoquinones carrying hydroxyl groups in the 5 or 8 positions are also good substrates, as indicated by the large k_{cat}/K_m values determined with these substrates. Addition of methyl groups on the benzoquinone ring or methoxy groups in the 2 position results in a significant decrease in the k_{cat}/K_m value, possibly due to increased steric constraints for the formation of a catalytically competent enzyme-substrate complex. Interestingly, PA1024 does not react when the hydroxyl group is in the 2 position of the naphthoquinone substrate. Non-reactivity with 2-hydroxy-1,4-napthoquinone is in stark contrast to *Enterococcus cloacae* nitroreductase, which shows a marked preference for this substrate (21).

PA1024 reduces quinones to the hydroquinone form through a two-electron mechanism. Two lines of evidence support this conclusion. First, single-electron fluxes considerably smaller than 1 were obtained with a number of quinone substrates when the obligatory one-electron acceptor Cyt *c* was used in a coupled enzymatic assay (Figure 4.5). In this context, a single-electron flux is the ratio of the rate constant for Cyt *c* reduction to the doubled rate constant for NADH oxidation (15). The data rule out the alternative possibility of a single-electron reduction of the quinones by the enzyme-bound flavin of PA1024, since if this were the case single-electron fluxes of 1 would have been observed. The different single-electron fluxes determined with the various quinone substrates tested can be reconciled with their autoxidation rates, which were previously shown for naphthohydroquinones to follow the order of 5-hydroxy > 2-methoxy > 2-methyl > unsubstituted hydroquinone (22). In essence, hydroquinones that are more prone to

non-enzymatic autoxidation can indirectly reduce Cyt *c* at faster rates through the products of autoxidation. The effect of SOD on the enzymatic activity of the enzyme in the Cyt *c* coupled assay provides independent evidence for quinone reduction to the hydroquinone rather than the semiquinone state. With all quinone substrates tested except 2,6-dimethoxy-1,4-benzoquinone, the presence of SOD decreased the initial rates for the coupled Cyt *c* reduction catalyzed by PA1024 by 50% or more (Table 4.2). In the presence of Cyt *c*, if a semiquinone radical were produced in the quinone reduction catalyzed by PA1024 it would redox cycle without reducing oxygen and bypass superoxide formation (23). This property explains the ability to significantly inhibit the coupled Cyt *c* reduction by a 2-electron reductase with SOD, but not a 1-electron reductase, and the latter phenomenon has been observed in studies with ferric reductase B from *Paracoccus denitrificans* (23). Additional evidence of a two-electron reduction comes from the k_{cat}/K_m values, which did not show a linear relationship with the one-electron reduction potentials and were sensitive to the structure of the substrate. The last two features are common amongst most two-electron quinone reductases (21,24).

The two-electron reduction of quinones by PA1024 occurs through a Ping-Pong Bi-Bi steady-state kinetic mechanism, as demonstrated by the competitive inhibition pattern observed between NAD^+ and the quinone substrate (**Figure 4.4**). NAD^+ must first leave the reduced enzyme before the quinone can bind, and the napthoquinone and NAD^+ compete for the reduced free enzyme (**Scheme 4.1**). All known two-electron flavin-dependent NAD(P)H:quinone reductases operate via a Ping-Pong Bi-Bi mechanism (25). This is likely due to the requirement for both reducing and oxidizing substrates to alternately position close to the flavin for the transfer of a hydride in the reductive and oxidative half-reactions catalyzed by NADH:quinone reductases (26).

With benzoquinones, flavin reduction is fully rate-limiting for the overall turnover of the enzyme. Evidence for this conclusion comes from the comparison of the limiting rate constant for flavin reduction (k_{red}) and the k_{cat} value that define turnover at saturating concentrations of both substrates, showing similar values of 24-28 s^{-1}. In contrast, with all naphthoquinones used, flavin reduction is partially rate-limiting for the overall turnover of the enzyme, as indicated by the k_{red} value being significantly larger than the k_{cat} values. This may reflect a slower rate constant for the release of the product of the reaction for the bulkier naphthoquinones compared to the smaller benzoquinones.

The K_{is} value for NAD^+ of ~2 mM is at least 400 times larger than the K_m value for NADH. This substantial difference is consistent with an unfavorable interaction of the positively charged NAD^+ in the active site of the enzyme as compared to the neutral NADH. The crystallographic structure of PA1024 (PDB 2GJL) shows the presence of the side chain of K124 at ~4 Å from the N1-C2 locus of the flavin (Figure 4.2B), allowing us to speculate that this residue may be responsible for NAD^+ binding being weaker than NADH due to electrostatic repulsion.

PA1024 has a small NADH oxidase activity, with a turnover rate of ~1 s^{-1} at saturating NADH concentration and atmospheric oxygen. This indicates that the NADH oxidase activity is likely not the primary function of PA1024. Slow oxidase activity has been observed in the case of NADH:quinone oxidoreductases (27), chromate reductase (28), flavin-dependent monooxygenases (uncoupling) (16), and old yellow enzyme (OYE) (29,30). In contrast to PA1024, FAD-dependent NAD(P)H:quinone oxidoreductase 1 (NQO1) and the quinone reductase Lot6p are not oxidized by molecular oxygen (25). In PA1024, the presence of a positive charge near the N1-C2 locus of the flavin, i.e., on the side chain of K124, may

contribute to the small oxidase activity observed, as in the case of several other flavin-dependent oxidases (31).

The UV-visible absorption spectrum of purified PA1024 in **Figure 4.1** displays the characteristic flavin signature, but the low-energy band of the cofactor at 461 nm is significantly red shifted compared to free FMN (450 nm) and to Pa-NMO (443 nm) (6). A large red shift in the low-energy peak is a feature usually indicative of a more polar protein environment around a flavin cofactor (32,33). Accordingly, in the crystal structure of PA1024 (7) there is a polar T75 located 3.8 Å from the N3 atom of FMN, while in the same position in Pa-NMO (PDB 4Q4K) there is the hydrophobic F71 at 3.6 Å from N3 atom of FMN (6). Furthermore, the flavin in PA1024 is exposed to the solvent (**Figure 4.2B**), which could contribute to additional hydrogen bond interactions with water. The fluorescence emission peak of PA1024 upon exciting the enzyme-bound flavin at 461 nm demonstrates a significant red shift to 543 nm and is only 10 times less fluorescent than FMN free in solution (**Figure 4.1 inset**).

Enzymes with NAD(P)H:quinone reductase activity were recently reported from bacteria with the ability to detoxify azo dyes from the environment (34-36). Convergent evolution of azoreductases and quinone reductases has been proposed based on similar reaction mechanisms involving the flavin-mediated reduction of an organic molecule with NAD(P)H and substrate scope (37,38). The lack of enzymatic activity with the azo dye methyl red indicates that PA1024 is not an azoreductase. Although there are several azoreductases from *P. aeruginosa* capable of reducing quinones (38), WrbA is the only other two-electron NAD(P)H:quinone reductase identified to date that does not possess azoreductase activity (39) beside PA1024.

PA1024 is a novel NADH:quinone reductase as illustrated below. The enzyme shares little overall sequence similarity to the well-characterized human NQO1 and FAD-dependent

NAD(P)H:quinone oxidoreductase 2 (NQO2), with only 20% and 19% identity in its amino acid sequence, respectively. As shown in **Figure 4.6**, which compares the active sites of the three enzymes, there are prominent differences in the active site frameworks of the three enzymes.

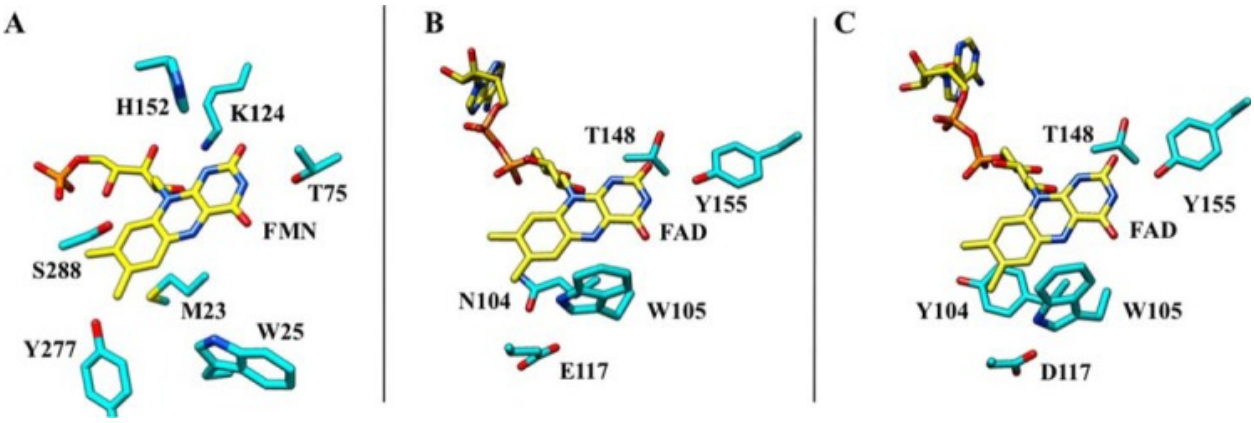

Figure 4.6 Comparison of the active sites of PA1024, NQO1, and NQO2.
FMN or FAD carbon atoms are in *yellow sticks,* and the side chain residue carbons are in *cyan sticks. A,* PA1024 (PDB 2GJL). *B,* NQO1 (PDB 1QBG) (66). *C,* NQO2 (PDB 1QR2) (67).

A major difference is the presence of H152 above the flavin of PA1024 and S288 near the C7/C8 methyls of the flavin, both of which are absent in the NQOs. Also, K124 is located near the N1 of PA1024, as opposed to T148 residue in the NQOs. Notably a M23 is positioned behind the re face of the flavin in PA1024, whereas a hydrophilic residue is present in NQO1 and NQO2. Similarities include the presence of a tryptophan below the flavin, and hydrophilic residues near the N1-C2(O) locus of the flavin. Besides the active site, PA1024 displays several differences with respect to mammalian NQOs. First, PA1024 contains FMN while the mammalian NQOs use FAD (7,25). Second, PA1024 has a clear preference for NADH, whereas NQO1 can utilize both NADH and NADPH with similar efficacy, and NQO2 prefers modified derivatives of NADH such as dihydronicotinamide riboside (40). Third, PA1024 is unable to reduce azo dyes, which are substrates of NQO1 and NQO2 (41-44).

Comparison of PA1024 with other known NADH:quinone reductases indicates that the

enzyme is distinct in sequence and structure from those enzymes as well. The overall fold of PA1024 is a TIM-barrel, distinguishing it from the flavodoxin-like fold of most NAD(P)H:quinone reductases characterized to date (25). As mentioned earlier, very few FMN-dependent quinone reductases specific for NADH have been identified. Other FMN-dependent quinone reductases, which however utilize both NADH and NADPH, have also been identified in bacteria, fungi and plants, including *Methanothermobacter marbergensis* NQO (45), Lot6p from *Saccharomyces cerevisiae* (46), YhdA (47), FQR1 (48) and NQR (49), among others. It is worth noting that other flavin-dependent enzymes with known functions have been shown to exhibit NAD(P)H:quinone reductase activity, for example bacterial nitroreductases and glucose oxidase (50). Thus, the possibility that the primary function of PA1024 may be different from the NADH:quinone reductase activity characterized in this study cannot be excluded.

The six consensus motifs identified in PA1024 contain critical differences to PaNMO that discriminate the reactivity and substrate preference between the two enzymes. Motif I and V may aid in binding the cofactor and possibly modulating the redox potential. Motif II is most likely related to the folding of the TIM barrel domain, yet a key difference being the presence of T75 in PA1024 as opposed to F71 in PaNMO. Motif III is also a part of the TIM barrel fold since all of the residues are not located near the active site, with the exception of the K124 which is unique to the PA1024-like class of quinone reductases. Motif IV is located on the surface above the active site cavity and may play a role in substrate preference. Motif VI is located in the putative substrate binding domain and is completely absent in PaNMO. Most importantly, the last part of motif II, motif III, and motif VI of PA1024 are the most helpful in identifying significant differences in the two classes of enzymes represented by PA1024 and Pa-NMO.

NAD(P)H:quinone oxidoreductases have been implicated in the detoxification of

quinones within intracellular pools, thereby exerting an antioxidant protective role. This is due to the fact that upon a two-electron reduction of quinones to the hydroquinones, the highly reactive semiquinones are bypassed, which in turn lowers free radical formation and consequent lipid peroxidation, formation of protein adducts, and DNA modifications (51-53). This could be the case for PA1024. However, when one considers that the operon containing *pa1024* includes hypothetical acyl-CoA dehydrogenases, a short chain dehydrogenase, an acyl-CoA hydratase/isomerase, and a porin, an alternative speculation is that PA1024 may be required to maintain an appropriate [NAD^+]/[NADH] ratio for the catabolism of fatty acids in *P. aeruginosa* PAO1. A link between a low [NAD^+]/[NADH] ratio and the stimulation of β-oxidation was observed previously (8,9). Furthermore, participation of an NADH:acceptor oxidoreductase as a physiological partner of a butyryl-CoA dehydrogenase was recently proposed in *Syntrophomonas wolfei*, although the enzyme was not identified (54).

In summary, the results presented in this study remedy the annotations of close to five hundred, mostly bacterial, hypothetical proteins in the databases, and define a new class of FMN-dependent quinone reductases with a TIM-barrel fold. There appears to be a widening gap between the benchtop and desktop that if left unchecked could potentially cause confusion, raising the necessity for computational biochemists and experimentalists to cooperate more closely in order to enhance gene function prediction. The results presented herein also highlight the structural diversity among quinone reductases and their deeply rooted evolutionary differences in nicotinamide preference and azoreductase activity. The biological significance of an NADH:quinone reductase activity is possibly more complex than previously considered, and the various effects of quinones and quinone reductases on the cellular setting have yet to be fully unraveled.

4.5 Experimental procedures

4.5.1 Materials

The enzymes *Xho*I, *Nde*I, *Dpn*I, calf intestinal alkaline phosphatase (CIP), and T4 DNA ligase were from New England BioLabs (Ipswich, MA), *Pfu* DNA polymerase from Stratagene (La Jolla, CA), and oligonucleotides from Sigma Genosys (The Woodlands, TX). *Escherichia coli* strain DH5α was purchased from Invitrogen Life Technologies (Grand Island, NY). *E. coli* strain Rosetta(DE3)pLysS and the expression vector pET20b(+) were from Novagen (Madison, WI), QIAprep Spin Miniprep kit, QIAquick PCR purification kit and QIAquick gel extraction kit were from Qiagen (Valencia, CA). The genomic DNA of *P. aeruginosa* PAO1 was a kind gift from Dr. Jim Spain, Georgia Institute of Technology, Atlanta, GA. HiTrapTM Chelating HP 5 mL affinity column was from GE Healthcare (Piscataway, NJ), and isopropyl-1-thio-β-D-galactopyranoside (IPTG) was from Promega (Madison, WI). Cytochrome *c* from bovine heart, superoxide dismutase, nitroalkanes and quinones were from Sigma-Aldrich (St. Louis, MO). All other reagents used were of the highest purity commercially available.

4.5.2 Cloning

The gene *pa1024* was amplified from the genomic DNA of *P. aeruginosa* PAO1 by PCR in presence of 5% DMSO. The PCR protocol included an initial denaturation step at 95 °C, 20 cycles of denaturation for 45 s at 95 °C, annealing for 30 s at 56 °C (with the annealing temperature progressively decreasing by 0.2 °C at each cycle), extension for 3 min at 72 °C, and a final step for 10 min at 72 °C.

The *pa1024* gene amplified by PCR was purified by agarose gel extraction with the QIAquick gel extraction kit. The amplicon and the expression vector pET20b(+) were subjected to double digestion with *Nde*I and *Xho*I and purified with the QIAquick PCR purification kit.

After a dephosphorylation step with 0.5 units of calf intestinal alkaline phosphatase for 30 min at 37 °C the dephosphorylated vector was purified with the QIAquick PCR purification kit and ligated to the insert with incubation for 15 h at 16 °C with T4 DNA ligase. A volume of 5 µL of the ligation mixtures was used to transform *E. coli* strain DH5α. The resulting colonies grown at 37 °C on Luria-Bertani agar plates containing 50 µg/mL ampicillin were screened for the presence of the desired insert by DNA sequencing at the Cell, Protein and DNA Core Facility at Georgia State University. The DNA sequencing confirmed the correct insertion of the gene in the plasmid vector and the absence of undesired mutations.

4.5.3 Recombinant expression and purification

E. coli expression strain Rosetta(DE3)pLysS transformed with the construct pET20b(+)/*pa1024* was used to inoculate 90 mL of Terrific Broth containing 50 µg/mL of ampicillin and 34 µg/mL of chloramphenicol, which was incubated at 37 °C for 15 h. One aliquot of 8 mL of this culture was used to inoculate 1 liter of Terrific Broth containing 50 µg/mL of ampicillin and 34 µg/mL of chloramphenicol, which was incubated at 37 °C until it reached an optical density at 600 nm of 0.8. IPTG was then added to a final concentration of 200 µM and the culture was incubated at 18 °C for 20 h. The wet cell paste of 8.5 g, recovered by centrifugation, was resuspended in 40 mL of lysis buffer containing 10 mM imidazole, 300 mM NaCl, 10% v/v glycerol, 1 mM phenylmethylsulfonyl fluoride, 5 mM $MgCl_2$, 2 mg/mL lysozyme, 5 µg/mL DNase, 5 µg/mL RNase, and 20 mM sodium phosphate, pH 7.4. The resuspended cells were subjected to several cycles of sonication. The cell free extract obtained after centrifugation at 12000 *g* for 20 min was loaded onto a HiTrap™ Chelating HP 5 mL affinity column equilibrated with 10 mM imidazole, 300 mM NaCl, 10% v/v glycerol, and 20 mM sodium phosphate, pH 7.4. After washing with 10 column volumes of equilibrating buffer,

the column was treated with four intermediate steps at 50, 100, 150 and 250 mM imidazole in equilibration buffer to remove possible contaminants. PA1024 was eluted with 500 mM imidazole in equilibration buffer. The purest fractions based on SDS-PAGE analysis were pooled, dialyzed against 20 mM Tris-Cl, pH 8.0, 200 mM NaCl, 10 % glycerol and stored at -20 °C.

4.5.4 Spectroscopic studies

UV-visible absorbance was recorded with an Agilent Technologies diode-array spectrophotometer Model HP 8453 PC (Santa Clara, CA) equipped with a thermostated water bath in 20 mM TRIS-Cl, pH 8.0, 200 mM NaCl, plus 10 % glycerol at 25 °C. The extinction coefficient of purified PA1024 was determined by extracting the FMN cofactor by heat denaturation of the enzyme. After removing the denatured protein by centrifugation, the concentration of free FMN was determined spectroscopically by using ε_{450} = 12,500 M^{-1} cm^{-1} (55). The concentration of flavin-bound active enzyme was determined by using the experimentally determined extinction coefficient ε_{461} of 12,400 M^{-1} cm^{-1} (this study). The total protein concentration was determined using the Bradford method with bovine serum albumin as standard (56). Initial rates of enzymatic reaction were normalized for the concentration of enzyme-bound flavin.

Fluorescence emission spectra were recorded in 20 mM TRIS-Cl, pH 8.0, 200 mM NaCl, 10 % glycerol, at 25 °C, with a Shimadzu model RF-5301 PC spectrofluorometer (Kyoto, Japan) using a 1 cm path length quartz cuvette. All fluorescence spectra were corrected with the corresponding blanks for Rayleigh and Raman scatterings. For flavin fluorescence, the sample at an FMN concentration of 3.2 μM was excited at 461 nm (447 nm for free FMN) and the emission scan was determined from 480 to 680 nm. Free FMN was obtained by boiling the

native enzyme followed by centrifugation.

4.5.5 Enzymatic assays

Reduction of the enzyme-bound flavin with NAD(P)H was carried out anaerobically with an SF-61DX2 Hi-Tech KinetAsyst high-performance stopped-flow spectrophotometer (Bradford-on-Avon, U.K.), thermostated at 25 ºC. Anaerobiosis of the instrument was obtained by overnight incubation with glucose (5 mM)/glucose oxidase (1 μM) in sodium pyrophosphate, pH 6.0. The enzyme was passed through a desalting PD-10 column equilibrated with 20 mM potassium phosphate, pH 7.0, 200 mM NaCl, transferred in a tonometer and subjected to 20 cycles of degassing by applying vacuum and flushing with argon. The syringes containing 20 mM potassium phosphate, pH 7.0, 200 mM NaCl, as buffer, or the substrate NAD(P)H dissolved in buffer were flushed for 30 min with ultrapure argon before mounting onto the stopped-flow spectrophotometer. To ensure complete removal of traces of oxygen, glucose (2 mM) and glucose oxidase (0.5 μM) were present in the buffer, enzyme and substrate solutions. The concentration of the substrate NAD(P)H was determined spectrophotometrically at 340 nm with the extinction coefficient 6,220 M^{-1} cm^{-1} (57). The concentration of the enzyme after mixing was 15 μM and of NAD(P)H ranged from 90 to 500 μM to maintain pseudo first order conditions.

Turnover of PA1024 with NADH was monitored with a suitable quinone in 20 mM potassium phosphate, 200 mM NaCl, pH 7.0, at 25 °C. NADH was kept at a constant, saturating concentration of 100 μM. Stock solutions of quinones were prepared in 100% ethanol, except 2,6-dimethoxy-1,4-benzoquinone, which was dissolved in DMSO. The final ethanol or DMSO concentration in all reaction mixtures was kept fixed at 1% to minimize possible effects on enzymatic activity. Reaction rates were measured by following NADH consumption at 340 nm, using ε_{340} = 6,220 M^{-1} cm^{-1} (58). In the case of 2-methyl-1,4-naphthoquinone, 343 nm was

followed instead, since its oxidized and reduced forms are isosbestic at this wavelength. The coupled Cyt *c* reduction was monitored by measuring the increase of absorbance at 550 nm using an ε_{550} = 29,500 M^{-1} cm^{-1} in 20 mM potassium phosphate, 200 mM NaCl, pH 7.0, at 25 °C. The final concentrations of NADH and Cyt *c* were saturating at 100 μM and 8.4 μM, respectively. For the experiments that compared the NADH oxidation versus the coupled Cyt *c* reduction, assays were done in triplicate in the presence and absence of 330 units of superoxide dismutase (SOD). Control reactions were run in the absence of the enzyme for all experiments.

NADH oxidase activity was monitored on an Oxy-32 oxygen-monitoring system at atmospheric oxygen in 20 mM potassium phosphate, 200 mM NaCl, pH 7.0 and 25 ^{o}C, by following the initial rate of oxygen consumption. Final concentrations of NADH and the enzyme were 100 μM and 0.14 μM, respectively. To test whether hydrogen peroxide was produced during enzymatic turnover, the rate of oxygen consumption was measured at a fixed substrate concentration in the presence and absence of 170 units of catalase.

The NMO activity assay was performed as previously described (5,6,13,59), following the initial rate of oxygen consumption with a Hansatech Instruments computer-interfaced Oxy-32 oxygen-monitoring system at atmospheric oxygen, i.e., 230 μM oxygen, and 30 °C. Stock solutions of nitronates and nitroalkanes were prepared as previously described (5,13). Enzyme concentration was 180 nM and substrate concentration was 1 mM for P3N or 3-NPA, and 20 mM for 2-nitropropane, propyl-2-nitronate, nitroethane, or ethylnitronate. A positive control for nitronate monooxygenase activity was performed in parallel with purified Pa-NMO to a final concentration of 1.4 nM and 1 mM P3N as previously described (6).

The azoreductase activity of PA1024 was tested as previously described (19,60), by monitoring the reduction of methyl red at 430 nm, using ε_{430} = 23,360 M^{-1} cm^{-1}, in 20 mM

potassium phosphate, 200 mM NaCl, pH 7.0, at 25 °C. The final concentrations of NADH, methyl red and enzyme were 100 μM, 25 μM, and 0.20 μM. The control reaction run in the absence of the enzyme was negligible, consistent with the non-enzymatic reaction between NADH and methyl red occurring only at low pH (61).

4.5.6 Product inhibition of PA1024 with NAD^+

Product inhibition of PA1024 was carried out using NAD^+ as the inhibitor with NADH and 5-hydroxy-1,4-naphthoquinone as substrates in 20 mM potassium phosphate, 200 mM NaCl, pH 7.0, at 25 °C. The final concentration of NADH was held fixed at 100 μM, whereas 5-hydroxy-1,4-naphthoquinone concentrations ranged from 2 μM to 17 μM. The concentration of NAD^+ was kept fixed at 0.4, 1.2, and 3 mM and a set in the absence of NAD^+ was included.

4.5.6.1 Data analysis

The steady-state kinetic parameters for the enzymatic assays were obtained from the fitting of the experimental points to the Michaelis-Menten equation for one substrate using KaleidaGraph software (Synergy Software, Reading, PA). Double reciprocal plots were constructed for product inhibition patterns using KaleidaGraph, and global analysis was carried out using Enzfitter software (Biosoft, Cambridge, U.K.). Stopped-flow traces were fit with the software KinetAsyst 3 (TgK-Scientific, Bradford-on-Avon, U.K.) to Equation 1, which represents a double-exponential process. A represents the absorbance at 461 nm at time t, B_1 and B_2 are the amplitudes of the decrease in absorbance, k_{obs1} and k_{obs2} represent the observed rate constants for the change in absorbance, and C is an offset value accounting for the nonzero absorbance of the enzyme-bound reduced flavin at infinite time.

$$A = B_1^{-k\text{obs1t}} + B_2^{-k\text{obs2t}} + \text{C} \qquad \text{Eq. 1}$$

Concentration dependence of the observed rate constants for flavin reduction was analyzed with Equation 2, where S represents the concentration of organic substrate, k_{red} is the rate constant for flavin reduction at saturating substrate concentration, and K_d is the apparent dissociation constant for substrate binding.

$$k_{obs} = \frac{k_{red}S}{K_d+S} \quad \text{Eq. 2}$$

4.5.7 Bioinformatic analysis

The analysis of the protein sequence of PA1024 was performed with BlastP (62), selecting the non-redundant protein sequence database. Multiple sequence alignments were also created with Clustal Omega (63) and Jalview 2.8 (64). To find hypothetical proteins sharing the 6 motifs of PA1024, the PHI-BLAST (65) feature was utilized. The modifications to the conserved motifs were designed manually based on the multiple sequence alignment generated by BlastP, analysis of potential critical residues, and multiple PHI-BLAST reiterations of varying patterns.

4.6 Acknowledgements

The authors thank Dr. Hongling Yuan for the initial cloning of PA1024 into *P. aeruginosa* PAO1, Daniel Ouedraogo for assistance with the stopped-flow experiments, and Dr. Jim C. Spain for insightful discussions.

4.7 References

1. Roberts, R. J., Chang, Y. C., Hu, Z., Rachlin, J. N., Anton, B. P., Pokrzywa, R. M., Choi, H. P., Faller, L. L., Guleria, J., Housman, G., Klitgord, N., Mazumdar, V., McGettrick, M. G., Osmani, L., Swaminathan, R., Tao, K. R., Letovsky, S., Vitkup, D., Segre, D.,

Salzberg, S. L., Delisi, C., Steffen, M., and Kasif, S. (2011) COMBREX: a project to accelerate the functional annotation of prokaryotic genomes, Nucleic Acids Res 39, D11-14.

2. Anton, B. P., Chang, Y. C., Brown, P., Choi, H. P., Faller, L. L., Guleria, J., Hu, Z., Klitgord, N., Levy-Moonshine, A., Maksad, A., Mazumdar, V., McGettrick, M., Osmani, L., Pokrzywa, R., Rachlin, J., Swaminathan, R., Allen, B., Housman, G., Monahan, C., Rochussen, K., Tao, K., Bhagwat, A. S., Brenner, S. E., Columbus, L., de Crecy-Lagard, V., Ferguson, D., Fomenkov, A., Gadda, G., Morgan, R. D., Osterman, A. L., Rodionov, D. A., Rodionova, I. A., Rudd, K. E., Soll, D., Spain, J., Xu, S. Y., Bateman, A., Blumenthal, R. M., Bollinger, J. M., Chang, W. S., Ferrer, M., Friedberg, I., Galperin, M. Y., Gobeill, J., Haft, D., Hunt, J., Karp, P., Klimke, W., Krebs, C., Macelis, D., Madupu, R., Martin, M. J., Miller, J. H., O'Donovan, C., Palsson, B., Ruch, P., Setterdahl, A., Sutton, G., Tate, J., Yakunin, A., Tchigvintsev, D., Plata, G., Hu, J., Greiner, R., Horn, D., Sjolander, K., Salzberg, S. L., Vitkup, D., Letovsky, S., Segre, D., DeLisi, C., Roberts, R. J., Steffen, M., and Kasif, S. (2013) The COMBREX project: design, methodology, and initial results, PLoS Biol 11, e1001638.

3. Francis, K., Smitherman, C., Nishino, S. F., Spain, J. C., and Gadda, G. (2013) The biochemistry of the metabolic poison propionate 3-nitronate and its conjugate acid, 3-nitropropionate, IUBMB Life 65, 759-768.

4. Francis, K., Russell, B., and Gadda, G. (2005) Involvement of a flavosemiquinone in the enzymatic oxidation of nitroalkanes catalyzed by 2-nitropropane dioxygenase, J. Biol. Chem. 280, 5195-5204.

5. Smitherman, C., and Gadda, G. (2013) Evidence for a transient peroxynitro acid in the reaction catalyzed by nitronate monooxygenase with propionate 3-nitronate, Biochemistry. 52, 2694-2704.

6. Salvi, F., Agniswamy, J., Yuan, H., Vercammen, K., Pelicaen, R., Cornelis, P., Spain, J. C., Weber, I. T., and Gadda, G. (2014) The combined structural and kinetic characterization of a bacterial nitronate monooxygenase from Pseudomonas aeruginosa PAO1 establishes NMO class I and II, J. Biol. Chem. 289, 23764-23775.

7. Ha, J. Y., Min, J. Y., Lee, S. K., Kim, H. S., Kim do, J., Kim, K. H., Lee, H. H., Kim, H. K., Yoon, H. J., and Suh, S. W. (2006) Crystal structure of 2-nitropropane dioxygenase complexed with FMN and substrate. Identification of the catalytic base, J Biol Chem. 281, 18660-18667.

8. Kimura, R. E., and Warshaw, J. B. (1988) Control of fatty acid oxidation by intramitochondrial [NADH]/[NAD+] in developing rat small intestine, Pediatr. Res. 23, 262-265.

9. Le-Quoc, D., and Le-Quoc, K. (1989) Relationships between the NAD(P) redox state, fatty acid oxidation, and inner membrane permeability in rat liver mitochondria, Arch. Biochem. Biophys. 273, 466-478.

10. Wakil, S. J., Green, D. E., Mii, S., and Mahler, H. R. (1954) Studies on the fatty acid oxidizing system of animal tissues. VI. beta-Hydroxyacyl coenzyme A dehydrogenase, J. Biol. Chem. 207, 631-638.

11. Pintea, A. M. (2008) Other Natural Pigments, Food Colorants: Chem. Func. Prop. 101-124.

12. Thomson, R. H. (1991) Distribution of naturally occurring quinones, Pharm. Weekbl. Sci. 13, 70-73.

13. Mijatovic, S., and Gadda, G. (2008) Oxidation of alkyl nitronates catalyzed by 2-nitropropane dioxygenase from Hansenula mrakii, Arch. Biochem. Biophys. 473, 61-68.

14. Soballe, B., and Poole, R. K. (1999) Microbial ubiquinones: multiple roles in respiration, gene regulation and oxidative stress management, Microbiology 145 (Pt 8), 1817-1830.

15. Iyanagi, T. (1990) On the mechanism of one-electron and two-electron reduction of quinones by microsomal flavin enzymes — the kinetic analysis between cyto- chrome-B5 and menadione., Free Radic. Res. Commun. 8, 259-268.

16. Huijbers, M. M., Montersino, S., Westphal, A. H., Tischler, D., and van Berkel, W. J. (2014) Flavin dependent monooxygenases, Arch. Biochem. Biophys. 544, 2-17.

17. Patridge, E. V., and Ferry, J. G. (2006) WrbA from Escherichia coli and Archaeoglobus fulgidus is an NAD(P)H:quinone oxidoreductase, J. Bacteriol. 188, 3498-3506.

18. Chen, H., Wang, R. F., and Cerniglia, C. E. (2004) Molecular cloning, overexpression, purification, and characterization of an aerobic FMN-dependent azoreductase from Enterococcus faecalis, Protein Expr. Purif. 34, 302-310.

19. Nakanishi, M., Yatome, C., Ishida, N., and Kitade, Y. (2001) Putative ACP phosphodiesterase gene (acpD) encodes an azoreductase, J. Biol. Chem. 276, 46394-46399.

20. Bin, Y., Jiti, Z., Jing, W., Cuihong, D., Hongman, H., Zhiyong, S., and Yongming, B. (2004) Expression and characteristics of the gene encoding azoreductase from Rhodobacter sphaeroides AS1.1737, FEMS Microbiol. Lett. 236, 129-136.

21. Nivinskas, H., Staskeviciene, S., Sarlauskas, J., Koder, R. L., Miller, A. F., and Cenas, N. (2002) Two-electron reduction of quinones by Enterobacter cloacae NAD(P)H:nitroreductase: quantitative structure-activity relationships, Arch. Biochem. Biophys. 403, 249-258.

22. Munday, R. (2000) Autoxidation of naphthohydroquinones: effects of pH, naphthoquinones and superoxide dismutase, Free Radic. Res. 32, 245-253.

23. Sedlacek, V., van Spanning, R. J., and Kucera, I. (2009) Characterization of the quinone reductase activity of the ferric reductase B protein from Paracoccus denitrificans, Arch. Biochem. Biophys. 483, 29-36.

24. Anusevicius, Z., Miseviciene, L., Medina, M., Martinez-Julvez, M., Gomez-Moreno, C., and Cenas, N. (2005) FAD semiquinone stability regulates single- and two-electron reduction of quinones by Anabaena PCC7119 ferredoxin:NADP+ reductase and its Glu301Ala mutant, Arch. Biochem. Biophys. 437, 144-150.

25. Deller, S., Macheroux, P., and Sollner, S. (2008) Flavin-dependent quinone reductases, Cell Mol. Life Sci. 65, 141-160.

26. Li, R., Bianchet, M. A., Talalay, P., and Amzel, L. M. (1995) The three-dimensional structure of NAD(P)H:quinone reductase, a flavoprotein involved in cancer chemoprotection and chemotherapy: mechanism of the two-electron reduction, Proc. Natl. Acad. Sci. U. S. A. 92, 8846-8850.

27. Bogachev, A. V., and Verkhovsky, M. I. (2005) Na(+)-Translocating NADH:quinone oxidoreductase: progress achieved and prospects of investigations, Biochemistry (Mosc.) 70, 143-149.

28. Opperman, D. J., Piater, L. A., and van Heerden, E. (2008) A novel chromate reductase from Thermus scotoductus SA-01 related to old yellow enzyme, J. Bacteriol. 190, 3076-3082.

29. Niino, Y. S., Chakraborty, S., Brown, B. J., and Massey, V. (1995) A new old yellow enzyme of Saccharomyces cerevisiae, J. Biol. Chem. 270, 1983-1991.

30. Karplus, P. A., Fox, K. M., and Massey, V. (1995) Flavoprotein structure and mechanism. 8. Structure-function relations for old yellow enzyme, FASEB J. 9, 1518-1526.

31. Gadda, G. (2012) Oxygen activation in flavoprotein oxidases: the importance of being positive, Biochemistry 51, 2662-2669.

32. Jordan, B. J., Cooke, G., Garety, J. F., Pollier, M. A., Kryvokhyzha, N., Bayir, A., Rabani, G., and Rotello, V. M. (2007) Polymeric model systems for flavoenzyme activity: towards synthetic flavoenzymes, Chem. Commun. (Camb). 1248-1250.

33. Nishimoto, K., Watanabe, Y., and Yagi, K. (1978) Hydrogen bonding of flavoprotein. I. Effect of hydrogen bonding on electronic spectra of flavoprotein, Biochim. Biophys. Acta. 526, 34-41.

34. Zhao, M., Sun, P. F., Du, L. N., Wang, G., Jia, X. M., and Zhao, Y. H. (2014) Biodegradation of methyl red by Bacillus sp. strain UN2: decolorization capacity, metabolites characterization, and enzyme analysis, Environ. Sci. Pollut. Res. Int. 21, 6136-6145.

35. Jadhav, S. B., Patil, N. S., Watharkar, A. D., Apine, O. A., and Jadhav, J. P. (2013) Batch and continuous biodegradation of Amaranth in plain distilled water by P. aeruginosa

BCH and toxicological scrutiny using oxidative stress studies, Environ. Sci. Pollut. Res. Int. 20, 2854-2866.

36. Kabra, A. N., Khandare, R. V., and Govindwar, S. P. (2013) Development of a bioreactor for remediation of textile effluent and dye mixture: a plant-bacterial synergistic strategy, Water Res. 47, 1035-1048.

37. Ryan, A., Wang, C. J., Laurieri, N., Westwood, I., and Sim, E. (2010) Reaction mechanism of azoreductases suggests convergent evolution with quinone oxidoreductases, Protein Cell. 1, 780-790.

38. Ryan, A., Kaplan, E., Nebel, J. C., Polycarpou, E., Crescente, V., Lowe, E., Preston, G. M., and Sim, E. (2014) Identification of NAD(P)H quinone oxidoreductase activity in azoreductases from P. aeruginosa: azoreductases and NAD(P)H quinone oxidoreductases belong to the same FMN-dependent superfamily of enzymes, PLoS One 9, e98551.

39. Green, L. K., La Flamme, A. C., and Ackerley, D. F. (2014) Pseudomonas aeruginosa MdaB and WrbA are water-soluble two-electron quinone oxidoreductases with the potential to defend against oxidative stress, J. Microbiol. 52, 771-777.

40. Knox, R. J., Jenkins, T. C., Hobbs, S. M., Chen, S., Melton, R. G., and Burke, P. J. (2000) Bioactivation of 5-(aziridin-1-yl)-2,4-dinitrobenzamide (CB 1954) by human NAD(P)H quinone oxidoreductase 2: a novel co-substrate-mediated antitumor prodrug therapy, Cancer Res. 60, 4179-4186.

41. Ross, D., Siegel, D., Beall, H., Prakash, A. S., Mulcahy, R. T., and Gibson, N. W. (1993) DT-diaphorase in activation and detoxification of quinones. Bioreductive activation of mitomycin C, Cancer Metastasis Rev. 12, 83-101.

42. Knox, R. J., Boland, M. P., Friedlos, F., Coles, B., Southan, C., and Roberts, J. J. (1988) The nitroreductase enzyme in Walker cells that activates 5-(aziridin-1-yl)-2,4-dinitrobenzamide (CB 1954) to 5-(aziridin-1-yl)-4-hydroxylamino-2-nitrobenzamide is a form of NAD(P)H dehydrogenase (quinone) (EC 1.6.99.2), Biochem. Pharmacol. 37, 4671-4677.

43. Knox, R. J., Friedlos, F., Jarman, M., and Roberts, J. J. (1988) A new cytotoxic, DNA interstrand crosslinking agent, 5-(aziridin-1-yl)-4-hydroxylamino-2-nitrobenzamide, is formed from 5-(aziridin-1-yl)-2,4-dinitrobenzamide (CB 1954) by a nitroreductase enzyme in Walker carcinoma cells, Biochem. Pharmacol. 37, 4661-4669.

44. Tedeschi, G., Chen, S., and Massey, V. (1995) DT-diaphorase. Redox potential, steady-state, and rapid reaction studies, J. Biol. Chem. 270, 1198-1204.

45. Ullmann, E., Tan, T. C., Gundinger, T., Herwig, C., Divne, C., and Spadiut, O. (2014) A novel cytosolic NADH:quinone oxidoreductase from Methanothermobacter marburgensis, Biosci. Rep. 34, e00167.

46. Sollner, S., Nebauer, R., Ehammer, H., Prem, A., Deller, S., Palfey, B. A., Daum, G., and Macheroux, P. (2007) Lot6p from Saccharomyces cerevisiae is a FMN-dependent reductase with a potential role in quinone detoxification, FEBS J. 274, 1328-1339.

47. Suzuki, Y., Yoda, T., Ruhul, A., and Sugiura, W. (2001) Molecular cloning and characterization of the gene coding for azoreductase from Bacillus sp. OY1-2 isolated from soil, J. Biol. Chem. 276, 9059-9065.

48. Laskowski, M. J., Dreher, K. A., Gehring, M. A., Abel, S., Gensler, A. L., and Sussex, I. M. (2002) FQR1, a novel primary auxin-response gene, encodes a flavin mononucleotide-binding quinone reductase, Plant Physiol. 128, 578-590.

49. Sparla, F., Tedeschi, G., Pupillo, P., and Trost, P. (1999) Cloning and heterologous expression of NAD(P)H:quinone reductase of Arabidopsis thaliana, a functional homologue of animal DT-diaphorase, FEBS Lett. 463, 382-386.

50. Leskovac, V., Trivic, S., Wohlfahrt, G., Kandrac, J., and Pericin, D. (2005) Glucose oxidase from Aspergillus niger: the mechanism of action with molecular oxygen, quinones, and one-electron acceptors, Int. J. Biochem. Cell Biol. 37, 731-750.

51. Siegel, D., Reigan, P., Ross, D. (2008) One- and Two-Electron-Mediated Reduction of Quinones: Enzymology and Toxilogical Implications, Adv. Bioact. Res. 169-197.

52. Chesis, P. L., Levin, D. E., Smith, M. T., Ernster, L., and Ames, B. N. (1984) Mutagenicity of quinones: pathways of metabolic activation and detoxification, Proc. Natl. Acad. Sci. U. S. A. 81, 1696-1700.

53. Gonzalez, C. F., Ackerley, D. F., Lynch, S. V., and Matin, A. (2005) ChrR, a soluble quinone reductase of Pseudomonas putida that defends against H2O2, J. Biol. Chem. 280, 22590-22595.

54. Muller, N., Schleheck, D., and Schink, B. (2009) Involvement of NADH:acceptor oxidoreductase and butyryl coenzyme A dehydrogenase in reversed electron transport during syntrophic butyrate oxidation by Syntrophomonas wolfei, J. Bacteriol. 191, 6167-6177.

55. Whitby, L. G. (1953) A new method for preparing flavin-adenine dinucleotide, Biochem. J. 54, 437-442.

56. Bradford, M. M. (1976) A rapid and sensitive method for the quantitation of microgram quantities of protein utilizing the principle of protein-dye binding, Anal. Biochem. 72, 248-254.

57. McComb, R. B., Bond, L. W., Burnett, R. W., Keech, R. C., and Bowers, G. N., Jr. (1976) Determination of the molar absorptivity of NADH, Clin. Chem. 22, 141-150.

58. Matthews, R. G. (1986) Methylenetetrahydrofolate reductase from pig liver, Methods Enzymol. 122, 372-381.

59. Francis, K., and Gadda, G. (2009) Kinetic evidence for an anion binding pocket in the active site of nitronate monooxygenase, Bioorg. Chem. 37, 167-172.

60. Punj, S., and John, G. H. (2009) Purification and identification of an FMN-dependent NAD(P)H azoreductase from Enterococcus faecalis, Curr. Issues. Mol. Biol. 11, 59-65.

61. Nam, S., and Renganathan, V. (2000) Non-enzymatic reduction of azo dyes by NADH, Chemosphere 40, 351-357.

62. Altschul, S. F., Madden, T. L., Schaffer, A. A., Zhang, J., Zhang, Z., Miller, W., and Lipman, D. J. (1997) Gapped BLAST and PSI-BLAST: a new generation of protein database search programs, Nucleic Acids Res. 25, 3389-3402.

63. Sievers, F., and Higgins, D. G. (2014) Clustal Omega, accurate alignment of very large numbers of sequences, Methods Mol. Biol. 1079, 105-116.

64. Waterhouse, A. M., Procter, J. B., Martin, D. M., Clamp, M., and Barton, G. J. (2009) Jalview Version 2--a multiple sequence alignment editor and analysis workbench, Bioinformatics 25, 1189-1191.

65. Zhang, Z., Schaffer, A. A., Miller, W., Madden, T. L., Lipman, D. J., Koonin, E. V., and Altschul, S. F. (1998) Protein sequence similarity searches using patterns as seeds, Nucleic Acids Res. 26, 3986-3990.

66. Skelly, J. V., Sanderson, M. R., Suter, D. A., Baumann, U., Read, M. A., Gregory, D. S., Bennett, M., Hobbs, S. M., and Neidle, S. (1999) Crystal structure of human DT-

diaphorase: a model for interaction with the cytotoxic prodrug 5-(aziridin-1-yl)-2,4-dinitrobenzamide (CB1954), J. Med. Chem. 42, 4325-4330.

67. Foster, C. E., Bianchet, M. A., Talalay, P., Zhao, Q., and Amzel, L. M. (1999) Crystal structure of human quinone reductase type 2, a metalloflavoprotein, Biochemistry 38, 9881-9886.

5 PH EFFECTS DEMONSTRATE TWO CATALYTIC REGIMES IN A FLAVIN-DEPENDENT NADH:QUINONE OXIDOREDUCTASE

5.1 Abstract

NAD(P)H:quinone oxidoreductases (NQOs) catalyze the flavin-mediated two electron reduction of quinones to hydroquinones using NAD(P)H as an electron donor. NQOs are proposed to detoxify quinones by preventing one-electron reductases from reducing the quinone to the semiquinone, the latter of which wreaks cellular havoc though chain radical reactions resulting in superoxide generation. PA1024 is a recently discovered NQO from *Pseudomonas aeruginosa* with proposed roles in quinone detoxification and maintenance of the cellular [NAD^+]/[NADH] balance. The present study utilizes pH and viscosity effects on the reductive half-reaction and steady-state kinetics of PA1024 to gain additional mechanistic clues on the general NQO reaction. The results revealed that PA1024 has two competent, catalytic regimes of activity at low and high pH modulated by a separate deprotonation event with pK_a ~6. The slow and fast regimes of activity may have implications in the *P. aeruginosa* pH-influenced metabolic stress response.

5.2 Introduction

The NASA spacecraft STARDUST collected interstellar dust particles in 2004 and determined the main class of compounds present were quinone-type molecules, suggesting they are some of the most ancient organic molecules in the universe.[1] Quinones are cyclic unsaturated compounds containing two carbonyl groups either adjacent or separated by a vinylene group in a six-membered ring.[2] Found in all domains of life from Bacteria to Archaea to Eurkarya[3], quinones are essential to biological processes such as electron transfer and oxidative

phosphorylation[4], which utilize ubiquinone (Coenzyme Q10) or some variation of it to carry out redox reactions. Quinones can participate in a wide array of chemistry in addition to redox catalysis including cycloadditions, halogenations, and radical reactions.[5]

NAD(P)H:quinone oxidoreductases (NQOs) catalyze the flavin-mediated two-electron reduction of quinones via the oxidation of NAD(P)H. The most well studied member of these enzymes is NAD(P)H:quinone oxidoreductase 1 (NQO1). The consensus among the majority of the scientific community is the enzyme serves to detoxify quinones through the two electron reduction to the hydroquinone, thereby preventing one electron reductases such as cytochrome p450 reductase that act on the quinone to produce toxic semiquinone radicals.[6-9] On the other hand, several quinone-containing drugs are activated upon NQO1 action to become cytotoxic such as β-lapachome and mitomycin C.[6, 8, 10] The bioactivation of specific quinones by NQO1 has prompted the development of antitumor and chemotherapeutic compounds incorporating quinone moieties.

An alternative role for these enzymes could entail maintenance of the [NADH]/[NAD^+] ratio in the cell. The [NADH]/[NAD^+] ratio has a significant impact on the ability to break down fatty acids, as a low ratio stimulates β-oxidation.[11] This role was speculated for a newly discovered NQO in *Pseudomonas aeruginosa*, PA1024, based on the genomic context and kinetic specificity for NADH. The operon PA1024 belongs to consists of probable acyl-CoA dehydrogenases, a β-hydroxylacyl CoA dehydrogenase, an enoyl-CoA hydratase/isomerase, a short chain dehydrogenase, and a porin,[12, 13] all of which are proteins typically involved in β-oxidation. The requirement for NAD^+ in β-oxidation stems from the enzyme β-hydroxylacyl CoA dehydrogenase.[14]

PA1024 was originally annotated in the GenBank™ and PDB databases as a nitronate monooxygenase (NMO), and the highest levels of sequence identity are shared with *P. aeruginosa* NMO and *Streptococcus pneumoniae* enoyl-acyl carrier protein reductase (FabK) at 32% and 31%, respectively. Despite the considerable levels of sequence identity and structural overlap, subsequent kinetic studies demonstrated PA1024 does not possess NMO nor enoyl-acyl carrier protein reductase activity[15, 16], but instead the enzyme catalyzes the FMN-dependent oxidation of NADH utilizing quinones as electron acceptors (**Scheme 5.1**)[15]. Closer inspection of PA1024 revealed the active sites of NMO and FabK contain key differences from PA1024 and that may explain the divergence in catalytic function.[15, 17]

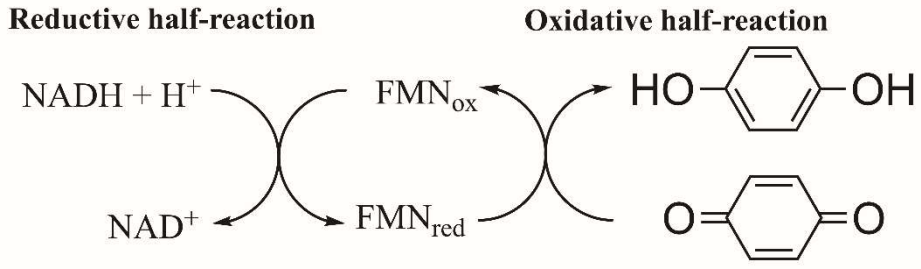

Scheme 5.1 Reaction catalyzed by PA1024

PA1024 shares little sequence similarity (< 25 %) to known flavin-dependent NQOs such as eukaryotic NQO1[18, 19], eukaryotic N-ribosyldihydronicotinamide:quinone reductase 2 (NQO2)[20], lot6p from *Saccharomyces cerevisiae*[7], tryptophan repressor binding protein from *Escherichia coli* (WrbA)[9, 21, 22], or Pst2p (protoplasts-secreted 2).[23] PA1024 demonstrates a strict specificity for NADH with virtually no reactivity with NADPH, and the best quinone substrates for the enzyme based on the second order rate constant k_{cat}/K_m are 1,4-benzoquinone, 5,8-dihydroxy-1,4-naphthoquinone and 5-hydroxy-1,4-naphthoquinone.[15] The TIM-barrel fold of the 34 kDa monomer of PA1024[24] is in contrast to most NAD(P)H quinone oxidoreductases reported to date which are typically a dimer in a flavodoxin-like fold.[25]

In the present study we sought to gain insights on the catalytic mechanism through a detailed investigation into the effect of pH on the reductive half-reaction and pH and viscosity on the steady-state kinetics of PA1024. The pH effects reveal two regimes of catalytic activity for the enzyme dictated by a deprotonation event with pK_a ~6. The two catalytic regimes are discussed in the context of the pH effect on *P. aeruginosa* virulence.

5.3 Materials and Methods

5.3.1 Materials

Nicotinoamide adenine dinucleotide reduced (NADH) was from VWR (Randor, PA). 1,4-benzoquinone, 5-hydroxy-1,4-naphthoquinone, sucrose, glucose, glucose oxidase, and piperazine were from Sigma-Aldrich (St. Louis, MO). Sodium chloride, sodium phosphate and sodium pyrophosphate were from Fischer Scientific (Fairlawn, NJ). PA1024 was prepared as described previously.[15] All other reagents used were of the highest purity commercially available.

5.3.2 Enzymatic Assays

All assays were conducted in buffer consisting of 20 mM sodium phosphate, sodium pyrophosphate, or piperazine (depending on the pH) and 200 mM sodium chloride at 25 ^{o}C. The reduction of enzyme-bound FMN by NADH was monitored at 461 nm on a SF-61DX2 Hi-Tech KinetAsyst high-performance stopped-flow spectrophotometer (Bradford-on-Avon, U.K.), thermostatted at 25 ºC. Anaerobiosis of the instrument and all buffers, substrate, and enzyme solutions was achieved according to published procedures.[15] The concentration of the substrate NADH was determined using the extinction coefficient at 340 nm of 6,220 M^{-1} cm^{-1}.[26] The concentration of the enzyme after mixing was 15 μM and of NADH ranged from 90 to 500 μM to maintain pseudo first order conditions.

The steady-state kinetic parameters of PA1024 were monitored on an Agilent Technologies UV-visible Spectrophotometer (Santa Clara, CA) thermostatted at 25 ^{o}C in 20 mM sodium phosphate, sodium pyrophosphate, or piperazine (depending on the pH) and 200 mM sodium chloride. The reducing substrate was NADH and the electron acceptor was either 1,4-benzoquinone or 5-hydroxy-1,4-naphthoquinone. Initially, a fixed concentration of 100 μM NADH was used across the pH range of 5-11 and variable quinone concentrations ranging from 4 μM to 200 μM for 1,4-benzoquinone and 12.5 μM to 200 μM for 5-hydroxy-1,4-naphthoquinone. Because of the requirement for steady-state kinetics where the [S] » [E], accurate K_m values lower than roughly 10 μM concentration were not measureable. The K_m of 1,4-benzoquinone could only be measured at pHs 5-7.5, and 10-11. The K_m for each of these pH values for 1,4-benzoquinone was less than 20 μM (data not shown). Because of these complications, very little emphasis is put on the K_m and k_{cat}/K_m values of the quinone substrates. To ensure NADH was saturating at all pH values, the steady-state kinetic values were measured at varying concentrations of NADH and a saturating concentration for each quinone at the pH extremes of 5 and 11. The kinetics at pH 5 demonstrated no dependence on the concentration of NADH. Upon determining 100 μM was not sufficient to fully saturate at pH 11, which yielded a K_m value for NADH of 80 μM, pHs 10.5, 10, 9.5 and 8.5 were assayed at variable NADH concentrations and a fixed, saturating quinone concentration of 200 μM to obtain a K_m value for NADH and an close estimate of the true k_{cat} values. A limiting value of 30 μM was calculated for the K_m of NADH at low pH. Consequently, when the apparent steady-state kinetic parameters were determined at a fixed concentration of 100 μM NADH and variable quinone concentration from pH 5 to 8.5, they approximate about 80% of the true k_{cat} values. Since the values are plotted on a log scale, the overall pK_a's and limiting values would be similar if 100% saturation was

achieved. Stock solutions of quinones were prepared in 100% ethanol. The final ethanol concentration in all reaction mixtures was kept fixed at 1% to minimize possible effects on enzymatic activity. Reaction rates were measured by following the disappearance of NADH absorption at 340 nm, using ε_{340} = 6,220 M^{-1} cm^{-1}.[26] Final enzyme concentrations ranged from 100-200 nM. All steady-state kinetic assays were initiated by the addition of NADH.

Solvent viscosity effects on steady-state kinetic parameters were measured in 20 mM sodium pyrophosphate, 200 mM NaCl at pH 6.0 and 8.5. Glucose and sucrose were investigated independently as viscosigens at both pH 6.0 and 8.5. The relative viscosity values at 25 °C were calculated according to the reference values at 20 °C from Lide.[27] For each set of viscosigen concentration, NADH was held constant at 100 μM and 5-hydroxy-1,4-naphthoquinone was varied from 10-140 μM. The final enzyme concentration was 140 nM.

5.3.3 Data Analysis

The steady-state kinetic parameters were obtained from the fitting of the experimental points of the enzymatic assays to the Michaelis-Menten equation for one substrate using KaleidaGraph software (Synergy Software, Reading, PA). The pH profiles of the k_{red} values for NADH were fit to eq 1, which describes a curve that plateaus to a limiting value (C_L) at low pH and increases with increasing pH with slope of +1 and plateaus to a limiting value (C_H) at high pH. The pH profiles of the k_{cat} values for 1,4-benzoquinone and k_{cat} and k_{cat}/K_m values for 5-hydroxy-1,4-naphthoquinone were fit to eq 2, which describes a curve that plateaus to a limiting value (C_L) at low pH and increases with increasing pH with slope of +1 and plateaus to a limiting value (C_H) at pH 8-9 to decrease at pH 10-12 with a slope of -1. Eq 2 is also known as a bell-shaped dependence with an offset at low pH.

$$\log(k_{red}) = \log\frac{C_H + C_L(10^{(pKa-pH)})}{1+10^{(pKa-pH)}} \quad \text{Eq. 1}$$

$$\log(k_{cat}, k_{cat}/K_m) = \log\left(\frac{C_H + C_L(10^{(pKa1-pH)})}{1+10^{(pKa1-pH)}+10^{(pH-pKa2)}}\right) \quad \text{Eq. 2}$$

Stopped-flow traces were fit using the software KinetAsyst 3 (TgK-Scientific, Bradford-on-Avon, U.K.) to eq 3, which defines a double-exponential process. *A* represents the absorbance at 461 nm at time t, B_1 and B_2 are the amplitudes of the decrease in absorbance, k_{obs1} and k_{obs2} represent the observed rate constants for the change in absorbance, and C is an offset value accounting for the nonzero absorbance of the enzyme-bound reduced flavin at infinite time. For the stopped-flow traces that were triphasic, eq 4 was used, which is similar to eq 3, except an additional B_3 amplitude and k_{obs3} are included for the third phase. Concentration dependence of the observed rate constants for flavin reduction was analyzed with eq 5, where *S* represents the concentration of substrate, k_{red} is the rate constant for flavin reduction at saturating concentration of substrate, and K_d is the apparent dissociation constant for substrate binding. Viscosity effects on the k_{cat} values were fit to eq 6; those on the k_{cat}/K_m values were fit to eq 7. In these equations $(k)_o$ and $(k)_\eta$ are the kinetic parameters in the absence and presence of viscosigen, respectively, *S* is the degree of viscosity dependence, η_{rel} is the relative viscosity of the aqueous buffered solution, and Y_H is the limiting value of the steady-state kinetic parameter of interest at high concentration of viscosigen. Sequence identities reported in the introduction were performed with ClustalOmega.[28]

$$A = B_1^{-k\text{obs1t}} + B_2^{-k\text{obs2t}} + \text{C} \quad \text{Eq. 3}$$

$$A = B_1^{-k\text{obs1t}} + B_2^{-k\text{obs2t}} + B_3^{-k\text{obs3t}} + \text{C} \quad \text{Eq. 4}$$

$$k_{\text{obs}} = \frac{k_{\text{red}} S}{K_{\text{d}} + S} \quad \text{Eq. 5}$$

$$k_{\text{obs}} \frac{(k)_o}{(k)_\eta} = \text{S}(\eta_{\text{rel}} - 1) + 1 \quad \text{Eq. 6}$$

$$k_{\text{obs}} \frac{(k)_o}{(k)_\eta} = \frac{1}{1 + \frac{Y_H(\eta_{\text{rel}} - 1)}{(\eta_{\text{rel}} - 1) + S}} \quad \text{Eq. 7}$$

5.4 Results

5.4.1 Reductive half-reaction at pH 8.0

To evaluate the oxidation of NADH by PA1024, the reduction of the enzyme-bound FMN was followed by monitoring the decrease at 461 nm under anaerobic conditions at pH 8.0 and 25 ^{o}C with the use of a stopped-flow spectrophotometer. The stopped-flow traces and concentration dependence of NADH for the observed rate constant of flavin reduction, k_{obs}, are shown in **Figure 5.1** as an example. The enzyme was fully reduced in a triphasic manner with the fast phase accounting for 93% of the amplitude change. The slow phases accounted for a combined 7 % of the total amplitude change and could be the result of a fraction of damaged enzyme. Stopped-flow traces were analyzed with eq 3, and the resulting parameters were fit to eq 5, demonstrating the enzyme was fully saturated from 90-500 μM NADH, with a k_{red} value of 38

± 1 s^{-1}. The K_d value was not measurable because 90 µM was the lowest concentration of NADH possible without compromising pseudo-first order conditions; however, the fact that the enzyme was fully saturated with 90 µM suggests a K_d value equal to or less than 10 µM.

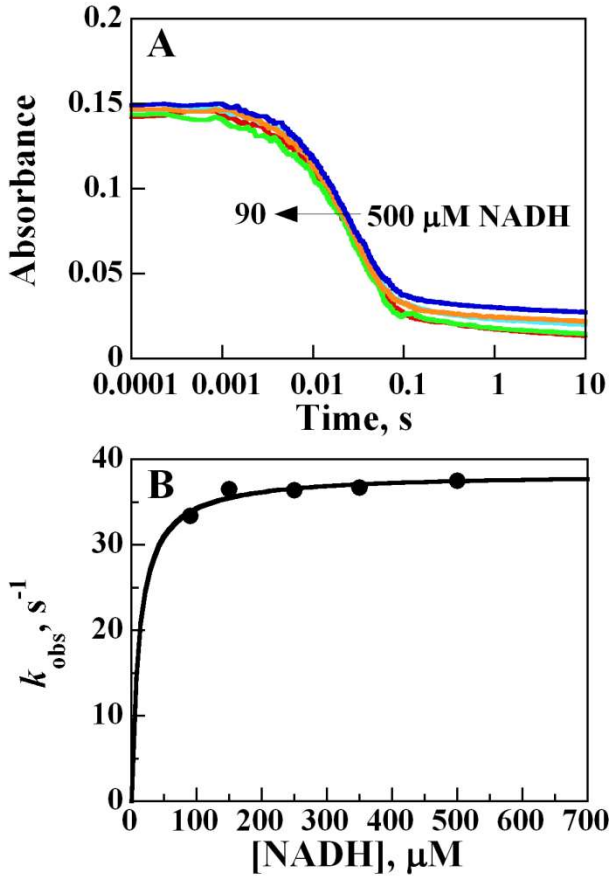

Figure 5.1 Anaerobic reduction of PA1024 by NADH at pH 8.0.
(A) Anaerobic reduction with 90-500 µM NADH of PA1024 at 8.0 and 25 °C. (B) Observed rate constants of flavin reduction as a function of NADH concentration
Note the log time scale on the x axis. The dead time of the instrument was 2.2 ms. 20 mM sodium phosphate and 200 mM NaCl were the buffer conditions.

5.4.2 Effect of pH on the reductive half-reaction

The pH dependence of the rate constant of flavin reduction, k_{red}, was determined to establish relevant ionizations involved in the reductive half-reaction (**Figure 5.2**). The k_{red} values

were determined over a pH range of 6-11 on a stopped-flow spectrophotometer by measuring the decrease in FMN absorbance at 461 upon reduction by NADH. The concentration of NADH was varied from 90-500 μM at all pHs. Biphasic stopped-flow traces were analyzed with eq 3 and triphasic traces were analyzed with eq 4. The resulting parameters were fit to eq 5 to give a k_{red} and K_d value. All pH values were biphasic or triphasic in nature with the fast phase accounting for more than 90% of the total amplitude change and the NADH K_d was below 90 uM for all pH values except pH 11, which gave a measureable K_d value of 140 ± 25 μM. An accurate y-intercept of zero could be obtained for pH 11, indicating that flavin reduction is irreversible. The other pH values may be irreversible as well, but it is not possible to verify since accurate y-intercepts could not be calculated.

As shown in **Figure 5.2**, the k_{red} values showed an offset at low pH and increased with increasing pH to a limiting value at high pH. The two catalytic regimes are modulated by a group with a pK_a value of 6.3 ± 0.2, which is required to be deprotonated for maximal k_{red}. The k_{red} pH profile values are listed in the top of Table 1. At all concentrations of NADH in all pHs tested, there was no accumulation of a charge transfer band between 500-700 nm, the absence of which indicates no detectable formation of a E_{red}-NAD^+ complex[29] (data not shown).

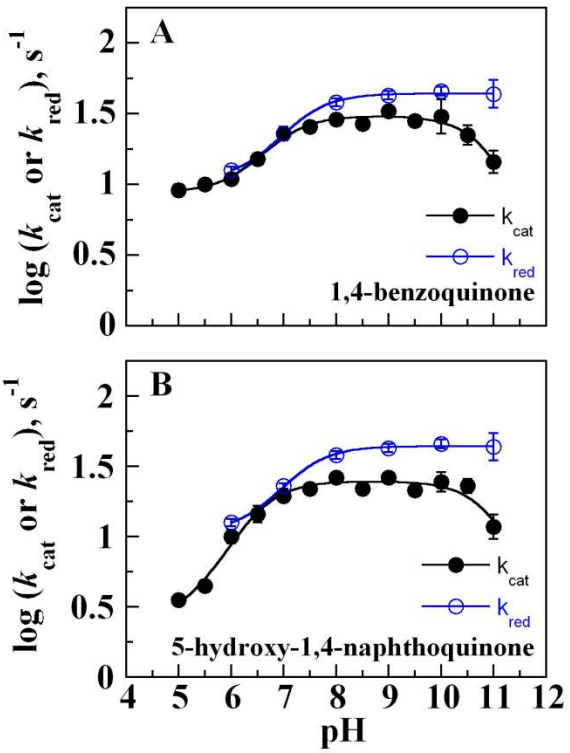

Figure 5.2 Effect of pH on the k_{red} and k_{cat} of PA1024.
(A and B - blue open circles) effect of pH on the k_{red} and (A – solid black circles) effect of pH on the k_{cat} of PA1024 with 1,4-benzoquinone and (B - solid black circles) effect of pH on the k_{cat} with 5-hydroxy-1,4-naphthoquinone.
Assays were carried out in 20 mM sodium phosphate or sodium pyrophosphate (depending on the pH) and 200 mM sodium chloride at 25 ^{o}C. NADH was varied from 90 µM to 500 µM. Curves with open blue circles were fit to eq 1. Curves with solid black circles were fit to eq 2.

5.4.3 Effect of pH on the steady-state kinetics

The pH-dependences of the steady-state kinetic parameters k_{cat} and k_{cat}/K_m were determined with 1,4-benzoquinone and 5-hydroxy-1,4-naphthoquinone as substrates to establish relevant ionizations of groups involved in the overall catalytic cycle. The k_{cat} and k_{cat}/K_m values were obtained over a pH range of 5-11 by measuring the decrease in absorbance at 340 nm, indicating the oxidation of NADH to NAD^+. NADH was held at a constant 100 µM and the quinone was varied for the pH range of 5-8.0. NADH was varied and the quinone was held at a saturating concentration for the pH range of 8.5-11 (See materials and methods for explanation).

All of the pK_a values and limiting values for the steady-state kinetics are listed in the bottom of **Table 5.1**. As shown in **Figure 5.2**, the k_{cat} pH-profile with 1,4-benzoquinone was different from the k_{red} pH profile, in that it contained an additional group at high pH required to be protonated for maximal k_{cat}. The two groups are distinct as the number of pH unit separation between the pair is greater than 2. The group at 6.4 is required to be deprotonated for maximal k_{cat}, whereas the group at is 11.0 required to be protonated for maximal k_{cat}, defining an optimal pH of 8.5 for the NADH:benzoquinone reductase activity.

The k_{cat} pH-profile with 5-hydroxy-1,4-naphthoquinone in **Figure 5.2B** demonstrated a bell-shape dependence with an offset at low pH, defining two separate pK_as with an optimal pH of 8.4. The second pK_a seen in both k_{cat} profiles of the quinone substrates was absent in the k_{red} pH profile, indicating the second pK_a occurs in the oxidative half-reaction; however, the second pK_a of 11 is not well defined since the highest pH tested was pH 11, thus we cannot definitively conclude this pK_a is real and cannot elaborate further on the significance of this pKa. The k_{cat}/K_m pH profile for 5-hydroxy-1,4-NQ shown in Figure S2 of the supplemental information was qualitatively similar to the k_{cat} pH profile but displayed large errors due to the barely measureable, low μM K_M values for the quinone substrate. 4 μM was the lowest quinone concentration possible without violating the first requirement of steady-state kinetics, ie; [S] » [E]. The fact that the k_{cat} and k_{cat}/K_m pH profiles have almost identical shapes establishes these two pK_as are purely catalytic and not related to any binding event.

Table 5.1 pH effects on the k_{red} and k_{cat} of PA1024.

		k_{red} (s^{-1})		
Substrate	pK_a [c]		$(k_{red})_L$ [a]	$(k_{red})_H$ [b]
NADH	7.3 [e]		11 [f]	44 [f]
		k_{cat} (s^{-1})		
Substrate*	pK_{a1} [d]	pK_{a2} [d]	$(k_{cat})_L$ [a]	$(k_{cat})_H$ [b]
5-H-1,4-NQ	6.4 [e]	11.0 [e]	3 [f]	25 [f]
1,4-BQ	6.9 [e]	11.0 [e]	9 [f]	31 [f]

1,4-BQ: 1,4-benzoquinone; 5-H-1,4-NQ: 5-hydroxy-1,4-naphthoquinone
[a] pH-independent limiting value at low pH
[b] pH-independent limiting value at high pH
[c] Determined by using eq 1
[d] Determined by using eq 2
[e] (± 0.1)
[f] (± 1)
*NADH was used as the reducing substrate

5.4.4 Effect of viscosity on the steady-state kinetics

The effect of viscosity on the kinetic parameters of PA1024 with 5-hydroxy-1,4-napthoquinone at pH 8.5 was carried out to assess the presence or absence of diffusion-controlled events during the catalytic cycle. The k_{cat} and k_{cat}/K_m values were determined at different concentrations of viscosigen on a UV-Visible spectrophotometer by measuring the decrease in NADH absorbance at 340 nm. NADH was fixed at 100 μM and the quinone was varied. As shown in **Figure 5.3A**, the effect of glucose on k_{cat} at pH 8.5 was linear with a slope of 34 ± 3 %, demonstrating the presence of a diffusion-controlled event in k_{cat}.

Because the K_m for 5-hydroxy-1,4-naphthoquinone was not measurable at pH 8.5 at increased relative viscosities, accurate k_{cat}/K_m values could not be obtained at different relative viscosities for pH 8.5. Thus, the pH was lowered to 6.0 and the effect of glucose was performed. For the k_{cat} value, glucose gave a value of 20 ± 2 % (**Figure 5.3B**). For the k_{cat}/K_m value, glucose (**Figure 5.3C**) gave an inverse solvent effect of 77 ± 11 %. The effect of viscosity at pH 11 could

not be measured due to an apparent side reaction between glucose with the quinone substrate that prevented accurate determination of initial rates.

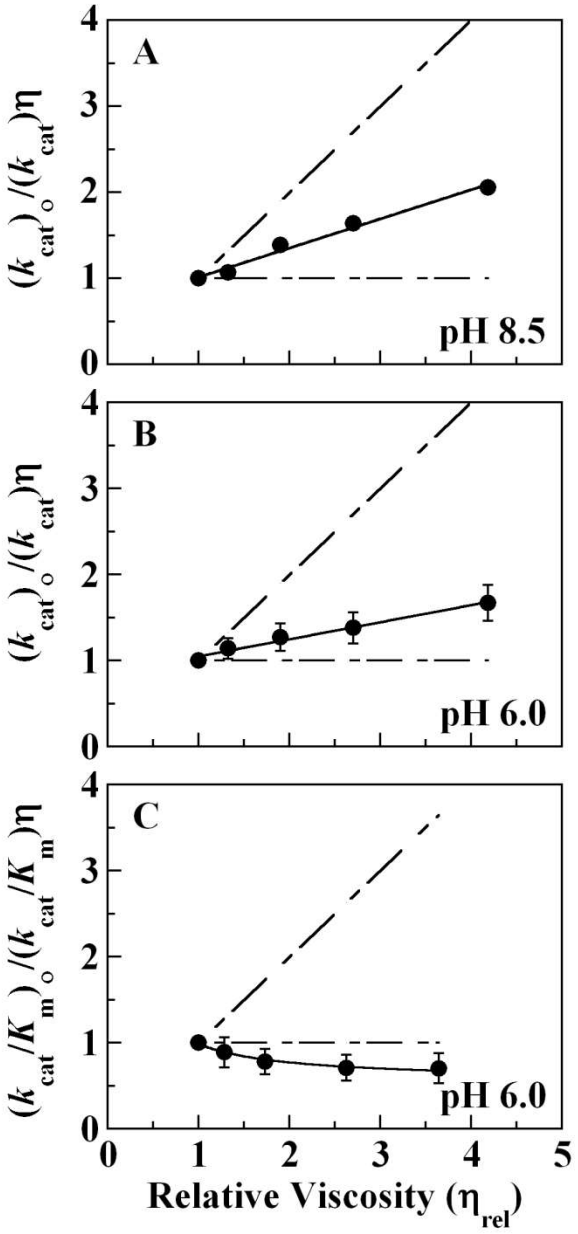

Figure 5.3 Effect of viscosity on k_{cat} and k_{cat}/K_m of PA1024.
(A) Effect of viscosity on the k_{cat} of PA1024 at pH 8.5 and 25 ^{o}C. (B) Effect of viscosity on the k_{cat} of PA1024 at pH 6.0 and 25 ^{o}C. Panel C. Effect of viscosity on the k_{cat}/K_m of PA1024 at pH 6.0 and 25 ^{o}C.
PA1024 activity was measured at varying concentrations of 5-hydroxy-1,4-naphthoquinone and 100 μM NADH at different concentrations of glucose. The buffer consisted of 20 mM sodium phosphate and 200 mM NaCl. The normalized k_{cat} or k_{cat}/K_m values are shown as a function of relative viscosity. Panels A and B were fit to eq 6. Panel C was fit to eq 7. The dashed line with a

slope of 1 represents the theoretical limit for a fully diffusion controlled process, whereas the dashed line with a slope of 0 represents a process that lacks diffusion control.

5.5 Discussion

The present study aimed to examine to the effect of pH and viscosity on the kinetic parameters of PA1024 to gain mechanistic insights on the catalytic cycle. The results indicate there are two active states of the enzyme, a slow regime at low pH and a fast regime at high pH, which are controlled by the depronation of an enzymatic group with pK_a ~7. The two regimes could have implications in the *P. aeruginosa* pH-influenced stress response. An additional group with pK_a ~11 is required to be protonated, indicating the oxidative half-reaction concludes with protonation of the hydroquinolate, which has been proposed for the prototypical eukaryotic NQO1.[30] Viscosity effects on the kinetics of PA1024 have been employed to gain additional mechanistic clues. The details are discussed below.

5.5.1 PA1024 possesses two competent pH regimes of catalytic activity

PA1024 operates over a broad pH range with two catalytic regimes of activity that are modulated by the deprotonation of an enzymatic group (**Figure 5.2**). Evidence of this conclusion stems from the effect of pH on the k_{red} and k_{cat} values. The fast regime at basic pH is four fold faster than the slow regime at acidic pH. Although this may seem like a small fold increase, even small fluctuations in the [NADH]/[NAD^+] ratio can have significant effects on various metabolic processes.[31, 32]

The pH-driven change in the catalytic rate of PA0124 may have implications in *P. aeruginosa* antibiotic resistance and metabolic versatility. The airway surface liquid (ASL) of the lungs have been shown to be acidified in cystic fibrosis (CF) patients, which is a disease that primarily afflicts the lungs and dramatically increases susceptibility of *P. aeruginosa* infection.[33,

[34] The acidification of the ASL results from the impairment of bicarbonate ion transport in CF patients.[35] Studies have demonstrated that the antimicrobial compounds present in the ASL, which are critical components of the host defense mechanism, and various commercial antibiotics are rendered ineffective at acidic pH, allowing *P. aeruginosa* to thrive in acidic environments.[36-38] Another study demonstrated that biofilm production is enhanced at high pH, representing yet another important pH-influenced mechanism by which the bacterium increases survival chances.[39] We speculate that perhaps at acidic pHs, PA1024 and the bacterium are in a resting state, therefore only the slow catalytic regime is required to maintain the [NADH]/[NAD^+] balance. But as the pH increases to neutral or slightly higher than neutral pHs, the bacterium faces more metabolic stress, therefore the fast catalytic regime is employed to quickly produce NAD^+ in order to upregulate β-oxidation pathways for increased virulence and survival.

5.5.2 Rate-limiting contributions are altered as pH changes

Comparison of the rate of flavin reduction to the k_{cat} value (Figure 2) indicates flavin reduction is the principal rate-limiting step for the overall turnover from pHs 6-7. (Ref lot6p paper for comparison) After the deprotonation of group with pK_a ~7.3, another step becomes rate limiting based on the comparison of k_{cat} and k_{red} values in **Figure 5.2**. The results of the viscosity effects on k_{cat} are consistent with a partially rate-limiting unimolecular step contributing to overall turnover, such as the release of the hydroquinone or NAD^+. Evidence of this conclusion comes from the effect of solvent viscosity on k_{cat} at pH 6.0 and 8.5, which are 20% and 35% diffusion controlled, respectively, based on the slopes of the linear plots (Figure 3). However, a slow release of the NAD^+ is a less likely possibility because there was no accumulation of the

E_{red}-NAD^+ complex over 60 secs with excess of NADH, which typically generates a charge transfer band in the 500-700 nm region of the visible spectrum.[29]

5.5.3 A conformational change may be required to bind the quinone

A conformational change of the reduced PA1024 may be required to efficiently bind the quinone. This conclusion was drawn based on the observation of inverse viscosity effects on the k_{cat}/K_m values with 5-hydroxy-1,4-naphthoquinone (**Figure 5.3C**). Inverse viscosity effects have been reported for the NAD-malic enzyme, which were accredited to an enzyme conformational change that may involve small motions or rotations.[40] In the case of choline oxidase, the inverse viscosity effects observed were attributed to the movement of a phenylalanine residue acting as an oxygen gate. [41] The inverse effect reported here could be the result of a minor conformational change to a configuration that favors quinone binding.

5.5.4 Conclusions

To summarize, we have employed pH and viscosity effects to elucidate key features of the overall catalytic mechanism of PA1024. The overall turnover is principally limited by flavin reduction and, to a lesser extent, the release of the hydroquinone product for pHs 5-9, however at higher pHs 10-11, presumably the release of the hydroquinone product becomes more rate limiting based on the comparison of the reductive half-reaction and steady-state kinetics. The enzyme functions with two catalytic regimes that are dictated by the deprotonation of a group on the enzyme with pK_a ~6 that elicits the fast regime.

5.6 References

[1] Krueger, F. R., Werther, W., Kissel, J., and Schmid, E. R. (2004) Assignment of quinone derivatives as the main compound class composing 'interstellar' grains based on both polarity ions detected by the 'Cometary and Interstellar Dust Analyser' (CIDA) onboard the spacecraft STARDUST, Rapid Commun Mass Spectrom 18, 103-111.

[2] (2017) Quinones, Encyclopaedia Brittanica: Chicago.

[3] Thomas, R. H. (1997) Naturally Occuring Quinones IV. Recent Advances, Blackie:London.

[4] Morton, R. A. (1965) Biochemistry of Quinones, Academic Press:New York.

[5] Abraham, I., Joshi, R., Pardasani, P., and Pardasani, R. T. (2011) Recent Advances in 1,4-Benzoquinone Chemistry, J. Braz. Chem. Soc. 22, 385-421.

[6] Ross, D., Siegel, D., Beall, H., Prakash, A. S., Mulcahy, R. T., and Gibson, N. W. (1993) DT-diaphorase in activation and detoxification of quinones. Bioreductive activation of mitomycin C, Cancer Metastasis Rev 12, 83-101.

[7] Sollner, S., Nebauer, R., Ehammer, H., Prem, A., Deller, S., Palfey, B. A., Daum, G., and Macheroux, P. (2007) Lot6p from Saccharomyces cerevisiae is a FMN-dependent reductase with a potential role in quinone detoxification, FEBS J 274, 1328-1339.

[8] Chesis, P. L., Levin, D. E., Smith, M. T., Ernster, L., and Ames, B. N. (1984) Mutagenicity of quinones: pathways of metabolic activation and detoxification, Proc Natl Acad Sci U S A 81, 1696-1700.

[9] Green, L. K., La Flamme, A. C., and Ackerley, D. F. (2014) Pseudomonas aeruginosa MdaB and WrbA are water-soluble two-electron quinone oxidoreductases with the potential to defend against oxidative stress, J Microbiol 52, 771-777.

[10] Ross, D., Siegel, D., Gibson, N. W., Pacheco, D., Thomas, D. J., Reasor, M., and Wierda, D. (1990) Activation and deactivation of quinones catalyzed by DT-diaphorase. Evidence for bioreductive activation of diaziquone (AZQ) in human tumor cells and detoxification of benzene metabolites in bone marrow stroma, Free Radic Res 8, 373-381.

[11] Kimura, R. E., and Warshaw, J. B. (1988) Control of fatty acid oxidation by intramitochondrial [NADH]/[NAD+] in developing rat small intestine, Pediatr Res 23, 262-265.

[12] Mao, F., Dam, P., Chou, J., Olman, V., and Xu, Y. (2009) DOOR: a database for prokaryotic operons, Nucleic Acids Res 37, D459-463.

[13] Winsor, G. L., Griffiths, E. J., Lo, R., Dhillon, B. K., Shay, J. A., and Brinkman, F. S. (2016) Enhanced annotations and features for comparing thousands of Pseudomonas genomes in the Pseudomonas genome database, Nucleic Acids Res 44, D646-653.

[14] Wakil, S. J., Green, D. E., Mii, S., and Mahler, H. R. (1954) Studies on the fatty acid oxidizing system of animal tissues. VI. beta-Hydroxyacyl coenzyme A dehydrogenase, J Biol Chem 207, 631-638.

[15] Ball, J., Salvi, F., and Gadda, G. (2016) Functional Annotation of a Presumed Nitronate Monoxygenase Reveals a New Class of NADH:Quinone Reductases, J Biol Chem 291, 21160-21170.

[16] Zhu, L., Lin, J., Ma, J., Cronan, J. E., and Wang, H. (2010) Triclosan resistance of Pseudomonas aeruginosa PAO1 is due to FabV, a triclosan-resistant enoyl-acyl carrier protein reductase, Antimicrob Agents Chemother 54, 689-698.

[17] Saito, J., Yamada, M., Watanabe, T., Iida, M., Kitagawa, H., Takahata, S., Ozawa, T., Takeuchi, Y., and Ohsawa, F. (2008) Crystal structure of enoyl-acyl carrier protein

reductase (FabK) from Streptococcus pneumoniae reveals the binding mode of an inhibitor, Prot Sci 17, 691-699.

[18] Ernster, L., Danielson, L., and Ljunggren, M. (1962) DT diaphorase. I. Purification from the soluble fraction of rat-liver cytoplasm, and properties, Biochim Biophys Acta 58, 171-188.

[19] Chalmers, J., Joshi, R., and Patel, A. (2008) Advances in reducing the burden of vascular disease in type 2 diabetes, Clin Exp Pharmacol Physiol 35, 434-437.

[20] Zhao, Q., Yang, X. L., Holtzclaw, W. D., and Talalay, P. (1997) Unexpected genetic and structural relationships of a long-forgotten flavoenzyme to NAD(P)H:quinone reductase (DT-diaphorase), Proc Natl Acad Sci U S A 94, 1669-1674.

[21] Andrade, S. L., Patridge, E. V., Ferry, J. G., and Einsle, O. (2007) Crystal structure of the NADH:quinone oxidoreductase WrbA from Escherichia coli, J Bacteriol 189, 9101-9107.

[22] Patridge, E. V., and Ferry, J. G. (2006) WrbA from Escherichia coli and Archaeoglobus fulgidus is an NAD(P)H:quinone oxidoreductase, J Bacteriol 188, 3498-3506.

[23] Koch, K., Hromic, A., Sorokina, M., Strandback, E., Reisinger, M., Gruber, K., and Macheroux, P. (2017) Structure, biochemical and kinetic properties of recombinant Pst2p from Saccharomyces cerevisiae, a FMN-dependent NAD(P)H:quinone oxidoreductase, Biochim Biophys Acta 1865, 1046-1056.

[24] Ha, J. Y., Min, J. Y., Lee, S. K., Kim, H. S., Kim do, J., Kim, K. H., Lee, H. H., Kim, H. K., Yoon, H. J., and Suh, S. W. (2006) Crystal structure of 2-nitropropane dioxygenase complexed with FMN and substrate. Identification of the catalytic base, J biol Chem 281, 18660-18667.

[25] Deller, S., Macheroux, P., and Sollner, S. (2008) Flavin-dependent quinone reductases, Cellular and molecular life sciences : CMLS 65, 141-160.

[26] McComb, R. B., Bond, L. W., Burnett, R. W., Keech, R. C., and Bowers, G. N., Jr. (1976) Determination of the molar absorptivity of NADH, Clin Chem 22, 141-150.

[27] Saldova, R., Kilcoyne, M., Stockmann, H., Millan Martin, S., Lewis, A. M., Tuite, C. M., Gerlach, J. Q., Le Berre, M., Borys, M. C., Li, Z. J., Abu-Absi, N. R., Leister, K., Joshi, L., and Rudd, P. M. (2017) Advances in analytical methodologies to guide bioprocess engineering for bio-therapeutics, Methods 116, 63-83.

[28] Sievers, F., and Higgins, D. G. (2014) Clustal Omega, accurate alignment of very large numbers of sequences, Methods Mol Biol 1079, 105-116.

[29] Massey, V., and Palmer, G. (1962) Charge transfer complexes of lipoyl dehydrogenase and free flavins, J Biol Chem 237, 2347-2358.

[30] Li, R., Bianchet, M. A., Talalay, P., and Amzel, L. M. (1995) The three-dimensional structure of NAD(P)H:quinone reductase, a flavoprotein involved in cancer chemoprotection and chemotherapy: mechanism of the two-electron reduction, Proc Natl Acad Sci U S A 92, 8846-8850.

[31] Ying, W. (2006) NAD+ and NADH in cellular functions and cell death, Front Biosci 11, 3129-3148.

[32] Christensen, C. E., Karlsson, M., Winther, J. R., Jensen, P. R., and Lerche, M. H. (2014) Non-invasive in-cell determination of free cytosolic [NAD+]/[NADH] ratios using hyperpolarized glucose show large variations in metabolic phenotypes, J Biol Chem 289, 2344-2352.

[33] Tate, S., MacGregor, G., Davis, M., Innes, J. A., and Greening, A. P. (2002) Airways in cystic fibrosis are acidified: detection by exhaled breath condensate, Thorax 57, 926-929.

[34] Shah, V. S., Meyerholz, D. K., Tang, X. X., Reznikov, L., Abou Alaiwa, M., Ernst, S. E., Karp, P. H., Wohlford-Lenane, C. L., Heilmann, K. P., Leidinger, M. R., Allen, P. D., Zabner, J., McCray, P. B., Jr., Ostedgaard, L. S., Stoltz, D. A., Randak, C. O., and Welsh, M. J. (2016) Airway acidification initiates host defense abnormalities in cystic fibrosis mice, Science 351, 503-507.

[35] Smith, J. J., and Welsh, M. J. (1992) cAMP stimulates bicarbonate secretion across normal, but not cystic fibrosis airway epithelia, J Clin Invest 89, 1148-1153.

[36] Abou Alaiwa, M. H., Reznikov, L. R., Gansemer, N. D., Sheets, K. A., Horswill, A. R., Stoltz, D. A., Zabner, J., and Welsh, M. J. (2014) pH modulates the activity and synergism of the airway surface liquid antimicrobials beta-defensin-3 and LL-37, Proc Natl Acad Sci U S A 111, 18703-18708.

[37] Xiong, Y. Q., Caillon, J., Drugeon, H., Potel, G., and Baron, D. (1996) Influence of pH on adaptive resistance of Pseudomonas aeruginosa to aminoglycosides and their postantibiotic effects, Antimicrob. Agents Chemother 40, 35-39.

[38] Torres, I. M., Demirdjian, S., Vargas, J., Goodale, B. C., and Berwin, B. (2017) Acidosis increases the susceptibility of respiratory epithelial cells to Pseudomonas aeruginosa-induced cytotoxicity, Am J Physiol Lung Cell Mol Physiol 313, L126-L137.

[39] Hostacka, A., Ciznar, I., and Stefkovicova, M. (2010) Temperature and pH affect the production of bacterial biofilm, Folia Microbiol 55, 75-78.

[40] Karsten, W. E., Lai, C. J., and Cook, P. F. (1995) Inverse Solvent Isotope Effects in the Nad-Malic Enzyme Reaction Are the Result of the Viscosity Difference between D2o

and H2o - Implications for Solvent Isotope Effect Studies, J Am Chem Soc 117, 5914-5918.

[41] Salvi, F., Rodriguez, I., Hamelberg, D., and Gadda, G. (2016) Role of F357 as an Oxygen Gate in the Oxidative Half-Reaction of Choline Oxidase, Biochemistry 55, 1473-1484.

6 STERIC HINDRANCE CONTROLS THE PYRIDINE NUCLEOTIDE SPECIFICTY OF A FLAVIN-DEPENDENT NADH:QUINONE OXIDOREDUCTASE

6.1 Abstract

The crystal structure of the NADH:quinone oxidoreductase PA1024 has been solved in complex with the reaction product NAD^+. The nicotinamide C4 is located 3.6 Å from the FMN N5 atom, representing a suitable separation and conformation for hydride transfer. NAD^+ is bound at the interface of the TIM-barrel domain and the extended domain of the enzyme in a folded conformation, with the two ribose groups close to each other. The steric hindrance of the ribose of NAD^+ and a nearby P78 controls the strict coenzyme specificity for NADH in PA1024. The comparison of the structure with that of the ligand-free enzyme revealed a different conformation of a short loop (75-86) that retains the NAD^+ bound and an unusual interrupted helix that binds the pyrophosphate moiety of NAD^+. The structure of the PA1024-NAD^+ complex contributes to ongoing efforts to understand pyridine nucleotide specificity, NAD^+ conformational diversity, and enzyme active site gates.

6.2 Statement of importance

Understanding the coenzyme specificity of nicotinamide-dependent enzymes is crucial to the advancement of protein engineering efforts. NADH is a far less expensive than NADPH, and many efforts by various research groups are currently underway to alter coenzyme specificity towards NADH. The coenzyme specificity in enzymes commonly relies on electrostatics, but rarely on steric hindrance as we have reported here for the NAD^+-PA1024 complex. The steric hindrance of the ribose groups of NAD^+ and a nearby P78 in the putative 2'phosphate-binding region of $NADP^+$ in the model controls the strict substrate specificity for NADH in PA1024.

6.3 Introduction

Pyridine nucleotides are ubiquitous and important biological molecules that are vital to the function of living cells.[1] The two primary forms, reduced nicotinamide adenine dinucleotide (NADH) and reduced nicotinamide adenine dinucleotide phosphate (NADPH), along with their oxidized counterparts NAD^+ and $NADP^+$, participate in numerous biological processes, including among others cellular energy production, mitochondrial functions, calcium regulation, oxidative stress, gene expression, immune functions, the aging process, and cell death.[2] The chemical structures of NADH and NADPH differ only by the presence of an extra phosphate group on the 2'hydroxyl of the adenine ribose moiety. NADH is commonly involved in catabolic pathways, whereas NADPH serves in anabolic pathways.[3] The small structural difference between the two molecules of a phosphate versus a hydroxyl group is responsible for eliciting different roles for each molecule and the enzymes that catalyze these reactions.

A plethora of enzymes with varying functions employ pyridine nucleotides as substrates or, more seldom, cofactors. Major classes include, but are not limited to, oxidoreductases, such as NAD(P)H quinone oxidoreductases[4] (NQOs) and azoreductases;[5] reductases, such as cytochrome P450 reductases[6] and glutathione reductase;[7] and dehydrogenases, such as lactate dehydrogenase[8] and glutamate dehydrogenase.[9] These enzymes often show a preference for NADH or NADPH; however, among the NQOs, lot6p and NQO1 can utilize both NADH and NADPH.[10, 11] YhdA from *Bacillus subtilis* and PA1225 from *Pseudomonas aeruginosa* are NQOs specific for NADPH,[12, 13] while AzoA from *Enterococcus faecalis* and tryptophan repressor binding protein (WrbA) are specific for NADH.[14, 15]

The most common fold that binds pyridine nucleotides is the βαβαβ motif, also known as the Rossmann fold,[16, 17] yet other folds have been discovered to bind NAD(P)H, such as the

TIM-barrel fold[18] and the flavodoxin-like fold.[4] The pyridine nucleotide is usually bound to the protein in an extended conformation.[16] The adenine portion of NAD(P)H typically binds a mostly hydrophobic pocket, whereas the pyrophosphate portion binds to the backbone amide groups of glycine residues positioned on α-helices or loops. NADPH-specific enzymes frequently have insertions of basic residues within the nicotinamide-binding region to bind the extra phosphate group, while NADH-specific enzymes have acidic residues positioned to repel the additional phosphate on NADPH. Numerous reports describe alteration or switching of the specificity of NADPH- and NADH-dependent enzymes through site-directed mutagenesis.[19-25] Despite the wealth of knowledge accumulated, the structural rules governing pyridine nucleotides specificity have yet to be fully elucidated.

PA1024 is a recently characterized FMN-dependent NADH:quinone oxidoreductase that demonstrates a strict specificity for NADH.[26] The rate of flavin reduction at pH 7.0 with 500 μM NADH is 22 s^{-1}, whereas the reaction with an equivalent concentration of NADPH is 3,500 times slower.[26] A previous study determined the ligand-free structure of PA1024, indicating the overall fold of the enzyme is a TIM-barrel fold.[27] In the present study, we have solved the crystal structure to 2.2 Å resolution of PA1024 in complex with the reaction product NAD^+ at pH 7.0. The complex reveals the structural basis for the strict NADH specificity of the enzyme and its lack of reactivity with NADPH. The results also reveal an active site gate that assumes a different conformation in the PA1024-NAD^+ complex as compared to the ligand-free enzyme structure and an unusual "interrupted helix" that binds the pyrophosphate moiety of NAD^+. The findings of this study contribute to the overall understanding of nicotinamide coenzyme specificity and aid in protein engineering efforts with related enzymes.

6.4 Results and Discussion

6.4.1 Overall structure of the PA1024-NAD$^+$ complex

PA1024 was co-crystallized with NAD^+. The structure was solved in the trigonal space group $P3_121$ with one molecule per asymmetric unit by molecular replacement using the coordinates of the ligand-free form of PA1024 as the initial search model. The structure was refined to R_{work} and R_{free} values of 15.6% and 20.3%, respectively, to 2.2 Å resolution. The resolution cutoff was determined by combining several criteria including $CC_{1/2}$, $\langle I/\sigma(I)\rangle$, and completeness, but not the R_{merge} values because they are poorly suited for determining high-resolution limits.[28] The crystallographic data and refinement statistics are summarized in **Table 6.1**. The final model of PA1024 in complex with NAD^+ (Protein Data Bank - PDB code 6E2A) accounts for one polypeptide chain containing 326 residues from G^2 to G^{327}, 150 solvent sites treated as water oxygens, one FMN molecule, one NAD^+ molecule and two glycerol molecules in the asymmetric unit. The N-terminal residue M^1 and the C-terminal residue V^{328}, as well as the C-terminal polyhistidine-tag, were excluded from the final structure due to lack of observable electron density.

Table 6.1 X-ray diffraction data collection and refinement statistics.

Data collection	
Space group	$P3_121$
a, *b*, *c* (Å)	93.38, 93.38, 80.76
α, β, γ (°)	90, 90, 120
Mosaicity (°)	0.64
Resolution range (Å)	80.76 – 2.20 (2.27-2.20)
Total No. of observed reflections	133527 (11413)
No. of unique reflections	21045 (1789)
Completeness (%)	99.9 (100)
Redundancy	6.3 (6.4)
$CC_{1/2}$	0.995 (0.684)
$\langle I/\sigma(I)\rangle$	9.6 (2.3)
R_{merge}	0.137 (0.952)
Overall *B* factor from Wilson plot (Å^2)	24.1
Refinement	
Refinement resolution range (Å)	40.44 – 2.20 (2.27-2.20)
R_{work}	0.156
R_{free}	0.203
RMS deviations from ideality	
Bonds lengths (Å)	0.007
Angles (°)	0.830
Number of atoms	
Protein	2427
Water	150
FMN	31
NAD^+	44
Glycerol	12
Average *B* factors (Å^2)	
Protein	33.7
Water	38.4
FMN	26.3
NAD	55.2
Glycerol	46.1
Ramachandran analyses	
Most favoured (%)	97
Allowed (%)	3

Values for the outer shell are given in parentheses.

The monomeric enzyme consists of two domains, a TIM-barrel domain and an inserted domain, which are connected by two loops. The TIM-barrel domain (M^1 – P^{211} and E^{299} – V^{328}) consists of eight α-helices and eight parallel β-strands, with the FMN and substrate binding sites

capping the barrel. In the PA1024-NAD^+ complex, the FMN-binding site is practically identical to the ligand-free structure of the enzyme previously reported. The overall structure of PA1024 in complex with NAD^+ is highly similar to the ligand-free structure determined by Ha et al. with an RMSD value of 0.13 Å on 326 equivalent Cα atoms (**Figure 6.1**).[27]

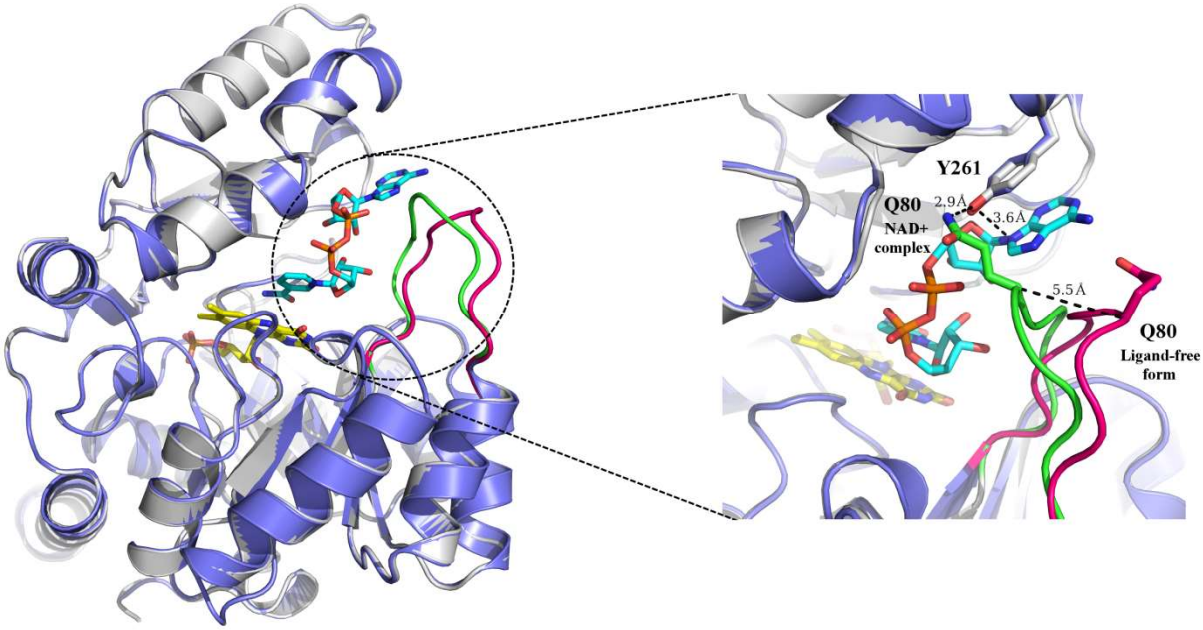

Figure 6.1 Superimposition of the ligand-free and NAD+-complex structures of PA1024.
The overall structure of the ligand-free form of PA1024 (PDB ID: 2GJL) is in blue and the PA1024- NAD^+ complex (PDB ID: 6E2A) is in grey. The loop residues 75-86 are highlighted in red (ligand-free form) and green (PA1024-NAD^+ complex). The FMN carbons are in yellow sticks and the NAD^+ carbons are in cyan. The dashed line represents the distance between the position of the C_α atom of Q80 in the ligand-free and NAD^+-complex structures.

Comparison of the structure of the PA1024-NAD^+ complex to the ligand-free structure of PA1024 indicates a conformational change occurs at a loop comprised of residues 75-86 (**Figure 6.1**). The loop residues P78, P82, and P84, which are fully conserved in over 500 sequences that share high identity and similarity with PA1024, are likely necessary to provide internal rigidity to the loop. Q80 on the loop shows the greatest variability from the ligand-free conformation, as it moves 5.5 Å to form a hydrogen bond with the side chain of Y261 (2.9 Å) and latches an

apparent active site "gate" to secure the NAD^+ (**Figure 6.2**). Q80 is highly conserved, but isoleucine or leucine occurs at this position in some cases, suggesting that a long side-chain is required to physically block the active site entrance and contain the NADH. Active site gates or "lids" at the entrance of the active site have also been observed in D-amino acid oxidase from pig kidney[29] and human[30], *Pseudomonas aeruginosa* D-arginine dehydrogenase,[31] choline oxidase,[32] dihydrofolate reductase,[33] RNA polymerase,[34] and many more enzymes.[35]

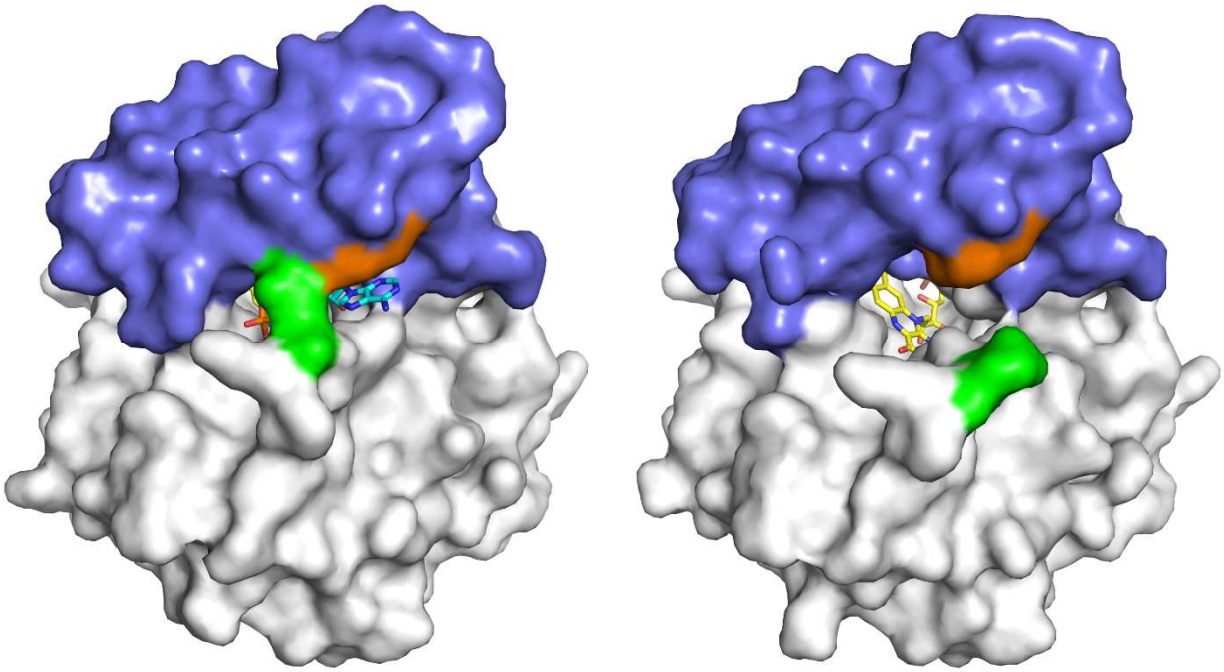

Figure 6.2 Surface depiction of ligand-free structure (left) and the PA1024-NAD+ complex structure (right).
The TIM-barrel domain is in grey surface and the inserted domain is in blue surface. Q80 is in green surface and Y261 is in orange surface. The NAD^+ carbons are in cyan sticks and the FMN carbons are in yellow sticks.

The NAD^+ molecule is bound to the *si*-face of the FMN. The *re*-face of the cofactor instead is buried in the protein environment, making it impossible for the NAD^+ to access. NQO1 and NQO2 are similar to PA1024 in this regard, as the *re*-face of FAD is buried in these proteins and the pyridine nucleotide substrate binds to the *si*-face.[36, 37] In contrast to PA1024,

which is FMN-dependent and has TIM-barrel fold, NQO1 and NQO1 utilize FAD as a cofactor and adopt a flavodoxin-like fold.

6.4.2 "Folded" conformation of NAD^+ bound to PA1024

The electron density of the NAD^+ bound to PA1024 is well defined (**Figure 6.3**) and the occupancy is ~80%. The average *B*-factor for 44 NAD^+ atoms is 55 $Å^2$, which is higher than the average value for the protein atoms, 34 $Å^2$, and the protein residues in the NAD^+-binding site, 40 $Å^2$. The high *B*-factor suggests some degree of flexibility of the NAD^+, which agrees well with the observation that the NAD^+-binding site is between the TIM-barrel domain and the inserted domain and includes a mobile loop (**Figure 6.1**). NAD^+ is bound to the enzyme in a "folded" fashion (**Figure 6.4**), rather than in an extended conformation. The nicotinamide ring binds close to the FMN, whereas the adenine ring resides close to the enzyme surface (Fig. 2). Variations of the folded binding mode of NAD^+ have been observed in other FMN-dependent enzymes, such as the NADH:quinone oxidoreductase WrbA[38] and flavin reductase P.[39] It is worth noting that NAD^+ is an inhibitor of flavin reductase P and that the conformation of NAD^+ in WrbA does not appear to be catalytically relevant because the nicotinamide C4 atom is located away from the flavin. A folded binding mode has also been observed in both the NAD^+ and $NADP^+$ complex with the short-chain flavin reductase HpaC from *Sulfolobus tokodaii* strain 7[40] and the $NADP^+$ complex with catalase from beef liver.[41] In contrast, FMN-dependent enzymes that have been co-crystallized with NAD^+/NADH in the extended conformation include pentaerythritol tetranitrate reductase,[42] PfaD from *Shewanella oneidensis*, and the hydrophilic domain of respiratory complex I from *Thermus thermophilus*.[43]

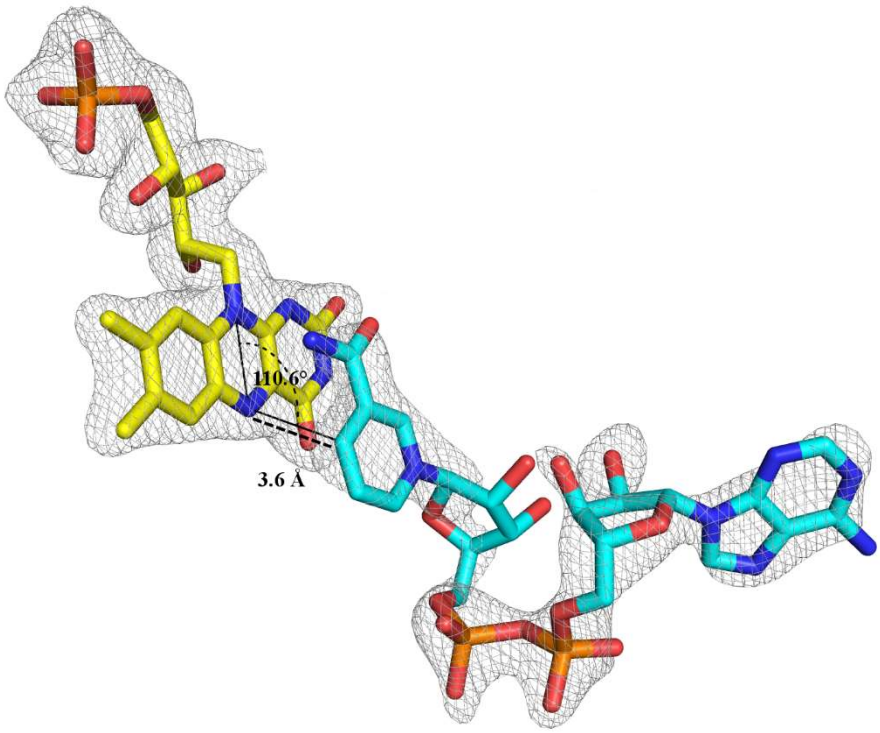

Figure 6.3 Binding mode of NAD^+ to PA1024.
σ_A-weighted $2F_o$-F_c electron density map countered at 1 σ level (where σ is the root mean square value of the electron density) is shown for FMN and NAD^+. The NAD^+ carbons are in cyan sticks and the FMN carbons are in yellow sticks. The dashed line indicates the distance between the C4 atom of the nicotinamide and the N5 atom of the FMN and the angle between the N10 and N5 atoms of the FMN and C4 atom of the nicotinamide.

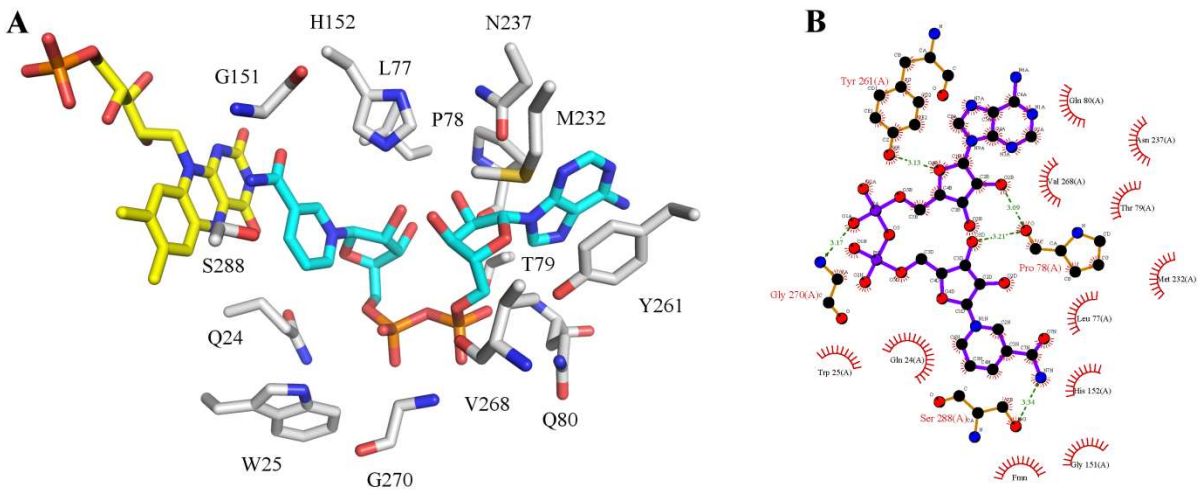

Figure 6.4 Interactions of PA1024 residues with NAD^+.
A) Residues that participate in the binding of NAD. FMN carbons are in yellow sticks, NAD^+ carbons are in cyan sticks, and PA1024 residue carbons are in grey. B) Schematic representation of the interactions of NAD^+ with PA1024. The dashed lines represent distances between the heavy atoms of the protein and the FMN cofactor.

6.4.3 Interactions of NAD^+ with PA1024

Nicotinamide moiety

The nicotinamide NH_2 moiety of NAD^+ forms hydrogen bonds with the N10 atom of FMN (3.4 Å) and the side-chain hydroxyl of S288 (3.3 Å) (**Figure 6.4**). Two van der Waals contacts are made by the β- and γ-carbons of Q24 with the nicotinamide ring of NAD^+ (3.4 and 3.7 Å, respectively). As shown in Figure 3, the nicotinamide C4 of NAD^+ is 3.6 Å from the N5 of FMN with a donor/acceptor angle of 110.6° for the atoms involved in the hydride transfer reaction. Thus, the combination of the proximity and appropriate angle seen in the structure of the PA1024-NAD^+ complex represent a binding mode relevant for facile hydride transfer from the nicotinamide of the NAD^+ to the N5 atom of the FMN. The nicotinamide ring of the NAD^+ does not appear to directly π-π stack with the pyrazine ring of FMN. A conformation similar to that seen here was described in the crystal structure of PfaD from *Shewanella oneidensis* in complex with NAD^+ (PDB ID: 4Z9R). In contrast, complexes of 1,4,5,6-tetrahydro-NADH in

pentaerythritol tetranitrate reductase and NADH in the hydrophilic domain of respiratory complex I from *Thermus thermophilus* showed the nicotinamide ring π-π stacked with the pyrazine of FMN, but the carboxamide portion of the nicotinamide ring is tilted and aligns with the O4 and N3 atoms on the pyrimidine ring of FMN.[42, 43]

Ribose moieties

The 2'hydroxyl of the adenine ribose establishes a hydrogen bond with the backbone C=O of P78 (3.1 Å). The 3'hydroxyl of the adenine ribose forms a hydrogen bond with the side chain of H152 (3.5 Å). The ring O atom of the adenine ribose engages in a hydrogen bond with the side-chain hydroxyl of Y261 (3.1 Å) (**Figure 6.4**). The nicotinamide ribose instead is not well defined in the electron density map (**Figure 6.3**), thereby preventing a clear depiction of its interactions with the protein.

Pyrophosphate moiety

The O5 phosphate atom of the pyrophosphate moiety of NAD^+ is close to the NH group on the side-chain of Q24 (3.7 Å) (**Figure 6.4**). The O1 and O2 atoms of the adenine phosphate form hydrogen bonds with the backbone amides of G270 (3.1 Å) and Q80 (3.4 Å). G270 resides on a short loop (^{268}VSG^{270}) that is connected to two α-helices in what can be described as an interrupted helix (**Figure 6.5**). The interrupted helix is part of the inserted domain of PA1024 and appears to be a single helix that has been slightly unwound. Y261 anchors the helix by stacking on the adenine of NAD^+ and Q80 interacts with Y261. G270 is fully conserved in the 500 sequences that share high identity with PA1024; therefore, G270 is likely essential to

provide the necessary space to bind the pyrophosphate of NAD^+. Residues S271 and V272 are likely required to have unbulky side-chains to accommodate the pyrophosphate of NAD^+.

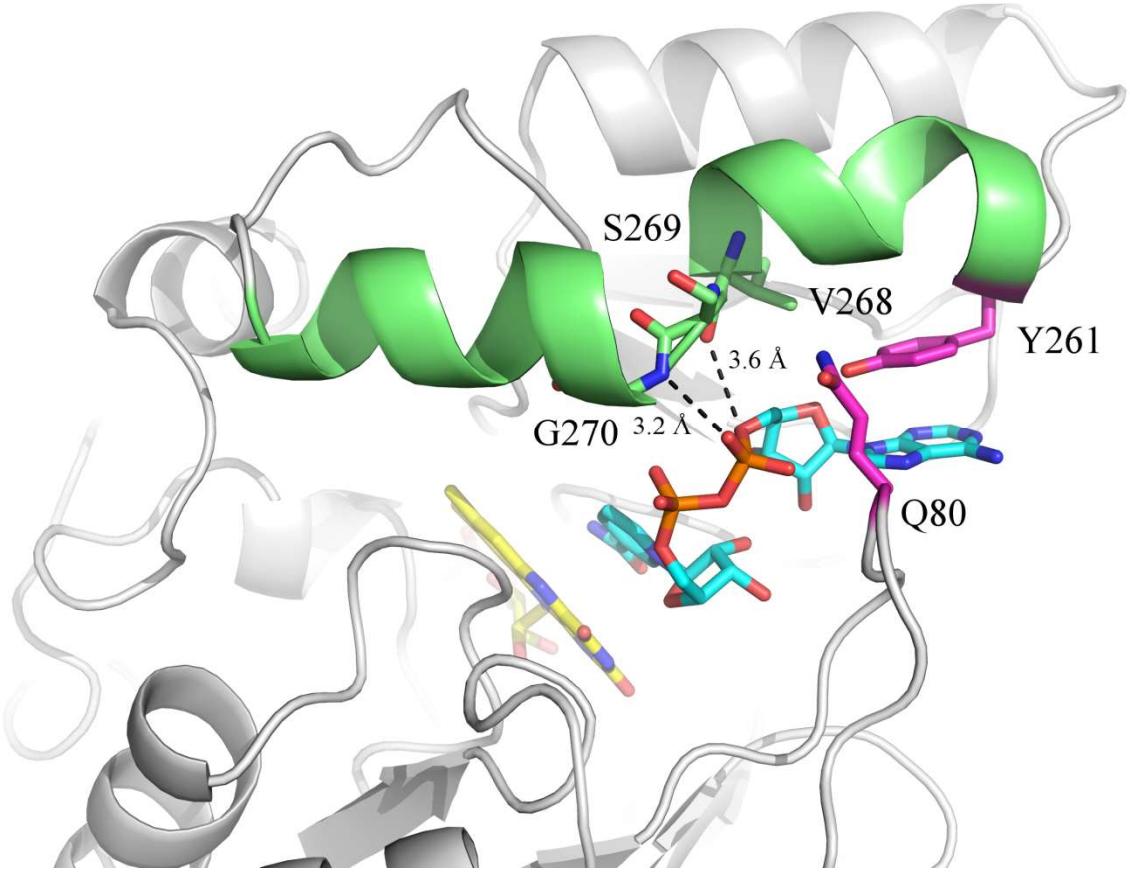

Figure 6.5 Pyrophosphate binding pocket of NAD^+ in PA1024.
The two α-helices in green are connected by a short loop composed of V268, S269, and G270 that form an "interrupted helix". The NAD^+ carbons are in cyan sticks and the FMN carbons are in yellow sticks. The dashed lines represent distances.

Adenine ring moiety

The N3 atom of the adenine moiety of NAD^+ forms a hydrogen bond with the side chain C=O of N237 (3.1 Å). The adenine moiety of NAD^+ appears to π-π stack with Y261 (Fig. 5). Comparison of 500 proteins sharing similar amino acid sequences to PA1024 indicates Y261 is highly conserved as either a tyrosine or phenylalanine, and in a few cases (<5%), an isoleucine. The important structural feature at position 261 for binding the pyridine nucleotide appears to be

an aromatic residue capable of π-π stacking interactions with the adenine moiety. A similar π-π stacking interaction with the adenine of ADP is well established in the aminoglycoside phosphotransferase class of enzymes.[44] In contrast, intramolecular π-π stacking of the adenine and nicotinamide has been observed in complexes with both NAD^+ and $NADP^+$ in the short-chain flavin reductase HpaC from *Sulfolobus tokodaii* strain 7.[40]

6.4.4 Structural features responsible for coenzyme specificity

The folded binding mode of the pyridine nucleotide would position the 2'phosphate on the adenine ribose of $NADP^+$ ~2 Å from the 2'hydroxyl on the nicotinamide ribose of $NADP^+$, creating a steric clash that likely prevents $NADP^+$ from binding to the enzyme (**Figure 6.6**). The 2'phosphate of the adenine ribose of $NADP^+$ also would likely clash with P78 of PA1024 at a distance of 1.9 Å (**Figure 6.6**). We propose that the steric constraint imposed by the folded conformation of the NAD^+ and P78 confer the strict specificity for NADH to PA1024. Intriguingly, charged residues do not appear to play a role in the coenzyme specificity of PA1024.

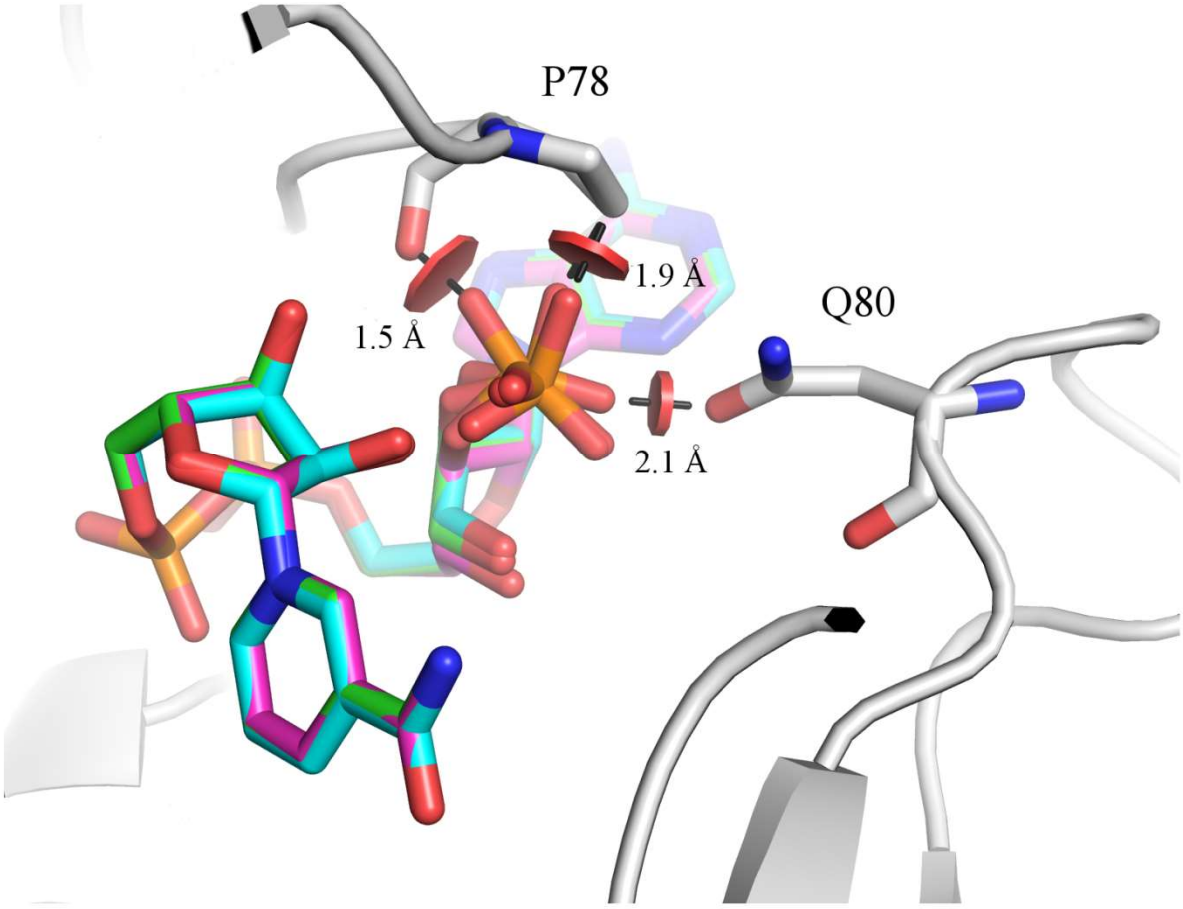

Figure 6.6 Model of the PA1024-$NADP^+$ complex.
Different conformations of the phosphate group in the $NADP^+$ were modeled. The $NADP^+$ carbons are in green, cyan and pink sticks, and the P78 and Q80 carbons and nearby loops of PA1024 are in grey. The red circles represent steric clashes.

The majority of the structure-function investigations on enzymes that utilize pyridine nucleotides attributes their specificity to electrostatics. An aspartate residue located in the 2'phosphate-binding region has commonly been shown to discriminate between NADH-NADPH in NADH-specific enzymes. Examples include D175 in *Lactobacillus bulgarius* D-lactate dehydrogenase, D53 in *Bacillus stearothermophilus* L-lactate dehydrogenase, and D223 in yeast alcohol dehydrogenase.[45] A recent study describes a variant of *Lactibacillus delbrueckii* 11842 D-lactate dehydrogenase with three point mutations (D176S/I177R/F178T) that displayed significantly improved catalytic activity on both NADH and NADPH.[21] In Type II NADH

dehydrogenase, a relatively NADH-specific enzyme, a variant of E203Q granted the enzyme the ability to oxidize NADH and NADPH with similar efficiency.[46]

The presence of arginine or lysine is typically observed in the 2'phosphate-binding region of $NADP^+$-specific enzymes. 4-hydroxyacetophenone monooxygenase exhibits a 700-fold preference for NADPH over NADH, and makes use of three basic residues (R339, K439, and R440) to dictate coenzyme specificity.[47] Crystallographic studies on 6-phosphogluconate dehydrogenase attribute the $NADP^+$ specificity to an interaction between the 2'-phosphate of $NADP^+$ and R33, since without that interaction there is no cleft for binding the adenine of NADH.[48] In the crystal structure of $NADP^+$ bound to NQO1, which can oxidize both NADH and NADPH, the backbone amide N atom of F232 interacts with one of the O atoms of the phosphate group on the adenine ribose of $NADP^+$.[36] This additional hydrogen bond is not present with NADH as substrate and may explain the differences in affinity between NADH and NADPH in NQO1, but the absence of fully charged side-chains interacting with the extra phosphate on the adenine ribose may grant NQO1 its dual specificity.

Only a few studies have described a steric factor as controlling specificity in pyridine nucleotide-dependent enzymes, as in the case reported here for PA1024. Homology modeling and docking analysis with NADPH of the bifunctional alcohol/aldehyde dehydrogenase from *Clostridium thermocellum* suggested the extra phosphate of NADPH would encounter electrostatic repulsion and steric hindrance with D494.[49] A variant of the enzyme with the mutation D494G increased the specificity with NADPH in *C. thermocellum* bifunctional alcohol/aldehyde dehydrogenase. A study on cytochrome P450 nitric oxide reductase, which prefers NADH but can oxidize NADPH at 20% the relative activity of NADH, attributed the

preference for NADH to steric clash of a serine residue (S75) with the 2'-phosphate moiety of NADPH.[50]

6.5 Conclusions

We have determined the crystal structure of the FMN-dependent NADH:quinone oxidoreductase PA1024 in complex with the reaction product NAD^+. The results have uncovered a different conformation of a short loop composed of residues 75-86 covering the nicotinamide-binding site in the structure of the PA1024-NAD^+ complex as compared to the ligand-free enzyme. P78, P82, and P84 provide internal rigidity to the loop. Q80 serves as an active site latch that secures the NAD^+ within the binding pocket. An interrupted helix that consists of two α-helices connected by a small three-residue loop serves to bind the pyrophosphate of NAD^+. Furthermore, the structural factors governing the strict coenzyme specificity of PA1204 for NADH have been determined. The $NADP^+$ likely cannot bind due to a steric clash of its 2'phosphate with P78. The availability of the structure of the PA1024-NAD^+ complex provides a firm framework for future structure-function studies aimed at the characterization of the FMN-dependent NADH:quinone oxidoreductase PA1024.

6.6 Materials and Methods

6.6.1 Protein production and crystallization

Recombinant PA1024 from *P. aeruginosa* was obtained through expression and purification methods previously described.[26] The recombinant PA1024 was dialyzed against 20 mM Tris-Cl, pH 8 (25°C), 200 mM NaCl and 10% glycerol. The purified enzyme was concentrated to 5 mg mL^{-1}, mixed with 2 mM NAD^+ (oxidized form of nicotinamide adenine dinucleotide) and incubated for 30 minutes at 4° C. The enzyme concentration was estimated based on the molar extinction coefficient of enzyme-bound FMN.[26] Crystallization was

performed by the hanging drop vapor diffusion method at room temperature in 4 µL drops of a 1:1 ratio of protein previously incubated with NAD^+ and the reservoir solution. Yellow crystals were obtained within a day in presence of 0.1 M HEPES at pH 7.0, 4% (*v/v*) tacsimate at pH 7.0, and 15% (*w/v*) poly-ethylene glycol methyl ether 5000 as previously described.[27] Prior to crystallization, PA1024 activity was determined by monitoring the NADH consumption in the presence of different quinones.[26]

6.6.2 Data collection and processing

The crystals were cryo-cooled in the mother liquor with 25% (*v/v*) glycerol and flash frozen immediately in liquid nitrogen. X-ray diffraction data were collected at 100 K on beamline 22-ID with detector Eiger 16M of the Southeast Regional Collaborative Access Team (SER-CAT) at the Advanced Photon Source, Argonne National Laboratory. 180 images of 1° oscillation per frame were collected with a 200 mm crystal-to-detector distance and an exposure time of 1 s per image. Data integration and analysis were carried out using iMOSFLM[51] and AIMLESS[52] in the CCP4 suite.[53] The resolution cutoff was determined by combining several criteria including $CC_{1/2}$ of > 0.5 for the highest resolution shell, $\langle I/\sigma(I)\rangle > 2$ and completeness. The data collection and processing statistics are summarized in Table 1.

6.6.3 Structure determination

The structure of the complex PA1024 with NAD^+ was solved by molecular replacement performed using the coordinates of the holo-form of PA1024 as the initial search model (PDB ID: 2GJL) (REF 2GJL). A unique solution was found by PhaserMR[54, 55] in the trigonal space group $P3_121$ with unit cell dimensions of a = 93.38, b = 93.38, c = 80.76 Å. The Matthews coefficient calculated with the CCP4i suite[53] suggested one monomer in the asymmetric unit. The model was subjected to several rounds of refinement using Phenix.refine.[56] Electron density

and difference map were inspected, and modifications to the model were made with COOT.[57] The refinement ended when inspection of the maps suggested no more changes were justified, and no significant changes in the R_{free} and R_{work} were observed. Solvent molecules were inserted at stereochemically reasonable positions in peaks of $2F_o$-F_c and F_o-F_c maps contoured at 1 and 3 sigma (σ) levels, respectively. Ligand restraint files were generated with *phenix.elbow.*[58] The final R_{work} and R_{free} values were 15.6% and 20.3% for the refined structure. The quality of the model was regularly checked for steric clashes, incorrect stereochemistry and rotamer outliers using MolProbity.[59] All structural figures were produced using PyMol (www.pymol.org). Refined atomic coordinates and experimental structure factors have been deposited in the Protein Data Bank (PDB entry 6E2A). Refinement statistics are given in Table 1.

6.7 Acknowledgements

This work was supported in part by Grant CHE-1506518 from the NSF (G.G.) and Georgia State University Molecular Basis of Disease Graduate Fellowship (J.B.) We thank the staff at the Southeast Regional-Collaborative Access Team (SER-CAT) at the Advanced Photon Source, Argonne National Laboratory, for assistance during X-ray data collection. Use of the Advanced Photon Source was supported by the U. S. Department of Energy, Office of Science, Office of Basic Energy Sciences, under Contract No. W-31-109-Eng-38.

6.8 References

[1] Walsh, C. T., Tu, B. P., and Tang, Y. (2018) Eight Kinetically Stable but Thermodynamically Activated Molecules that Power Cell Metabolism, Chem Rev 118, 1460-1494.

[2] Ying, W. (2008) NAD+/NADH and NADP+/NADPH in cellular functions and cell death: regulation and biological consequences, Antioxid Redox Signal 10, 179-206.

[3] Engel, P. C. (2014) Glutamate dehydrogenases: the why and how of coenzyme specificity, Neurochem Res 39, 426-432.

[4] Deller, S., Macheroux, P., and Sollner, S. (2008) Flavin-dependent quinone reductases, Cell Mol Life Sci 65, 141-160.

[5] Ryan, A., Kaplan, E., Nebel, J. C., Polycarpou, E., Crescente, V., Lowe, E., Preston, G. M., and Sim, E. (2014) Identification of NAD(P)H quinone oxidoreductase activity in azoreductases from P. aeruginosa: azoreductases and NAD(P)H quinone oxidoreductases belong to the same FMN-dependent superfamily of enzymes, PLoS One 9, e98551.

[6] Porter, T. D., and Kasper, C. B. (1986) NADPH-cytochrome P-450 oxidoreductase: flavin mononucleotide and flavin adenine dinucleotide domains evolved from different flavoproteins, Biochemistry 25, 1682-1687.

[7] Racker, E. (1955) Glutathione reductase from bakers' yeast and beef liver, J Biol Chem 217, 855-865.

[8] Valvona, C. J., Fillmore, H. L., Nunn, P. B., and Pilkington, G. J. (2016) The Regulation and Function of Lactate Dehydrogenase A: Therapeutic Potential in Brain Tumor, Brain Pathol 26, 3-17.

[9] Grabowska, A., Nowicki, M., and Kwinta, J. (2011) Glutamate dehydrogenase of the germinating triticale seeds: gene expression, activity distribution and kinetic characteristics, Acta Physiol Plant 33, 1981-1990.

[10] Lind, C., Cadenas, E., Hochstein, P., and Ernster, L. (1990) DT-diaphorase: purification, properties, and function, Methods Enzymol 186, 287-301.

[11] Sollner, S., Nebauer, R., Ehammer, H., Prem, A., Deller, S., Palfey, B. A., Daum, G., and Macheroux, P. (2007) Lot6p from Saccharomyces cerevisiae is a FMN-dependent reductase with a potential role in quinone detoxification, FEBS J 274, 1328-1339.

[12] Flores, E., and Gadda, G. (2018) Kinetic Characterization of PA1225 from Pseudomonas aeruginosa PAO1 Reveals a New NADPH:Quinone Reductase, Biochemistry 57, 3050-3058.

[13] Deller, S., Sollner, S., Trenker-El-Toukhy, R., Jelesarov, I., Gubitz, G. M., and Macheroux, P. (2006) Characterization of a thermostable NADPH:FMN oxidoreductase from the mesophilic bacterium Bacillus subtilis, Biochemistry 45, 7083-7091.

[14] Chen, H., Wang, R. F., and Cerniglia, C. E. (2004) Molecular cloning, overexpression, purification, and characterization of an aerobic FMN-dependent azoreductase from Enterococcus faecalis, Protein Expr Purif 34, 302-310.

[15] Patridge, E. V., and Ferry, J. G. (2006) WrbA from Escherichia coli and Archaeoglobus fulgidus is an NAD(P)H:quinone oxidoreductase, J Bacteriol 188, 3498-3506.

[16] Bellamacina, C. R. (1996) The nicotinamide dinucleotide binding motif: a comparison of nucleotide binding proteins, FASEB J 10, 1257-1269.

[17] Rossmann, M. G., Moras, D., and Olsen, K. W. (1974) Chemical and biological evolution of nucleotide-binding protein, Nature 250, 194-199.

[18] Wierenga, R. K. (2001) The TIM-barrel fold: a versatile framework for efficient enzymes, FEBS Lett 492, 193-198.

[19] Scrutton, N. S., Berry, A., and Perham, R. N. (1990) Redesign of the coenzyme specificity of a dehydrogenase by protein engineering, Nature 343, 38-43.

[20] Holmberg, N., Ryde, U., and Bulow, L. (1999) Redesign of the coenzyme specificity in L-lactate dehydrogenase from bacillus stearothermophilus using site-directed mutagenesis and media engineering, Protein Eng 12, 851-856.

[21] Meng, H., Liu, P., Sun, H., Cai, Z., Zhou, J., Lin, J., and Li, Y. (2016) Engineering a d-lactate dehydrogenase that can super-efficiently utilize NADPH and NADH as cofactors, Sci Rep 6, 24887.

[22] Petschacher, B., Leitgeb, S., Kavanagh, K. L., Wilson, D. K., and Nidetzky, B. (2005) The coenzyme specificity of Candida tenuis xylose reductase (AKR2B5) explored by site-directed mutagenesis and X-ray crystallography, Biochem J 385, 75-83.

[23] Moon, H. J., Tiwari, M. K., Singh, R., Kang, Y. C., and Lee, J. K. (2012) Molecular determinants of the cofactor specificity of ribitol dehydrogenase, a short-chain dehydrogenase/reductase, Appl Environ Microbiol 78, 3079-3086.

[24] Chanique, A. M., and Parra, L. P. (2018) Protein Engineering for Nicotinamide Coenzyme Specificity in Oxidoreductases: Attempts and Challenges, Front Microbiol 9, 194.

[25] Petschacher, B., Staunig, N., Muller, M., Schurmann, M., Mink, D., De Wildeman, S., Gruber, K., and Glieder, A. (2014) Cofactor Specificity Engineering of Streptococcus mutans NADH Oxidase 2 for NAD(P)(+) Regeneration in Biocatalytic Oxidations, Comput Struct Biotechnol J 9, e201402005.

[26] Ball, J., Salvi, F., and Gadda, G. (2016) Functional Annotation of a Presumed Nitronate Monoxygenase Reveals a New Class of NADH:Quinone Reductases, J Biol Chem 291, 21160-21170.

[27] Ha, J. Y., Min, J. Y., Lee, S. K., Kim, H. S., Kim, D. J., Kim, K. H., Lee, H. H., Kim, H. K., Yoon, H. J., and Suh, S. W. (2006) Crystal structure of 2-nitropropane dioxygenase complexed with FMN and substrate. Identification of the catalytic base, J Biol Chem 281, 18660-18667.

[28] Karplus, P. A., and Diederichs, K. (2012) Linking crystallographic model and data quality, Science 336, 1030-1033.

[29] Mattevi, A., Vanoni, M. A., Todone, F., Rizzi, M., Teplyakov, A., Coda, A., Bolognesi, M., and Curti, B. (1996) Crystal structure of D-amino acid oxidase: a case of active site mirror-image convergent evolution with flavocytochrome b2, Proc Natl Acad Sci U S A 93, 7496-7501.

[30] Terry-Lorenzo, R. T., Chun, L. E., Brown, S. P., Heffernan, M. L., Fang, Q. K., Orsini, M. A., Pollegioni, L., Hardy, L. W., Spear, K. L., and Large, T. H. (2014) Novel human D-amino acid oxidase inhibitors stabilize an active-site lid-open conformation, Biosci Rep 34.

[31] Fu, G., Yuan, H., Li, C., Lu, C. D., Gadda, G., and Weber, I. T. (2010) Conformational changes and substrate recognition in Pseudomonas aeruginosa D-arginine dehydrogenase, Biochemistry 49, 8535-8545.

[32] Salvi, F., Rodriguez, I., Hamelberg, D., and Gadda, G. (2016) Role of F357 as an Oxygen Gate in the Oxidative Half-Reaction of Choline Oxidase, Biochemistry 55, 1473-1484.

[33] Venkitakrishnan, R. P., Zaborowski, E., McElheny, D., Benkovic, S. J., Dyson, H. J., and Wright, P. E. (2004) Conformational changes in the active site loops of dihydrofolate reductase during the catalytic cycle, Biochemistry 43, 16046-16055.

[34] Sevostyanova, A., Belogurov, G. A., Mooney, R. A., Landick, R., and Artsimovitch, I. (2011) The beta subunit gate loop is required for RNA polymerase modification by RfaH and NusG, Mol Cell 43, 253-262.

[35] Gora, A., Brezovsky, J., and Damborsky, J. (2013) Gates of enzymes, Chem Rev 113, 5871-5923.

[36] Li, R., Bianchet, M. A., Talalay, P., and Amzel, L. M. (1995) The three-dimensional structure of NAD(P)H:quinone reductase, a flavoprotein involved in cancer chemoprotection and chemotherapy: mechanism of the two-electron reduction, Proc Natl Acad Sci U S A 92, 8846-8850.

[37] Al Massri, S. (2017) Characterizing the cofactor specificity of NQO2, Electronic Thesis and Dissertation Repository 4586.

[38] Andrade, S. L., Patridge, E. V., Ferry, J. G., and Einsle, O. (2007) Crystal structure of the NADH:quinone oxidoreductase WrbA from Escherichia coli, J Bacteriol 189, 9101-9107.

[39] Tanner, J. J., Tu, S. C., Barbour, L. J., Barnes, C. L., and Krause, K. L. (1999) Unusual folded conformation of nicotinamide adenine dinucleotide bound to flavin reductase P, Prot Sci 8, 1725-1732.

[40] Okai, M., Kudo, N., Lee, W. C., Kamo, M., Nagata, K., and Tanokura, M. (2006) Crystal structures of the short-chain flavin reductase HpaC from Sulfolobus tokodaii strain 7 in its three states: NAD(P)(+)(-)free, NAD(+)(-)bound, and NADP(+)(-)bound, Biochemistry 45, 5103-5110.

[41] Fita, I., and Rossmann, M. G. (1985) The NADPH binding site on beef liver catalase, Proc Natl Acad Sci U S A 82, 1604-1608.

[42] Pudney, C. R., Hay, S., Levy, C., Pang, J., Sutcliffe, M. J., Leys, D., and Scrutton, N. S. (2009) Evidence to support the hypothesis that promoting vibrations enhance the rate of an enzyme catalyzed H-tunneling reaction, J Am Chem Soc 131, 17072-17073.

[43] Berrisford, J. M., and Sazanov, L. A. (2009) Structural basis for the mechanism of respiratory complex I, J Biol Chem 284, 29773-29783.

[44] Boehr, D. D., Farley, A. R., Wright, G. D., and Cox, J. R. (2002) Analysis of the pi-pi stacking interactions between the aminoglycoside antibiotic kinase APH(3')-IIIa and its nucleotide ligands, Chem Biol 9, 1209-1217.

[45] Bernard, N., Johnsen, K., Holbrook, J. J., and Delcour, J. (1995) D175 discriminates between NADH and NADPH in the coenzyme binding site of Lactobacillus delbrueckii subsp. bulgaricus D-lactate dehydrogenase, Biochem Biophys Res Commun 208, 895-900.

[46] Desplats, C., Beyly, A., Cuine, S., Bernard, L., Cournac, L., and Peltier, G. (2007) Modification of substrate specificity in single point mutants of Agrobacterium tumefaciens type II NADH dehydrogenase, FEBS Lett 581, 4017-4022.

[47] Kamerbeek, N. M., Fraaije, M. W., and Janssen, D. B. (2004) Identifying determinants of NADPH specificity in Baeyer-Villiger monooxygenases, Eur J Biochem 271, 2107-2116.

[48] Adams, M. J., Ellis, G. H., Gover, S., Naylor, C. E., and Phillips, C. (1994) Crystallographic study of coenzyme, coenzyme analogue and substrate binding in 6-phosphogluconate dehydrogenase: implications for NADP specificity and the enzyme mechanism, Structure 2, 651-668.

[49] Zheng, T., Olson, D. G., Tian, L., Bomble, Y. J., Himmel, M. E., Lo, J., Hon, S., Shaw, A. J., van Dijken, J. P., and Lynd, L. R. (2015) Cofactor Specificity of the Bifunctional Alcohol and Aldehyde Dehydrogenase (AdhE) in Wild-Type and Mutant Clostridium thermocellum and Thermoanaerobacterium saccharolyticum, J Bacteriol 197, 2610-2619.

[50] Zhang, L., Kudo, T., Takaya, N., and Shoun, H. (2002) The B' helix determines cytochrome P450nor specificity for the electron donors NADH and NADPH, J Biol Chem 277, 33842-33847.

[51] Battye, T. G., Kontogiannis, L., Johnson, O., Powell, H. R., and Leslie, A. G. (2011) iMOSFLM: a new graphical interface for diffraction-image processing with MOSFLM, Acta Crystallogr D Biol Crystallogr 67, 271-281.

[52] Evans, P. R. (2011) An introduction to data reduction: space-group determination, scaling and intensity statistics, Acta Crystallogr D Biol Crystallogr 67, 282-292.

[53] Winn, M. D., Ballard, C. C., Cowtan, K. D., Dodson, E. J., Emsley, P., Evans, P. R., Keegan, R. M., Krissinel, E. B., Leslie, A. G., McCoy, A., McNicholas, S. J., Murshudov, G. N., Pannu, N. S., Potterton, E. A., Powell, H. R., Read, R. J., Vagin, A., and Wilson, K. S. (2011) Overview of the CCP4 suite and current developments, Acta Crystallogr D Biol Crystallogr 67, 235-242.

[54] Storoni, L. C., McCoy, A. J., and Read, R. J. (2004) Likelihood-enhanced fast rotation functions, Acta Crystallogr D Biol Crystallogr 60, 432-438.

[55] McCoy, A. J., Grosse-Kunstleve, R. W., Adams, P. D., Winn, M. D., Storoni, L. C., and Read, R. J. (2007) Phaser crystallographic software, J Appl Crystallogr 40, 658-674.

[56] Afonine, P. V., Grosse-Kunstleve, R. W., Echols, N., Headd, J. J., Moriarty, N. W., Mustyakimov, M., Terwilliger, T. C., Urzhumtsev, A., Zwart, P. H., and Adams, P. D.

(2012) Towards automated crystallographic structure refinement with phenix.refine, Acta Crystallogr D Biol Crystallogr 68, 352-367.

[57] Emsley, P., Lohkamp, B., Scott, W. G., and Cowtan, K. (2010) Features and development of Coot, Acta Crystallogr D Biol Crystallogr 66, 486-501.

[58] Adams, P. D., Grosse-Kunstleve, R. W., Hung, L. W., Ioerger, T. R., McCoy, A. J., Moriarty, N. W., Read, R. J., Sacchettini, J. C., Sauter, N. K., and Terwilliger, T. C. (2002) PHENIX: building new software for automated crystallographic structure determination, Acta Crystallogr D 58, 1948-1954.

[59] Chen, V. B., Arendall, W. B., 3rd, Headd, J. J., Keedy, D. A., Immormino, R. M., Kapral, G. J., Murray, L. W., Richardson, J. S., and Richardson, D. C. (2010) MolProbity: all-atom structure validation for macromolecular crystallography, Acta Crystallogr D Biol Crystallogr 66, 12-21.

7 GENERAL DISCUSSION AND CONCLUSIONS

*Pa*DADH has been studied in this dissertation by a combined approach of mutagenesis and pH kinetic effects. The mutagenesis was initially carried out in hopes of identifying the catalytic base that deprotonates the substrate α-amino group. However, the pH profiles of variants targeting H48, E87, Y53 and Y254 indicated the deprotonation was still occurring in the mechanism. This finding was taken as evidence that there is no catalytic base functioning in the mechanism, since all the potential bases were ruled out by mutagenesis, and consequently it was proposed that the pK_a belongs to the substrate α-amine that loses its proton to solvent possibly with the aid of enzymatic residues. H48 may be involving in transferring the proton to the bulk solvent, suggested by the hollowed pH profiles of the H48F variant. Hollowed pH profiles are indicative of a disruption in the fast equilibration of the proton on the ES complex.

Comparison of the the pH profiles of the E87L variant to the wild-type demonstrated the requirement of E87 to be depronated for tight binding of cationic substrates, as the binding pK_a seen in the k_{cat}/K_m pH profiles disappeared in the E87L variant. D-arginine and D-lysine most likely form strong electrostatic interactions with E87, and this residue is the principle factor controlling substrate specificity in *Pa*DADH.

In the second part of this dissertation, we demonstrated that PA1024 is not a nitronate monooxygenase, as it was annotated in the databanks. Instead, the enzyme exhibits an NADH:quinone reductase activity with a strict preference for NADH. The NADH specificity could have major implications in the physiological function of the enzyme, as NADH and NADPH often play very distinct roles within metabolic pathways. The biochemical characterization and bioinformatics anaylsis carried out established PA1024 as the founding

member of a new class of FMN-dependent NQRs with a TIM-barrel fold. All of the NQRs identified to date are a flavodoxin-like fold, making this the first TIM-barrel fold enzyme with demonstrated NQO activity.

The kinetic characterization in combination with the structural analysis led to the identification of structural motfis unique to the catalytic function of this class of NQRs. These motifs were then used in a PHI-BLAST to identify close to 500 hypothetical proteins that belong to this class of NQRs. The method utilized in this study of implementing both experimental and computational approaches to identify structural motifs that define the catalytic function could be used to enhance gene function prediction of hypothetical proteins from other enzyme familes, instead of the current annotation method which relies solely on overall amino acid sequence similarity. Key hypothetical proteins could be selected and characterized, and PHI-BLAST could be used to identify other enzymes with similar function.

The enzyme has a strict preference for NADH over NADPH. The structure of the enzyme in complex with NAD^+ has been solved, leading to the structural basis for the strict NADH specificity. P78 and Q80 are positioned in the NAD^+-complex to sterically clash with putative binding spot of the 2'-phosphate of $NADP^+$. In addition, Q80 assumes two distinct conformations in the ligand-free and NAD^+-complex structures, revealing a conformational gating mechanism of Q80 to secure the NAD^+ within the binding pocket. Lastly, an unusual interrupted helix that consists of (^{268}VSG^{270}) serves to bind the pyrophosphate of NAD^+ is observed in the structure of the NAD^+-complex. This interrupted helix could potentially be a novel structural motif to bind the pyrophosphate moieties in TIM-barrel enzymes.

The rate-limiting contributions of PA1024 are shifted as the pH increases. Product release becomes progressively more rate-limiting at high pH, whereas flavin reduction is principal rate

liming step at low pH. Kinetic solvent viscosity effects (KSVE) provided further evidence in favor of product release being partially rate-liming in the reaction catalyzed by PA1024. KSVE on the k_{cat}/K_m values with PA1024 suggested a conformational change may be required to bind the quinone. However, whether the release of the NAD^+ or hydroquinone or a combination of both product release is responsible for the observed KSVE requires additional experiments.

The *in vivo* deletion mutant of PA1024 could provide the necessary information to better determine to physiological role of the enzyme. The enzyme almost certainly oxidizes NADH to NAD^+ *in vivo*, but if quinones are the true physiological electron acceptors is still debatable. But given their high k_{cat}/K_m values and widespread occurrence in nature, it is conceivable they could possibly be the natural substrates of the enzyme. The operon to which PA1024 belongs to consists of enzymes typically involved the β-oxidation of fatty acids. This operon could potentially be a novel β-oxidation pathway yet to be characterized in *P. aeruginosa*. Another study on *Syntropos wolfei* provided evidence that an NADH:acceptor reductase was the possible physiological partner of a butyrl-Coa reductase, as the NADH:acceptor reductase was copurified with the butyrl-Coa reductase. That same study also demonstrated that known NQO1 inhibitors decreased the rate of β-oxidation, consistent with a biochemical link between NADH:quinone reductases and β-oxidation. We propose that PA1024 plays a pivotal role in the maintenance of the [NADH]/[NAD^+] ratio in the cell, and consequently the ability of *P. aeruginosa* to perform the β-oxidation of fatty acids through this hypothetical pathway. In order to verify this proposal, *in vivo* experiments targeting PA1024 and this operon would be necessary.